University of Calgary

PRISM Repository **https://prism.ucalgary.ca**

The Vault Open Theses and Dissertations

2024-01-24

Extrinsic Factors and RPE Regeneration

Selje, Sara J.

Selje, S. J. (2024). Extrinsic factors and RPE regeneration (Master's thesis, University of Calgary, Calgary, Canada). Retrieved from https://prism.ucalgary.ca.
https://hdl.handle.net/1880/118068
Downloaded from PRISM Repository, University of Calgary

UNIVERSITY OF CALGARY

Extrinsic Factors and RPE Regeneration

by

Sara J. Selje

A THESIS
SUBMITTED TO THE FACULTY OF GRADUATE STUDIES
IN PARTIAL FULFILMENT OF THE REQUIREMENTS FOR THE
DEGREE OF MASTER OF SCIENCE

GRADUATE PROGRAM IN NEUROSCIENCE
CALGARY, ALBERTA
JANUARY, 2024

© Sara J. Selje 2024

Abstract

The retinal pigment epithelium (RPE) is a monolayer of pigmented cells that closely interacts with photoreceptor outer segments of the outer vertebrate retina to maintain visual function. Damage to the RPE, for instance in a disease such as Age-Related Macular Degeneration, results in photoreceptor degeneration and subsequently, vision loss. In contrast to mammals, zebrafish can intrinsically regenerate a functional RPE layer after injury. Specific molecular pathways are known to regulate RPE proliferation in culture, but the pathways that function *in vivo* to promote RPE regeneration remain largely unknown. My aim is to determine potential pathways that influence RPE regeneration in zebrafish. First, I examine the importance of the secreted ligand Semaphorin 3F (SEMA3F), expressed in the RPE of both mammals and zebrafish, in RPE regeneration. I use a *sema3fa* homozygous mutant zebrafish on a transgenic RPE injury background (*Tg(rpe65a:NTR-EGFP)*) where timed application of the drug metronidazole (MTZ) to the bath results in nitroreductase-mediated RPE-specific cell death. My data suggest Sema3fa has no effect on the extent of RPE injury in this model, though RPE apoptosis may be delayed and increased in the absence of Sema3fa. Further, loss of Sema3fa may induce an initial increase in proliferation in the RPE as well as increased proliferation in the photoreceptor outer nuclear layer. Second, I provide an initial assessment of the involvement of additional pathways in zebrafish RPE regeneration. These pathways impact proliferation and/or migration of cells in culture and are expressed within the RPE. I use *in situ* hybridization to visualize larval RPE expression of 10 candidate genes before and after RPE injury. Genes that may show changes in expression post-injury include *bmp7b, caska, foxm1, her4.1, msnb, rpe65a, trpm7,* and *vrk1*. Future work could include using loss-of-function approaches in the RPE injury model to determine potential roles of

these genes in RPE regeneration. In the long-term, this work may impact gene therapies for patients suffering from retinal degenerative diseases.

Preface

This thesis is original, unpublished, independent work by the author, S. Selje with contributions from the following:

Sanjibani Sanyal (MSc Student) – probe synthesis for *foxm1* and *vrk1*

Katelyn Shewchuk (PhD Candidate) – primer design and probe synthesis for *her4.1*

The experiments reported in Chapters 2-4 were covered by the Certificate of Animal Use Protocol AC23-0127 issued by the University of Calgary Animal Care Committee on October 23, 2023.

Acknowledgements

I want to extend my heartfelt appreciation to the following individuals who have played a pivotal role in the completion of this master's thesis:

I am profoundly grateful to my supervisor, Dr. Sarah McFarlane, for her immense wisdom, support, and passion which has kept me motivated over the last two years. Thank you to my committee members, Drs. Jennifer Hocking and Mark Ungrin for their constructive feedback and guidance throughout this project. To all the members of the McFarlane lab, I will always cherish the enriching and collaborating environment you've provided me. Thanks to Carrie, for all her assistance and for keeping the lab running smoothly. Gabriel, Neda, Katie, Julia, Sam, and especially Sanji for their friendship, cooperation and for being some of my first friends in Calgary. I will always remember our fun chats in the cove. Thank you to Dr. Kevin Lam for sparking my love for research. Thank you to my friends outside the lab who were always curious as to what I was doing despite having no idea what I was talking about. Heartfelt thanks to my family, Mom, Dad, and Oma, that even from a distance were always there for emotional support. To my unwaveringly supportive partner Erik, who's love and encouragement has been the bedrock upon which this thesis stands. A final thanks to my loving dog Rex, who stayed up with me every late night to remind me to take a break.

Dedication

In loving memory of Travis,

Who will always inspire me to challenge myself.

Table of Contents

List of Equations and Tables

List of Figures and Illustrations

List of Symbols, Abbreviations, and Nomenclature

°C	degrees Celsius
%	percent
+	positive
µL	microliter
µm	micrometer
µM	micromolar
AAV	adeno-associated virus
aCsp3	active Caspase 3
AMD	Age-Related Macular Degeneration
ANOVA	analysis of variance statistical test
anti-DIG-POD	anti-digoxigenin antibody conjugated with horseradish peroxidase
β	beta
BF	brightfield
bmp7b	bone morphogenetic protein 7b
bp	base pair
BrdU	5-bromo-2'-deoxyuridine
Cas9	CRISPR-associated protein 9
CASK/*caska*	calcium-/calmodulin-dependent serine protein kinase a
cDNA	complimentary DNA
CMZ	ciliary marginal zone
col4a6	collagen IV, alpha 6
CRISPR	clustered regularly interspaced short palindromic repeats
DIG	digoxygenin
DMSO	dimethylsulfoxide
DNA	deoxyribonucleic acid
dpf	days post fertilization
dpr	days post removal
E2F2	E2F transcription factor 2
E3	zebrafish incubation medium
EdU	5-ethynyl-2'-deoxyuridine
EMT	epithelial-mesenchymal transition
ERM	Ezrin-Radixin-Moesin
F0	founder generation
FISH	fluorescent *in situ* hybridization
foxm1	forkhead box protein m1
GCL	ganglion cell layer
gDNA	genomic DNA
GFP/eGFP	green fluorescent protein

h	hour
her4.1	hairy-related 4, tandem duplicate 1
hpf	hours post fertilization
IPM	interphotoreceptor matrix
INL	inner nuclear layer
ISH	*in situ* hybridization
L	liter
MET	mesenchymal-epithelial transition
Mg^{2+}	magnesium
Mitf/*mitfa*	microphthalmia associated transcription factor a
mRNA	messenger RNA
msnb	moesin b
mTOR	mammalian target of rapamycin
MTZ	metronidazole
n	number of larval replicates
N	number of experimental replicates
NCBI	National Center for Biotechnology Information
NRP	neuropilin
ns	not significant
NTR	nitroreductase
ONL	outer nuclear layer
Otx2/*otx2b*	orthodenticle homeobox 2b
PBST	phosphate-buffered saline with Tween® 20
PCR	polymerase chain reaction
PEDF	Pigment Epithelium-Derived factor
PFA	paraformaldehyde
PI3K	phosphoinositide 3-kinases
PLXN	plexin
PP7	Polyphyllin VII
PTU	N-phenylthiourea
PVR	proliferative vitreoretinopathy
RNA	ribonucleic acid
RPE	retinal pigment epithelium
RPE65/*rpe65a*	retinal pigment epithelium-specific protein 65a
RT-qPCR	real time quantitative polymerase chain reaction
SEMA/Sema	Semaphorin
Sema3fa	Semaphorin 3fa
scRNA-seq	single cell RNA sequencing
SSC/SSCT	saline-sodium citrate (with Tween® 20) buffer
TEM	transmission electron microscopy

Tg	transgenic
trpm7	transient receptor potential cation channel m7
TUNEL	terminal deoxynucleotidyl transferase-mediated dUTP nick-end labeling
UMAP	uniform manifold approximation and projection for dimension reduction
VEGF	Vascular Endothelial Growth Factor
VRK1/*vrk1*	vaccinia-related kinase 1 (serine/threonine kinase 1)
Vsx2/*vsx2*	visual system homeobox 2
Wnt	Wingless-related integration site
WT	wild type
ZPR2	zebrafish RPE antibody

CHAPTER ONE: INTRODUCTION

1.1 Introduction

Humans, like many vertebrates, rely on their sense of sight to navigate the world. From acquiring necessities like food and housing to more anthropological appreciation, vision is essential to maximize our interaction with the world; so, losing this critical sense can be hugely detrimental. Besides losing a major sense, vision loss comes with other comorbidities such as increased risk of anxiety and depression, as well as substantial losses to the economy in the form of increased health costs and decreased productivity (Frick et al., 2007; Marques et al., 2021; Osaba et al., 2019; Schultz et al., 2021).

Our brains convert light into electrical signals that can be processed by the brain through a nervous system structure: the retina. Once light reaches the eye, it passes through the cornea, lens, vitreous humor and then reaches the retina. This highly laminar structure contains many different cell types: ganglion cells, amacrine cells, bipolar cells, horizontal cells, Müller glia, and finally the photoreceptors, all with their own individual functions (Masland, 2001). Retinal ganglion cells are the innermost neuron type in the retina, found in the ganglion cell layer (GCL) and are responsible for propagating visual stimuli to the brain via their axons which make up the optic nerve (Mead & Tomarev, 2016). Within the inner nuclear layer (INL) there are amacrine and horizontal cells, which both laterally modulate the signaling of other neurons of the retina (Lagnado, 1998). Bipolar cells mediate visual signal transduction between photoreceptors and ganglion cells, and their cell bodies are also located in the INL (Euler et al., 2014). Müller glia span the width of the retina and are the most common glial cell in the retina. They help maintain retinal homeostasis and integrity by responding to injury, but the extent to which varies by taxonomic class (Goldman, 2014). Finally, located in the outer nuclear layer (ONL) are photoreceptors, the cones and rods. These

specialized light-sensitive cells mediate the initial step of vision. The specialized outer segments of the photoreceptors capture light and convert it into electrical signals for vision transduction (Molday & Moritz, 2015).

My research focuses on a cell layer at the very back of the retina: the retinal pigment epithelium (RPE; **Figure 1.1**). This layer has important roles in maintaining the blood-retina barrier, preventing light scatter, supporting photoreceptors by facilitating nutrient and ion transport and maintaining photoreceptor excitability, phagocytosing and recycling photoreceptor debris by shuttling the building blocks of the broken down photoreceptor outer segments back to the photoreceptor layer, secreting molecules that maintain the structural integrity of surrounding cell layers, and maintaining the avascularity and immune privilege of the outer retina (**Figure 1.2**). Disruption of the RPE, or any of the vital retinal cell layers, can result in interference with the sensitive neuronal mechanics of the eye, leading to vision loss or even blindness. Because mammals cannot intrinsically regenerate the cells of the retina after moderate damage, cellular degeneration or death leads to permanent vision loss.

The RPE therefore, plays a critical role in the function of the healthy vertebrate retina, and disruption of this delicate balance can lead to disastrous consequences for the organism. Unlike mammals, certain teleosts such as zebrafish (*Danio rerio*) can regenerate a functional RPE layer after large scale RPE injury (Hanovice et al., 2019). Zebrafish are an attractive model organism, not only due to their high fecundity, transparent larvae, and huge eye to body ratio, they also have a functional retina by 3 days post fertilization (dpf) with cone-dominant vision, which is more like the human retina than the rod-dominated murine retina (Avanesov & Malicki, 2010; Chhetri et al., 2014). It would be of interest to be able to understand the molecular mechanisms of how the RPE layer is able to regenerate by using the zebrafish model. Acquiring a greater understanding of the

molecular mechanisms involved in RPE regeneration will hopefully allow us to treat certain retinal diseases in humans in the future.

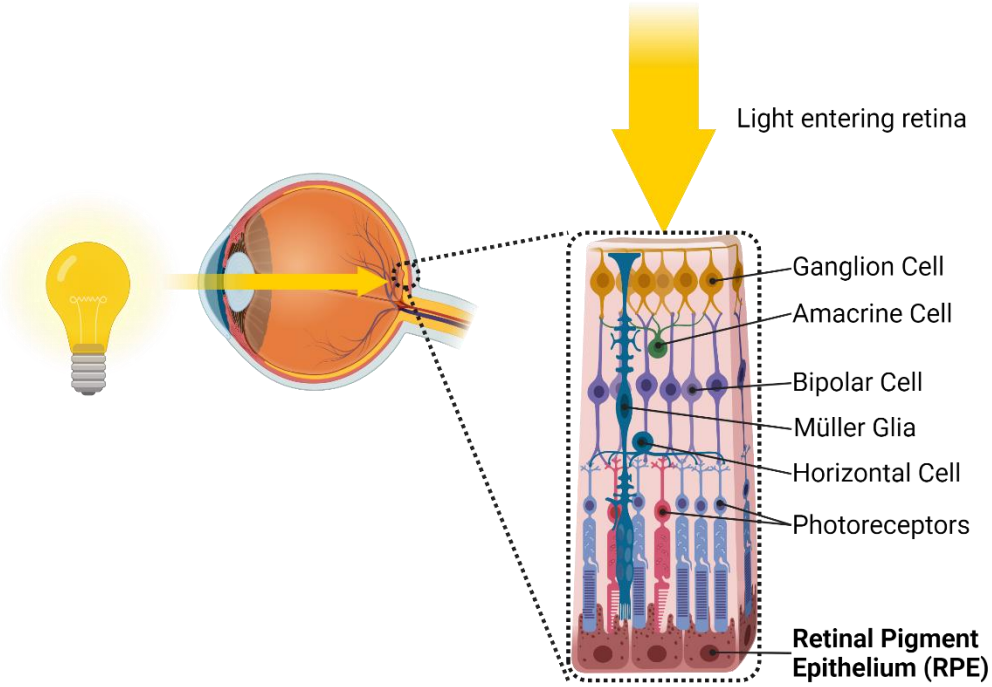

Figure 1.1 Schematic of the highly conserved retinal structure.

Light enters the eye, passes through the cornea, pupil, lens, through the vitreous and onto the retina (left). Light travels through the laminated cellular layers of the retinas and ultimately is captured by the outer segments of photoreceptors. The cells of the RPE form a layer of epithelium that is one cell thick that covers the back of the eye. The apical microvilli of the RPE cells interdigitate with the outer segments of the photoreceptors (insert). Created with BioRender.com.

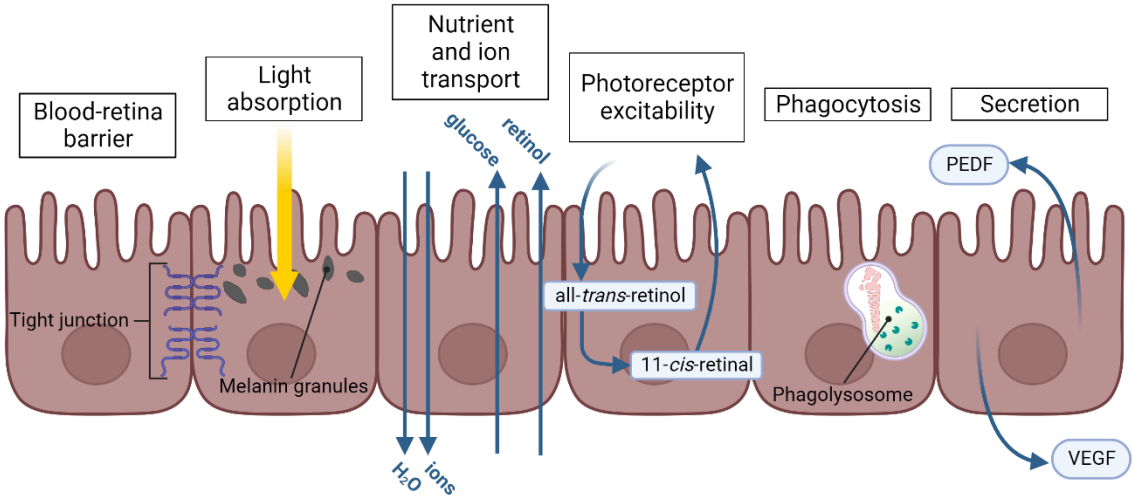

Figure 1.2 Schematic depicting the major functions of the RPE.

The RPE cells have multiple functions. The RPE cells use tight junctions to maintain the blood-retina barrier. Melanin granules within the RPE absorb stray light. Various ion channels facilitate water, nutrient, and ion transport between the retina and the choriocapillaris. The RPE cells reisomerize all-*trans*-retinol into its 11-*cis*-retinal form to maintain photoreceptor excitability. The RPE phagocytoses the outer segments of photoreceptors to recycle the basic components. Secretion of molecules such as growth factors helps maintain the structural integrity of the surrounding cell layers and maintains the avascularity and immune privilege of the outer retina. Created with BioRender.com.

1.2 Retinal Pigment Epithelium

1.2.1 RPE Structure

The RPE is a polarized monolayer of cuboidal cells located at the back of the retina. These cells interact apically with the outer segments of photoreceptors within the interphotoreceptor matrix (IPM) through microvilli. Basally, the RPE interacts with Bruch's membrane through small basal infoldings (Bonilha, 2014). The polarized nature of the RPE is critical for proper functionality of the neural retina and is maintained by cytoskeletal components that include microfilaments, microtubules, and intermediate filaments (Bonilha, 2014). The integrity and function of the RPE layer depends on cellular junctions, specifically basolateral tight junctions, adherens junctions, and desmosomes (Bonilha, 2014). The tight junctions are essential in maintaining the blood-retina barrier, while the adherens junctions form an adhesion belt, enclosing cells in a circumferential fashion. Both junction types contribute to maintaining an avascular outer retina (Bonilha, 2014). On the apical surface of the RPE, long and thin microvilli interlace with the outer segments of photoreceptors, and this is where the visual cycle components of the RPE are located (Nawrot et al., 2004).

1.2.2 Functions of the RPE

The RPE has multiple functions (**Figure 1.2)**. The RPE offers a support role to photoreceptors and is part of the blood-retina barrier. Some of the essential roles of the RPE include absorbing stray photons to focus light on the retina. The RPE also transports ions, water and metabolic end products from the retina to the blood, and takes up nutrients such as glucose, retinol, and fatty acids from the blood and passes them on to the energy-demanding photoreceptors (Strauss, 2005; Yang et al., 2021). The layered vasculature of the choriocapillaris is what provides

oxygen and other nutrients to nourish the RPE and its underlying photoreceptors (Lejoyeux et al., 2022). Additionally, the RPE is an important contributor to the visual cycle. Because photoreceptors are unable to reisomerize all-*trans*-retinal, which is formed after photon absorption, the RPE is essential to maintain photoreceptor excitability by reisomerizing all-*trans*-retinal back to the 11-*cis* form (Strauss, 2005). The RPE also maintain photoreceptor excitability by stabilizing the ion composition of the retinal space (Strauss, 2005). Another key function is in retinal recycling, which involves non-inflammatory clearing by phagocytosis; as the RPE phagocytoses photoreceptor outer segments, it digests them into their component macromolecules, which are then transported back to the photoreceptor cells to allow the outer segments to reform (Kwon & Freeman, 2020; Mazzoni et al., 2014). Finally, the RPE secretes growth factors such as Pigment Epithelium-Derived Factor (PEDF) and Vascular Endothelial Growth Factor (VEGF) to promote the structural integrity of the choriocapillaris and photoreceptors and maintain the avascularity and immune privilege of the outer retina (Ford et al., 2011; Polato & Becerra, 2016; Strauss, 2005; Yang et al., 2021). The failure of any one of these functions can quickly induce the degeneration of the retina, resulting in loss of visual function and ultimately blindness (Yang et al., 2021).

1.2.3 RPE Development

Development of the single layer RPE in vertebrates begins with the optic vesicle. This group of neuroepithelial progenitors is influenced by factors from surrounding tissues including the extraocular mesenchyme. The extrinsic factors cause different fated regions of the optic vesicles to express specific transcription factors (Fuhrmann, 2010). In vertebrates, like mouse and chick, the neuroepithelial cells begin to express a small network of regulatory genes such as *Microphthalmia Associated Transcription Factor* (*MITF*) and *Orthodenticle Homeobox 2* (*OTX2*)

(Moreno-Marmol et al., 2018). Initially, these genes are expressed within the entire optic vesicle. With the onset of expression of *Visual System Homeobox 2* (*VSX2*), which marks the neural retina, *OTX2* and *MITF* expression is downregulated in presumptive neural retina and remains in the prospective RPE (Lane & Lister, 2012). Below, I describe the development of the RPE in the model organism I am using for my studies, zebrafish. The Otx and Mitf transcription factors are both found in the embryonic zebrafish RPE at 16-18 hours post-fertilization (hpf), as the eye vesicles undergo morphogenesis to become the optic cups. Unlike in murine models, however, *otx2b* is a more important regulator of RPE target genes than *mitfa* (Cechmanek & McFarlane, 2017; Lane & Lister, 2012). By 18 hpf, the RPE cells in the dorsal/medial region of the optic vesicle begin to form a sheet of cuboidal cells (Moreno-Marmol et al., 2018). In mammals, the RPE cells remain cuboidal, but in teleosts, like zebrafish, the RPE cells further flatten and form squamous polygon-shaped cells (Moreno-Marmol et al., 2018). By 24 hpf, optic cup morphogenesis and RPE expansion over the retinal surface is complete (Cechmanek & McFarlane, 2017). Although my project focuses on RPE regeneration and not development, it is still important to understand the initial differentiation and proliferation of RPE cells as these processes may be similar in a regenerative scenario.

1.3 RPE Disease

1.3.1 Disease

There are many retinal diseases in humans. Diseases such as diabetic retinopathy, proliferative vitreoretinopathy (PVR), and Age-Related Macular Degeneration (AMD) involve the RPE. In diabetic retinopathy, glucose levels in the blood increase and can expedite the accumulation of excessive reactive oxygen species in cells, leading to oxidative stress and

inflammation in the RPE that causes cell damage (Yang et al., 2021; Yu et al., 2019). In PVR, which can occur after retinal detachment, the release of cytokines, growth factors, and chemokines facilitate pathologic RPE cell migration, proliferation, and epithelial-mesenchymal transition (Idrees et al., 2019). The subsequent RPE-derived fibrotic cells migrate into the vitreous and their contraction leads to recurring detachment of the retina as well as breakdown of the blood-retina barrier leading to photoreceptor death (Idrees et al., 2019). AMD is the major and primary RPE disease studied (Marmorstein, 2001). AMD is among the leading causes of blindness worldwide, only behind cataracts and glaucoma (Gheorghe et al., 2015). Due to AMD's prevalence in persons 75 years old and older, most of the individuals affected are in developed countries. Due to an aging population, AMD numbers are expected to increase and potentially double in the United States by 2050 (Moniz et al., 2022; Rein et al., 2009). AMD is the result of abnormal and increased RPE apoptosis and atrophy, and in more severe cases, choroid neovascularization due to disruption of the blood-retina barrier (Gheorghe et al., 2015; Yang et al., 2021). The comparison of the properties of *ex vivo* RPE cells from AMD and normal donors suggests a pathological mechanism for AMD that relates to the abnormal autophagy and apoptosis of RPE cells. RPE cells from AMD donors have increased amounts of lipid droplets, glycogen particles, disintegrated mitochondria, and autophagosomes, indicating decreased cell metabolism and increased autophagy (Golestaneh et al., 2017; Yang et al., 2021). This dysfunctional autophagy is also described by the ratio of autophagy markers LC3-II/LC3-I in the normal vs. AMD donor cultured cells; where AMD RPE fails to increase the LC3-II/LC3-I ratio seen in normal RPE (Golestaneh et al., 2017). Interestingly, the pathological LC3-II/LC3-I ratio is likely associated with defective AKT/mTOR signaling, as in the normal RPE the AKT/mTOR pathway promotes autophagy and LC3-I to LC3-II processing (Golestaneh et al., 2017).

1.3.2 Current Treatment Options for RPE-associated Retinal Diseases

Currently, the only widely used treatment for an RPE-associated disease, such as the wet (vascular) form of AMD, is anti-VEGF therapy. This therapy involves the ongoing injection into the intravitreal space of antibodies that bind and inhibit VEGF, to reduce neovascularization of the outer retina (Kovach et al., 2012). This treatment, however, only stabilizes vision. Thus, there are currently no effective nor practical methods of treatment to reverse the retinal damage caused by RPE-associated retinal degenerative diseases (Yorston, 2014).

Alternate treatment options include cell therapies, where embryonic, adult, or induced pluripotent stem cells are differentiated into either photoreceptors or RPE cells that are transplanted into the back of the eye (Yang et al., 2021). These stem-cell-derived RPE and photoreceptors have partially restored vision in pre-clinical models. However, the approach still has some major limitations that include allogenic rejection, donor pathogenic genes, and non-absolute immune privilege post transplantation (Yang et al., 2021). Gene therapy provides another potential opportunity to treat RPE degenerative diseases. Research into the genes and signal transduction pathways involved in retinal diseases has identified potential gene therapy targets to slow or reverse the retinal damage (Yang et al., 2021). The first approved ophthalmological gene therapy in humans uses recombinant adeno-associated viruses (AAVs) to deliver the *RPE65* gene into RPE cells that do not have functional RPE65, such as those in inherited retinal dystrophy. More research into the long-term clinical applications of gene therapy, however, is required (Dias et al., 2018; Russell et al., 2017). Although these therapies offer potential for ocular disease intervention, it is critical to first develop a greater understanding of the molecular determinants involved in the RPE and retinal cell degenerative processes before transitioning towards more translational research.

1.4 RPE Regeneration

1.4.1 Vertebrate RPE Regeneration

With the potential to successfully compensate for missing or dysfunctional genes, it is relevant to discover the genes and pathways responsible for RPE degeneration and perhaps regeneration. Human mature RPE is normally mitotically quiescent, but post-traumatic injury the RPE cells transform and proliferate, though the new RPE cells do not form a functional RPE layer (Chiba, 2014). Further, PVR is a detrimental process associated with this transformation. In PVR, RPE cells lose their epithelial quality and transition into fibroblast-like mesenchymal cells, leading to a scar-like non-functional RPE and retinal detachment (Chiba, 2014). Interestingly, some non-mammalian organisms can regenerate a functional RPE when the RPE is damaged, either in a transgenic ablation model or by pharmacological treatment. These models seek to replicate RPE degenerative diseases in humans (George et al., 2021). For instance, adult *Cynops pyrrhogaster* (newt), *Xenopus laevis* (frog), and *Danio rerio* (zebrafish) are all able to regenerate some form of functional RPE post-injury (George et al., 2021). It would then be of interest to identify the molecular pathways involved that allow these model organisms to regenerate this functional RPE layer.

1.4.2 MTZ-NTR Injury Model

A genetic RPE injury model was recently developed in zebrafish; the *Tg(rpe65a:NTR-EGFP)* (previously known as *Tg(rpe65a:nfsB-eGFP*) zebrafish line is an effective approach to specifically model RPE injury and subsequent recovery (Hanovice et al., 2019). This model utilizes what Hanovice et al. call “genetic ablation”, with large, contiguous areas of RPE injury, resembling the defects seen in late-stage AMD. As per the Hanovice et al. study, I will use the term ablation

when referring to the RPE injury. The size of the injury is potentially more clinically relevant than the small lesions produced with non-cell-specific injury techniques such as laser photocoagulation (Hanovice et al., 2019). This model was originally engineered by Dr. Jeff Gross's lab at the University of Pittsburgh and uses an *rpe65a* promoter element to selectively drive expression of an NTR-eGFP fusion protein in the mature RPE (**Figure 2.1A**) (Hanovice et al., 2019). GFP fluorescence can be used to confirm the expression of NTR-eGFP in the RPE. Upon bath application of the prodrug antibiotic metronidazole (MTZ), the E. coli nitroreductase (NTR) enzyme converts MTZ into a potent DNA cross-linking agent that induces apoptosis selectively in the GFP/NTR-expressing RPE cells (**Figure 2.1B**) (Curado et al., 2007; Curado et al., 2008). Previous analysis of the transgenic model confirmed ablation of the RPE, as assessed by loss of GFP-positive RPE, loss of RPE marker genes like ZPR2, and TUNEL-positive apoptotic nuclei in the RPE (Hanovice et al., 2019). Of note, because of the degeneration of the supportive RPE, the underlying photoreceptors degenerate in a similar time frame (Hanovice et al., 2019). Note that the MTZ treatment only causes damage in the presence of NTR, as apoptotic cells are basically absent from the RPE or ONL in non-transgenic fish (Hanovice et al., 2019). Post genetic ablation, the remaining non *rpe65a*-expressing RPE cells in the retinal periphery transition to becoming dividing proliferative cells that produce progeny that migrate centrally to the injury site and differentiate into mature RPE cells (**Figure 2.1C**). As a result of the production of new RPE cells, within one to two weeks of MTZ application and removal, the original RPE lesion is filled with differentiated and integrated RPE cells, with the underlying photoreceptors also regaining a normal morphology (Hanovice et al., 2019). Because of import restrictions, the McFarlane lab re-engineered this injury model using the constructs provided by the Gross lab. To analyse the role of a secreted Semaphorin, Semaphorin3fa (Sema3fa), in RPE regeneration, we also bred the re-

engineered line onto the *sema3fa*$^{ca304/ca304}$ null mutant line, where a 2 bp deletion in exon 2 of the *sema3fa* gene results in a premature stop codon (Halabi et al., 2021). Western analysis with an antibody that recognizes zebrafish Sema3fa verified that the fish are null for Sema3fa protein.

1.5 Molecular Determinants of RPE Regeneration

1.5.1 Molecular Factors known to Regulate RPE Regeneration

We know the identity of some molecular factors that affect RPE regeneration post-injury. Much of this work comes from studies that assess the ability of molecular pathways to influence the proliferation and migration of RPE cells *in vitro*. For example, overexpression of the transcription factor E2F2 in murine *in vitro* models induces RPE cell replication and regeneration (Kampik et al., 2017).

The zebrafish NTR transgenic model was used to investigate the molecular underpinnings of RPE regeneration *in vivo*. In zebrafish, transgenic mutants and drug treatment were used to show that the mechanistic Target of Rapamycin (mTOR) and Wnt pathways are required for RPE regeneration (Hanovice et al., 2019; Lu et al., 2022). The mTOR pathway regulates cell proliferation, autophagy and apoptosis, while the Wnt pathway regulates cell fate determination, cell migration, cell polarity, neural patterning, and organogenesis in development (Hanovice et al., 2019; Komiya & Habas, 2008; Lu et al., 2022; Zou et al., 2020). More specifically to the RPE, mTOR is essential for RPE regeneration, and disrupting the Wnt pathway causes qualitative lapses in RPE recovery (Hanovice et al., 2019; Lu et al., 2022). These types of studies show the strength of the NTR model for studying *in vivo* the candidate regulators of RPE regeneration post-injury. In this thesis I use a similar approach to test Sema3fa as a candidate regulator of the response of the to RPE injury. I also explore whether a subset of RPE genes, identified as potential regulators

of RPE proliferation and migration in *in vitro* mammalian RPE models, show changes in expression in the zebrafish RPE injury model. These genes could then serve in future studies using pharmacological and genetic loss-of-function approaches to investigate the roles they may play in regulating RPE regeneration.

1.5.2 Semaphorins

Semaphorins (SEMAs) are a multifunctional group of proteins composed of eight classes, all of which have the unifying feature of an approximately 500 amino acid extracellular "Sema" domain (Jackson & Eickholt, 2009). SEMA3s are secreted ligands for Plexin (PLXN) and Neuropilin (NRP) families of transmembrane receptors (Jackson & Eickholt, 2009). SEMA3s are known to alter actin cytoskeleton dynamics (Jackson & Eickholt, 2009). SEMAs were initially described for their roles as repulsive guidance cues, specifically for neuronal growth cones, neural crest cells, and endothelial cells (Jackson & Eickholt, 2009; Tran et al., 2007). Now, however, SEMAs are recognized as major contributors to the polarization, morphogenesis and homeostasis of many tissue types (Tran et al., 2007). There is also evidence that SEMAs are involved in tissue regeneration and repair. For instance, SEMA4-PLXNB2 signaling is essential for kidney repair in murine models (Xia et al., 2015).

1.5.3 Semaphorins in the Zebrafish Model

Sema3s are secreted ligands that bind to Nrp receptors, which then dimerize with Plxns to activate intracellular signaling pathways. Sema3s play key roles in development, including in the regulation of the proliferation and migration of specific cell types, including vascular cells. For example, Sema3s regulate zebrafish hindbrain neural cell crest migration (Yu & Moens, 2005).

Sema3s can control certain regenerative responses following central nervous system injury (Christie et al., 2021; Pasterkamp & Verhaagen, 2001). Sema3f is also expressed in the RPE of both human cells *in vitro* and zebrafish *in vivo* (Buehler et al., 2013; Halabi et al., 2021). Here it is proposed to serve as a key endogenous signal in maintaining an avascular outer retina, potentially through the specific Nrp1 receptor for both Sema3s and VEGF (Buehler et al., 2013; Soker et al., 1998). Interestingly, pathologic vascularization, as occurs in the wet form of AMD, is seen in a zebrafish *sema3fa* mutant line (Buehler et al., 2013; Halabi et al., 2021). In zebrafish, mRNA for *sema3fa* is present in the RPE by 72 hpf and maintained until at least 7 dpf with both cell autonomous and non-cell autonomous signalling (Halabi et al., 2021; Mori-Kreiner, 2020b). Since this gene is found in the mature RPE and appears to provide an anti-angiogenic signal to the choroid vasculature, it is reasonable to study a role for Sema3fa in RPE regeneration after injury.

1.6 Hypothesis and Aims

1.6.1 General Hypothesis

In zebrafish, the RPE can endogenously regenerate to produce a functional layer post-injury, but most of the genes responsible are not yet known. The Wnt and mTOR pathways were recently discovered as being essential to RPE regeneration, but there are many others to be explored (Hanovice et al., 2019; Lu et al., 2022, 2023). *sema3fa* mRNA is expressed early in zebrafish retinal development, plays a role in preventing pathologic choroid vessel growth in zebrafish, and regulates the mTOR pathway known to be essential in zebrafish RPE regeneration (Buehler et al., 2013; Callander et al., 2007; Halabi et al., 2021; Nakayama et al., 2015). These observations prompt further investigation of a role for Sema3fa in RPE regeneration. I hypothesize

that **secreted extrinsic signals, such as Sema3fa, promote RPE regeneration after injury and death**. This hypothesis was addressed by the following aims:

1.6.2 Specific Aim 1: To define the importance of the secreted ligand Sema3fa in RPE death and regeneration.

Previous findings from the McFarlane lab indicate that *sema3fa* mRNA is expressed by the RPE at 72 hpf and 7 dpf and that RPE development appears grossly normal in *sema3fa*$^{ca304/ca304}$ mutants (Halabi et al., 2021). Here I will assess if the loss of *sema3fa* causes a change in RPE cell death and regeneration post genetic ablation in an MTZ-NTR RPE injury model. Since this model is new to our lab, I will verify that the model works reliably in my hands and establish parameters for measuring RPE cell death and regeneration. I propose to quantify the injury response by assessing: 1) overall RPE health by measuring the transgenic GFP fluorescence post-injury, 2) cell death by measuring active caspase-3 (aCsp3) immunofluorescence, 3) proliferation by counting 5-ethynyl-2'-deoxyuridine (EdU) fluorescing cells. I will compare these parameters in wild type (WT) and *sema3fa*^{ca304} mutant uninjured RPE controls, WT control and injured RPE, *sema3fa*^{ca304} mutant control and injured RPE, and WT and *sema3fa*^{ca304} mutant injured RPE, at three different timepoints.

1.6.3 Specific Aim 2: To investigate candidate pathways that may regulate RPE death and/or regeneration.

Since the genes responsible in RPE regeneration are still largely unknown, I sought to initiate the investigation of other candidate pathways that may be involved in RPE regeneration post-injury. These pathways include those involved in mesenchymal-epithelial transition, cell

growth/division, and pathways involved in normal RPE function. I developed a list of ten candidate genes, based on three criteria; 1) the gene had to be physiologically relevant to the RPE, pertaining to a regeneration-associated biology, 2) the gene must be present in the control and/or injured zebrafish RPE at 5 dpf, and 3) the gene should have an available pharmacological inhibitor to simplify future experimental analysis. With each candidate gene, I will use an antisense riboprobe and conduct fluorescent *in situ* hybridization (FISH) on control and injured *Tg(rpe65a:NTR-EGFP)* larvae to observe if the gene is up or down-regulated in the RPE post-injury.

CHAPTER TWO: METHODS

2.1 Animals

2.1.1 Zebrafish strains and maintenance

Adult zebrafish (*Danio rerio*) were maintained according to standard conditions in a 14-hour light/10-hour dark cycle at 28°C. Embryos were obtained by natural spawning and after collection were raised in E3 medium supplemented with 0.25mg/L methylene blue and housed in an incubator following similar 14-hour light/10-hour dark cycle at 28°C. To inhibit pigmentation, embryos were transferred to the methylene blue-supplemented E3 medium treated with 0.003% (w/v) N-phenylthiourea (PTU) before 24 hpf, when initial pigment development is observed. PTU is a common reagent which inhibits melanization in zebrafish by reversibly inhibiting tyrosinase, a key enzyme in the melanogenic pathway (Li et al., 2012). At 24 hpf, embryos were screened and any that were unfertilized, deceased, or showed gross defects in morphological development were removed.

Zebrafish lines used in this study were *sema3fa*$^{ca304/ca304}$ mutants (Halabi et al., 2021) and their corresponding WT siblings on a *Tg(rpe65a:NTR-EGFP)* background re-engineered by using the constructs provided by the Gross lab (Hanovice et al., 2019). Ongoing familial generations were derived from heterozygous incrosses and screened for RPE-specific GFP expression at 72 hpf. The University of Calgary Animal Care Committee approved all procedures.

2.1.2 Genotyping

Genomic DNA (gDNA) was extracted from tissue from caudal fin clippings of tricaine methansulfonate (MS222; 160 mg/L) anesthetized adults. The tissue was placed in 100 µL of 50

mM NaOH, boiled for 10 minutes and neutralized with 10 µL of 100 mM Tris-HCL pH 7.4 (Meeker et al., 2007). Extracted gDNA was amplified by PCR using previously established *sema3fa* primers (Halabi, 2019). *sema3fa*$^{+/+}$ homozygotes, *sema3fa*$^{ca304/ca304}$ homozygotes, and *sema3fa*$^{+/ca304}$ heterozygotes were genotyped as previously described (Zheng et al., 2022), with the following substitutions: the PCR amplification had an annealing temperature of 55°C and an extension time of one minute, and the denaturation was conducted at 95°C for 5 minutes.

2.2 Injury Assay

2.2.1 MTZ-NTR mediated RPE ablation

To achieve the metronidazole (MTZ)-mediated RPE ablation, *Tg(rpe65a:NTR-EGFP)* larvae were removed from PTU at 5 dpf and placed for 24 hours in a 28°C incubator, either in 10 mM MTZ in E3 (Sigma-Aldrich) solution or in E3 as the control; 10-12 larvae were in each well. Aluminum foil was placed over the dish to protect the MTZ from light degradation. After treatment, the larvae were removed from the MTZ bath and washed 3x5 minutes in E3 and then allowed to recover. The day of removal from MTZ was designated as 0 days post removal (dpr). Those larvae used for the 0 dpr/6 dpf timepoint were removed from the bath and immediately euthanized with tricaine methanesulfonate (MS-222) and then fixed in 4% paraformaldehyde (PFA) overnight. Post recovery from the MTZ treatment, the remaining larvae were returned to a 14-hour light/10-hour dark cycle at 28°C until fixation at the desired timepoint (**Figure 2.1D**). Many preliminary experiments were conducted to ensure consistent and significant ablation of the RPE layer as assessed by quantifying GFP fluorescence of the RPE (**Figure 2.2**).

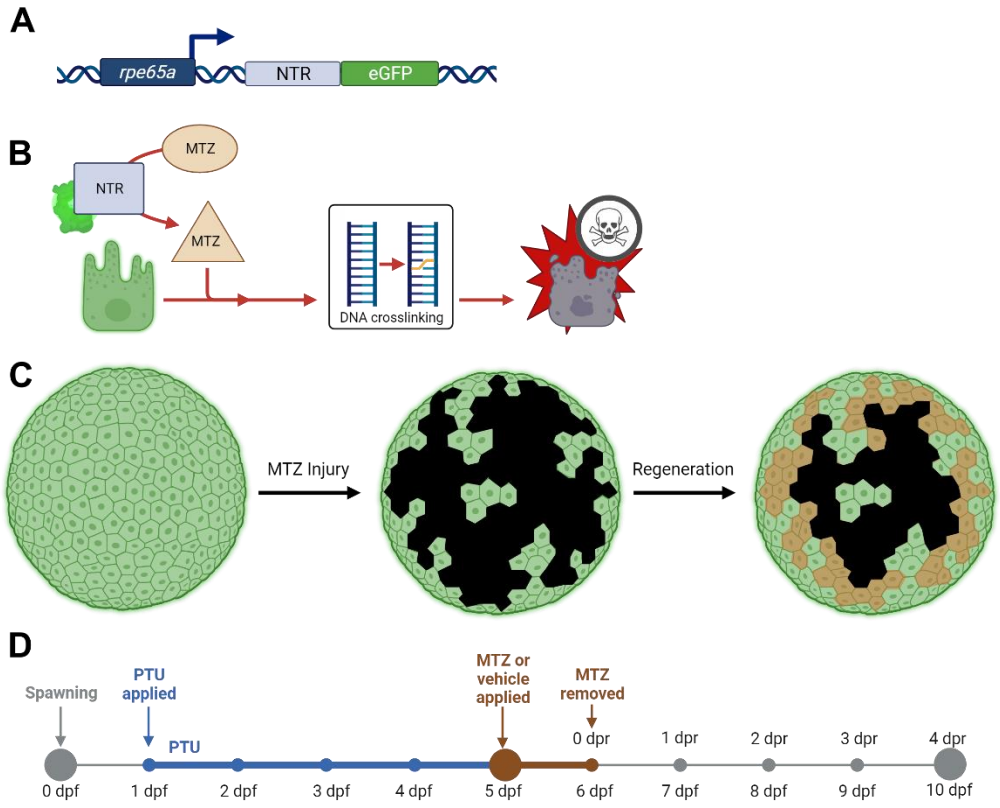

Figure 2.1 Schematic depicting the method of MTZ/NTR-mediated RPE ablation.

Schematic depicting the cDNA transgene with the RPE-specific *rpe65a* promoter upstream of the bacterial nitroreductase (NTR) enzyme fused to the eGFP coding sequence, which allowed me to confirm translation and identify NTR-expressing RPE cells (A). Translated NTR enzyme converts the prodrug metronidazole (MTZ) into a potent DNA crosslinking agent, inducing apoptosis within NTR/eGFP-expressing RPE cells (B). Representation of schematics of en-face whole mount transgenic eyes to show eGFP expression in an uninjured eye (left), loss of eGFP in the central eye after MTZ-mediated injury (middle), and subsequent regeneration of the RPE (new cells shown in brown) that occurs in a peripheral to central fashion (right) (C). Timeline of experiments. Larvae are placed in 1X phenylthiourea at 1 day-post fertilization (dpf) to minimize pigmentation for analysis purposes at the experimental endpoints. At 5 dpf, 10-12 larvae are grown for 24 hours in either 10 mM MTZ or E3 vehicle (control). After 24 hours, the MTZ/vehicle is removed (0 days post-removal (dpr)) and the fish are allowed to heal until fixation (D).

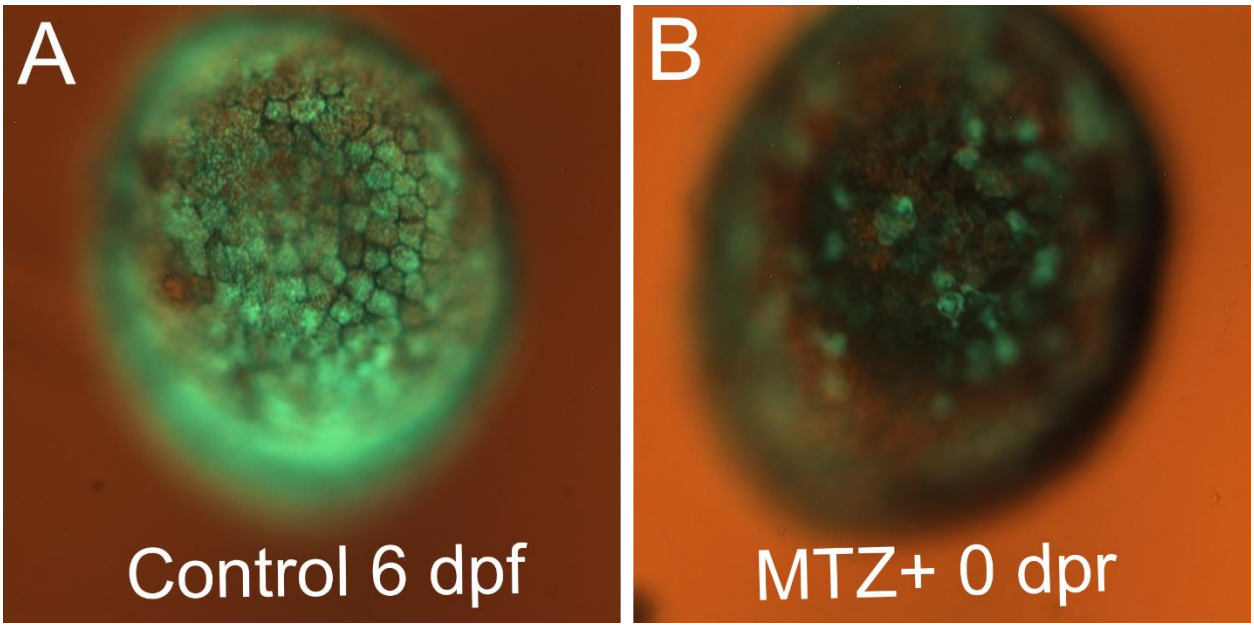

Figure 2.2 Robust MTZ/NTR-mediated ablation of the RPE.

Representative images of 6 dpf *sema3fa*$^{+/+}$ Tg(rpe65a:NTR-EGFP) whole mount eyes viewed en face. Shown is eGFP fluorescence with a brightfield background to reveal RPE pigmentation. There is complete coverage of the eye with eGFP-expressing RPE in the uninjured fish at 6 dpf (A), but the absence in the central eye of eGFP-expressing RPE cells at 6 dpf/0 dpr in the larva treated with 10 mM MTZ for 24 hours (injured) (B). MTZ-ablation decreases the extent of GFP-positive RPE coverage. The characterization of the MTZ RPE injury model by the Gross lab (Hanovice et al., 2019) indicates that this loss of eGFP expression reflects RPE cell death after being exposed to the MTZ.

2.3 Histology

2.3.1 Cryosection

Larvae were collected at desired developmental timepoints, anaesthetized with tricaine methanesulfonate (MS-222) and then fixed in 4% PFA in phosphate-buffered saline (PBS) for four hours at room temperature or overnight at 4°C. After fixation, samples were rinsed 3 times for 5 minutes with PBS and submersed in 25% sucrose in PBS overnight at 4°C. To further cryoprotect tissues, the larvae were submerged in 35% sucrose in PBS overnight at 4°C. The larvae were then embedded in Optimal Cutting Temperature medium (OCT; Tissue Tek) for transverse sections and frozen at -80°C for 10 minutes before storage in a container at -80°C. 12 µm sections were cut on a Leica CM 3050S cryostat and slides processed immediately or stored at -20°C.

2.4 Molecular Analysis

2.4.1 Immunohistochemistry (IHC)

I used active caspase 3 (aCsp3) as a marker of cell apoptosis within the RPE and retina (Yang et al., 2005). The timepoints chosen were 0 dpr (6 dpf), 1 dpr (7 dpf), and 3 dpr (9dpf). 0 dpr was chosen because it is when peak RPE apoptosis occurs (Hanovice et al., 2019). RPE apoptosis starts to decrease by 1 dpr, and while apoptosis at 3 dpr is not characterized, the 3 dpr time point is when RPE proliferation and recovery is at its peak. aCsp3 immunohistochemistry was run on cryosections (**2.3.1**) according to the protocol described (Uribe & Gross, 2007) with the following modifications. The addition of 1% dimethyl sulfoxide (DMSO) into the 1X PBS was omitted, and instead samples were rehydrated and washed with PBST (0.1% Tween-20 in 1X PBS). The primary antibody used was a 1:500 dilution of purified rabbit anti-Active Caspase-3 (Cat:559565; BD Biosciences) in blocking solution. The secondary antibody was a 1:1000 dilution

of Alexa Fluor® 555 goat anti-rabbit (Ref: A21429; Invitrogen) in blocking solution. A 10 minute 1:2000 Hoechst 33342 (Ref: H3570; Invitrogen) application was followed by a final four washes of PBT. Slides were mounted with a coverslip and Aqua-Poly/Mount (Ref: NC943924; Polysciences Inc.) and stored at -20°C until imaging.

2.4.2 EdU Click-iT™ Reaction

Timepoints of 0, 2, and 4 dpr were chosen as RPE proliferation post-injury peaks at 2 dpr and I wanted to observe temporal dynamics of RPE proliferation (Hanovice et al., 2019). Stock solutions were prepared as per manufacturer instructions. I exposed the larvae to a 400 µM EdU bath for 4 hours then fixed and cryosectioned as described above (**2.3.1**). Sections on slides were rehydrated with PBT for 20 minutes, and the Click-iT™ reaction (Ref: C10338; Thermo Fisher Scientific) performed as per the manufacturer's instructions. 1:2000 Hoechst 33342 (Ref: H3570; Invitrogen) was applied for 10 minutes, slides rinsed and mounted with a coverslip and Aqua-Poly/Mount (Ref: NC943924; Polysciences Inc.) and stored in -20°C until imaging.

2.4.3 Fluorescent *in situ* hybridization (FISH)

Primers for antisense riboprobes for candidate genes were designed using the Primer Blast program of the US National Centre for Biotechnology Information (NCBI) and synthesized by the University of Calgary Core DNA Services (**Table 1**). The reverse primer contained a T7 RNA polymerase binding sequence on the reverse primer at the 5' end (5'-GAAATTAATACGACTCACTATAGG-3'). Antisense RNA riboprobes were labeled with digoxigenin (DIG) and were generated through polymerase chain reaction (PCR) amplification.

RNA fluorescent *in situ* hybridization (FISH) was performed as previously described (Brend & Holley, 2009) with the following modifications. Larvae were fixed and cryosectioned after MTZ-treatment or control at 0 dpr/6 dpf as described in **2.3.1,** taking care to avoid RNAse contamination. 200 µL of 1% stock probe in hybridization buffer with 5% dextran sulfate was prewarmed to 65°C, added to the slides, then a cover slip was placed on top, and the slides were placed in a slide *in situ* box in a 65°C oven overnight. After removing the coverslip and the probe, sequential washes of 2X SSC (0%, 25%, 50%, 75%, 100%) in hybridization buffer were done for 5 minutes at 65°C. Then, two washes (one with 0.2X SSCT and then 0.1X SSCT) were done for 15 minutes at 65°C. Rehydration was done sequentially with 0.2X SSC in PBST (75%, 50%, 25%) for 5 minutes at room temperature until one final 5 minute 100% PBST wash at room temperature. Samples were blocked for 30 minutes at room temperature with 2% Blocking Reagent in 1X MAB (Roche). 200 µL per slide of anti-DIG-POD Fab fragment antibody (Ref: 11207733910; Roche) at 1:400 in the blocking solution was added for 1 hour at room temperature. Samples were washed five times five minutes in PBT, then 200 µL fluorescein tyramide solution was added for 30 minutes at room temperature: 1:50 tyramide solution in 1X amplification buffer (Cat: NEL702001KT; Akoya Biosciences) with 2% dextran sulfate. After rinsing in PBST, 1:2000 Hoechst 33342 (Ref: H3570; Invitrogen) was applied, and slides rinsed with PBST before being mounted with a coverslip and Aqua-Poly/Mount (Cat: NC943924; Polysciences Inc.) and stored in -20°C until imaging.

2.5 Imaging

2.5.1 Compound microscope

Sections were imaged on a Axioplan 2 (Zeiss) equipped with an AxioCam 305 Colour camera using ZENBlue (Zeiss) software. Cell counts were done on the microscope to best visualize cells in different focal planes. Every second section was counted to avoid counting a cell more than once, and the counts from three retinal sections per embryo were averaged. Only one eye was counted per embryo and slides were double blinded to avoid investigator bias. Hoechst labeling of cell nuclei was performed to identify cells. Images were collated in Adobe Photoshop for measurements and processing, and further processing was done with Fiji 1.54 (ImageJ) and Inkscape 1.3. The brightness and contrast of some images were altered.

2.5.2 Confocal

Sections were imaged on a LSM900 Observer inverted microscope with confocal laser scanning and detection with a PMT scan module (Zeiss) using ZENBlue (Zeiss) software.

2.6 Quantification

2.6.1 Percent GFP Fluorescence

Transverse cryosections were double blinded and imaged using a Axioplan 2 compound microscope with similar exposure parameters. Three sections per eye were imaged, with only one eye per embryo being selected. Images were exported and consolidated into a large multi-panel file in Photoshop (Adobe). While still blinded, GFP-positive RPE was manually traced and measured using Fiji software (Schindelin et al., 2012). “Total length” was defined as the GFP-

positive RPE from the dorsal CMZ-RPE boundary to the ventral CMZ-RPE boundary. Note that the peripheral GFP+ RPE is less disrupted in the model, so GFP fluorescence was present in the periphery of the retinal sections. CMZ-RPE boundary was readily identified through anatomical means as the region where the GFP-positive peripheral RPE cells meet the trapezoidal central CMZ cells. “eGFP-free length” is defined as the total measured gap in fluorescence of the RPE layer, considering both the fact that the RPE is absent at the optic nerve head and any tears in the RPE that occurred during cryosectioning.

$$\frac{\boldsymbol{total\ length\ -\ "eGFP\text{-}free\ length"}}{\boldsymbol{total\ length}} * \mathbf{100}\%$$

Equation 1 Formula for normalization of percent GFP fluorescence as a measure of RPE health.

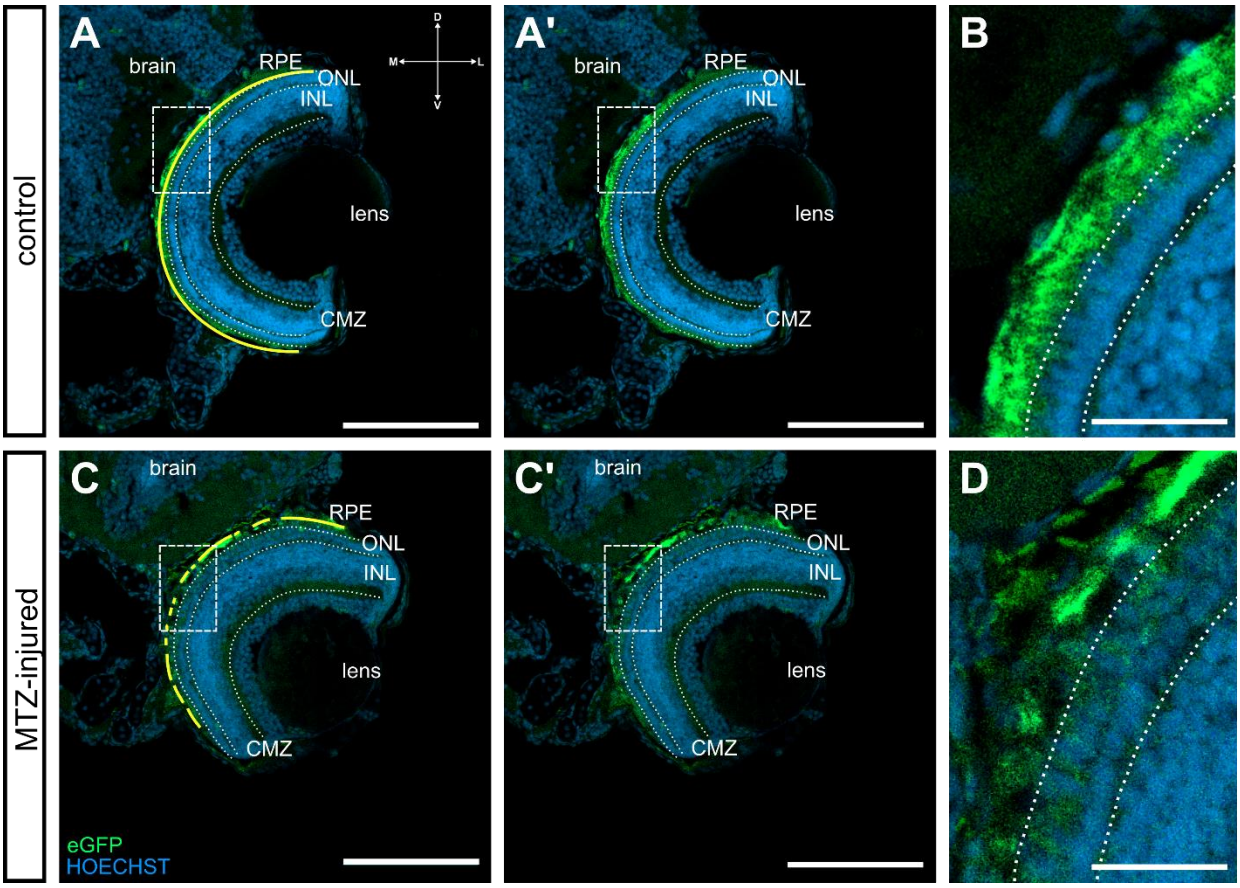

Figure 2.3 Verification of the MTZ-injury model as revealed by loss of GFP+ RPE in transverse retinal sections.

Confocal image (1µm) of transverse cryosection of the retina showing lamination and the intact GFP fluorescence in uninjured RPE of *sema3fa*^{ca304} *Tg(rpe65a:NTR-EGFP)* 6 dpf larvae (B), with the GFP+ RPE highlighted by a yellow line (A). Scale bar in A, A' denotes 100 µm. The boxed area in A is shown at higher magnification in B to reveal the intact RPE layer. Scale bar in B denotes 20 µm. Confocal image of transverse cryosection of the retina showing lamination and the loss of GFP fluorescence in MTZ-injured *sema3fa*^{ca304} *Tg(rpe65a:NTR-EGFP)* fish at 6 dpf/0 dpr (C'), with the yellow line representing GFP+ RPE that is still present after MTZ-injury (C). Scale bar in C, C' denotes 100 µm. The boxed area in C is shown at higher magnification in D to reveal the disrupted RPE layer. Scale bar in D denotes 20 µm. Dotted white lines separate the different retinal layers; RPE, outer nuclear layer (ONL), inner nuclear layer (INL), and the peripheral ciliary marginal zone (CMZ).

2.6.2 Counting of Active Caspase-3 Cells

Active Caspase-3 (aCsp3)-immunolabeling was used to identify cells undergoing apoptotic cell death and counted on an Axioplan 2 compound microscope. For each embryo, only one eye was quantified, and the number of aCsp3-positive cells counted per section for three retinal sections, skipping every second section to not double count a cell. Separate counts were made for aCsp3+ cells in the RPE (colocalized with GFP) and in the ONL. 7 to 11 embryos were counted per timepoint, from 3 separate experimental replicates. Active caspase-3-positive cells were defined as rounded, reddish-orange fluorescent, crenated cells, which were also Hoechst-labelled. All cell counts were done double blinded on the Axioplan 2 compound microscope, which allowed me to change focal plane and switch between fluorescent channels. In this way, I ensured that only aCsp3-positive cells were counted. Note that autofluorescence was yellow-orange in nature, and was also present in the green channel. In control retinas, where few apoptotic cells were present, apoptotic cells in the olfactory epithelium or jaw were used as a positive control to confirm the success of the immunohistochemistry.

2.6.3 Counting of EdU-positive cells

5-ethynyl-2'-deoxyuridine (EdU) -positive cells were quantified by conducting cell counts on an Axioplan 2 compound microscope. For each embryo, only one eye was considered, and the number of EdU-positive cells counted per section for three retinal sections, skipping every second section per embryo as to not double count a cell. 7 to 11 embryos were counted per timepoint over 3 independent experimental replicates. EdU-positive cells were defined as rounded/ovoid, Hoechst-positive, bright red-orange fluorescent cells. Only EdU+ cells located in the RPE, localized in line with the remaining transgenic GFP expression, were counted. All cell counts were

done double blinded on an Axioplan 2 compound microscope, as described above for the counting of the aCsp3 cells. For all retinal sections counted, labelling of proliferative cells in the peripheral ciliary marginal zone of the retina was used as an internal positive control for success of the immunohistochemistry.

2.6.4 Statistics

Sample size was calculated by using the resource equation method (Charan & Kantharia, 2013). This method is used in exploratory animal studies, such as conducted in this thesis, where previous literature is either minimal or unavailable. As such, we cannot assume effect size or standard deviation. Without knowledge of these two variables from the literature, we cannot perform *a priori* prediction for sample size using power analysis. To calculate whether a sample size is appropriate using the resource equation, we subtract the total number of animals used in the study by the number of treatment groups (**Equation 2**). This calculation gives the degree of freedom of analysis of variance (E) which is typically used in ANOVA calculations, but in exploratory animal studies it is appropriate for sample size calculations.

$$\boldsymbol{E = Total\ Number\ of\ Animals - Total\ Number\ of\ Groups}$$

Equation 2 Resource equation for the calculation of appropriate sample sizes.

If E is calculated to be between 10 and 20, then the chosen sample size is appropriate for the test. If the number is above 20 there are more than enough animals and if the number is below 10, more animals are needed. For all statistical tests conducted in this thesis, the number of animals used ranged from 7 to 11 per group (14 to 22 animals total) and I compared two groups at a time, whether it be comparing wild type (WT) versus mutant or control versus injured. Applying this

calculation results in an E value anywhere between 12 and 20, which is deemed an appropriate sample size according to the resource equation parameters.

Non-parametric Mann-Whitney U tests were used to compare two groups and all statistical analyses were performed on Prism 10 software (GraphPad). In graphs, each value (n) represents data from a separate embryo, with data pooled from several independent experimental replicates (N).

CHAPTER THREE: Investigating a Role for Sema3fa in RPE Injury and Regeneration

3.1 Introduction

The vertebrate retina is a highly complex, light-sensitive tissue composed of specifically organized neuronal layers that allows the transduction of visual stimuli to electrical signals that are received by the brain. The specifically laminated structure of the retina is essential for the function of the vertebrate eye. At the very back of the retina is a structure called the retinal pigment epithelium (RPE). In development, the early optic neuroepithelium is bipotential, having the ability to give rise to both neural retina and RPE progenitors. The neural retinal progenitor cells generate all seven retinal cell types: ganglion, horizontal, amacrine, bipolar, rods, cones, and Müller glia (Javed & Cayouette, 2017). The RPE, however, develops from RPE-specific progenitors whose emergence during development depends on both cell-intrinsic and cell-extrinsic factors (Fuhrmann et al., 2014). Given that extrinsic factors have an important influence on RPE development, I began to investigate whether extrinsic factors play a role in RPE apoptosis and regeneration, as similar cellular events (proliferation, migration, differentiation) are involved in both RPE development and regeneration.

RPE cells have many diverse functions that include maintaining an avascular retina, absorbing stray photons, nutrient and ion transport, and maintaining photoreceptor excitability. These roles mean the RPE contributes an important supportive role for proper photoreceptor function (**Figure 1.2**). Certain retinal diseases such as diabetic retinopathy, PVR, and AMD involve the irreversible degeneration of RPE. In diabetic retinopathy, oxidative stress and inflammation in the RPE causes cell damage and death (Yang et al., 2021). In PVR, the release of cytokines, chemokines, and growth factors after retinal detachment cause RPE cells to acquire a

fibrotic morphology and migrate into the vitreous (Idrees et al., 2019). In AMD, which is among the leading causes of blindness, decreased cell metabolism, increased autophagy, and increased apoptosis of RPE cells cause the breakdown of the RPE layer (Gheorghe et al., 2015; Yang et al., 2021). Degeneration of the RPE leads to degeneration of the underlying photoreceptors as they lose their support, causing irreversible vision loss in mammals (Dias et al., 2018; Jackson et al., 2002). To begin to understand how to successfully repair the RPE damaged in retinal disease I turned to an animal model that exhibits RPE regeneration, the zebrafish. We need to develop an understanding of the molecular determinants involved in RPE regeneration to perhaps harness endogenous RPE regeneration in the treatment of retinal degenerative diseases.

The zebrafish eye is an appealing model to use to gain an understanding of the molecular underpinnings of the function and dysfunction of the human eye. Zebrafish and mammalian eyes share a similar development, function, and structure, including a cone-rich adult retina. Interestingly, while mammals do not have the ability to effectively regenerate damaged RPE, zebrafish exhibit a robust intrinsic ability to regenerate large regions of damaged RPE in both adults and larvae (Hanovice et al., 2019). An NTR-MTZ zebrafish transgenic injury model can be used to specifically damage large regions of the RPE. The result is RPE cell apoptosis and the loss of RPE cells, followed by RPE cell de-differentiation and proliferation at the peripheral margins of the injury. In this model, peak RPE apoptosis occurs 24 hours after the initiation of RPE injury, at the time of removal (0 days post-removal, 0 dpr)) from the MTZ. In contrast, peak proliferation occurs around 2 dpr and occurs in a peripheral to central fashion. The proliferative cells produce post-mitotic daughters that differentiate into new RPE by 6 dpr (Hanovice et al., 2019). By 6-13 dpr with larval injuries, and by 1 month in injured adults, the entire RPE and underlying damaged photoreceptors are regenerated, even after widespread injury (Hanovice et al., 2019). This model

was used to show the importance of the Wnt and mTOR pathways in RPE regeneration *in vivo.* Both pathways are activated post RPE ablation, and loss of either pathway results in significantly impaired RPE regeneration (Hanovice et al., 2019; Lu et al., 2022). To further understand the mechanisms and pathways responsible for this large-scale regeneration, it is imperative to explore additional genes and pathways that may be involved.

One possible extrinsic factor that might influence RPE regeneration is Sema3f. Initially recognized as repulsive axon guidance cues, ongoing research has revealed that secreted Sema3s are key regulators of the morphology and motility of many cell types (Alto & Terman, 2017). Sema3f, specifically, has been explored by the McFarlane lab. *sema3fa* mRNA, but not its paralog *sema3fb*, is expressed by the RPE of the maturing eye, until at least 7 dpf (Halabi et al., 2021). The known *sema3fa* receptor *nrp2b* is also expressed in the RPE at 7 dpf, suggesting cell autonomous signalling (Mori-Kreiner, 2020b). Sema3fa may also provide a molecular barrier that prevents inappropriate growth of the choroid vasculature into the outer zebrafish retina in a non-cell autonomous fashion, with Nrp2b potentially located on the choroid vessels (Halabi et al., 2021). Interestingly, SEMA3F is found in RPE isolates of AMD patients, and the migration of human endothelial cells *in vitro* is inhibited by SEMA3F (Buehler et al., 2013; Halabi et al., 2021). As such, it is of interest to study the role of Sema3fa in the RPE response to injury.

In this chapter, I explore the role of Sema3fa in the regenerative response of the RPE as it pertains to overall RPE health, apoptosis, and proliferation post RPE injury. I establish in the McFarlane lab a zebrafish NTR-MTZ injury model that was previously shown to be effective at causing RPE injury and death (Hanovice et al., 2019). I take advantage of this model and the regenerative properties of the zebrafish RPE and retina to investigate potential functions of Sema3fa in RPE regeneration. My data suggest that although Sema3fa may not play a role in the

development and extent of MTZ-induced RPE injury, it may influence apoptosis and subsequent proliferation following RPE injury.

3.2 Results

3.2.1 Loss of Sema3fa does not appear to impact the larval RPE

sema3fa mRNA is expressed in the RPE of larval (Halabi et al., 2021) and juvenile zebrafish (Carrie Hehr, personal communication), and SEMA3F protein in the RPE of mouse pups (Sun et al., 2017). Further, Sema3f may play an important role in protecting against pathogenic neovascularization (Buehler et al., 2013; Halabi et al., 2021; Mori-Kreiner, 2020a; Sun et al., 2017). As such, I explored if Sema3fa has a role in RPE regeneration after injury. The RPE injury model I used was developed by the Gross lab; the MTZ-NTR RPE injury model. This model was reengineered by the McFarlane lab. I exposed 5 dpf *Tg(rpe65a:NTR-EGFP)* transgenic larvae to 10 μM MTZ for 24 hours. Larvae in E3 media alone served as control.

To verify that there was RPE cell loss in the MTZ-NTR RPE injury model, and to determine a way of quantifying the extent of cell loss, I developed a measure of overall RPE health; I used the GFP expressed by RPE cells in the *Tg(rpe65a:NTR-EGFP)* background as a marker of overall RPE health, as only healthy RPE cells appear to activate the *rpe65a* promoter (Hanovice et al., 2019). I compared the extent of GFP expression at the back of the retina, the RPE layer, of control and MTZ-treated *sema3fa* wild type (WT) and mutant larvae in the *Tg(rpe65a:NTR-EGFP)* background. First, it was important to determine if the loss of Sema3fa resulted either in the loss of the expression of GFP from the *rpe65a* promoter, and/or the larval development of the RPE in the absence of injury. Either scenario would complicate the analysis of the importance of Sema3fa in RPE loss and regeneration in the injury model.

I evaluated the RPE, via GFP fluorescence, in the control larvae grown from embryos PTU-treated at 24 hpf and raised in E3 to 6 dpf, 7 dpf, and 9 dpf. Note that these larvae served as the controls for the MTZ-treated RPE injury animals discussed below. Hoechst stain was used to identify the RPE cell layer, in addition to the transgenic GFP expression. A representative cross section of a control larva showed robust GFP expression in the RPE that covered the back of the retina, except for the peripheral-most retina (**Figure 3.1D; H**). To quantify the amount of healthy RPE, I measured the total length of the gaps in eGFP fluorescence in the RPE layer, subtracted this value from the total RPE length (not considering the peripheral RPE), and normalized the calculated value to the total GFP-positive RPE (**Equation 1**). Measurements were done in a manner blinded to genotype. The GFP+ RPE was manually traced, and the total length measured from the dorsal to the ventral CMZ-RPE boundaries. The normalization was performed because I found larval eyes varied in size. For both genotypes, and at all three timepoints tested, GFP fluorescence was present over almost the entire central RPE (**Figure 3.1I**). Further, there was no statistical difference in the extent of RPE coverage between WT larvae and mutants. These data suggest that the loss of Sema3fa has no effect on overall RPE health during normal larval development.

3.2.2 Loss of Sema3fa does not appear to impact the extent or time course of MTZ-induced RPE injury

To investigate a role for Sema3fa in RPE regeneration, I next sought to measure GFP+ RPE coverage post RPE injury in both WT and *sema3fa* mutants. I fixed the *Tg(rpe65a:NTR-EGFP)* larvae exposed at 5 dpf to 10 μM MTZ for 24 hours at different points post removal (dpr) from the MTZ; 0 dpr (peak of apoptosis), 1 dpr and 3 dpr (cessation of apoptosis) (n=7 to 11; N=3

independent experiments). I measured the RPE coverage in transverse retinal cryosections at each time point for MTZ-treated *sema3fa*$^{+/+}$ and *sema3fa*^{ca304} larvae, with the control measurements coming from the larvae described above (**3.2.1**). In MTZ-treated WT larvae, I observed a qualitative decrease in the retinal coverage by GFP+ RPE post-injury, often with large gaps present (**Figure 3.2D**). A similar decrease in GFP+ RPE coverage was also evident in the injured mutant eye (**Figure 3.2H**). Quantification revealed a significant loss of RPE coverage in the MTZ-treated (injured) larvae of both genotypes as compared to their corresponding controls at 0, 1, and 3 dpr (**Figure 3.3A; B**). These data confirm that MTZ-treatment injures the RPE in both *sema3fa* WT and mutants. When I compared the extent of loss of RPE coverage in the injured *sema3fa* WT and mutant eyes I found there was no statistically significant difference at 0, 1, and 3 dpr (**Figure 3.3C**). These data suggest that the loss of *sema3fa* has no effect on the extent of RPE injury.

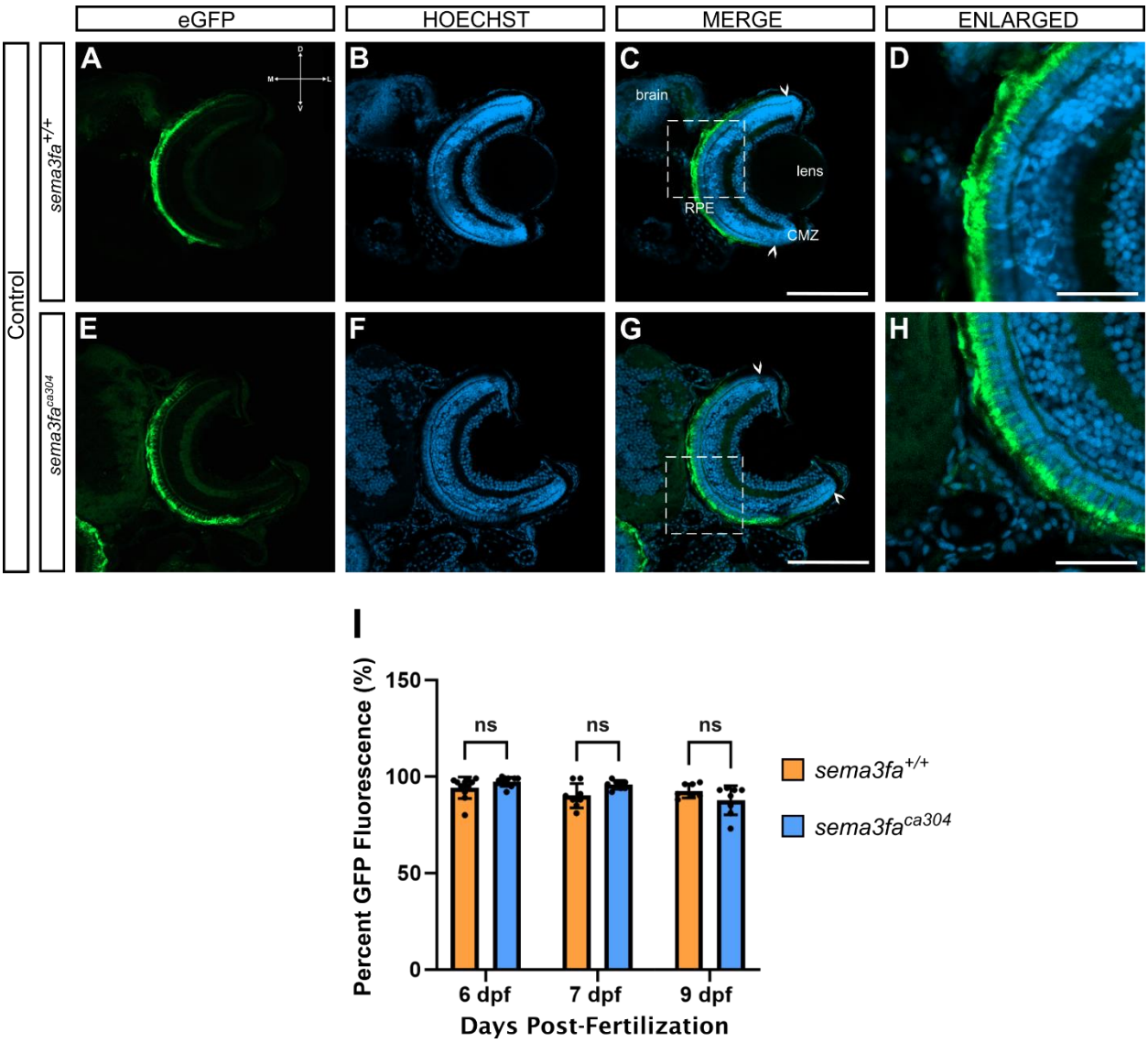

Figure 3.1 Loss of Sema3fa does not appear to impact RPE coverage of the eye over normal larval development.

Confocal images of transverse cryosections of uninjured (control) *sema3fa*$^{+/+}$ (A to D) and *sema3fa*^{ca304} (E to H) *Tg(rpe65a:NTR-EGFP)* retinas at 8 dpf with chevrons indicating the observed GFP+ RPE borders. In this transgenic, GFP (green) labels the RPE at the back of the eye. D and H show an enlargement of the boxed areas in C and G. Merge scale bar denotes 100 µm. Enlarged scale bar denotes 30 µm. Graph showing the quantitation of RPE coverage measured as

the normalized RPE-associated GFP fluorescence **i**n transverse retinal cryosections of control (non MTZ-treated) *sema3fa*$^{+/+}$ and *sema3fa*^{ca304} *Tg(rpe65a:NTR-EGFP)* larvae. Measurements were made at 6 dpf (0 dpr) to 9 dpf (3 dpr) (I). Both *sema3fa*$^{+/+}$ and *sema3fa*^{ca304} fish displayed a virtually intact RPE layer with coverage close to 100%, with no significant difference across the two genotypes at any of the time points. Data is pooled data from N=3 independent experiments. Each point represents an average of three retinal sections for an individual embryo (n=7 to 11 embryos/time point and per genotype). Data show the mean and standard deviation. Statistical significance was tested by using Mann-Whitney U tests.

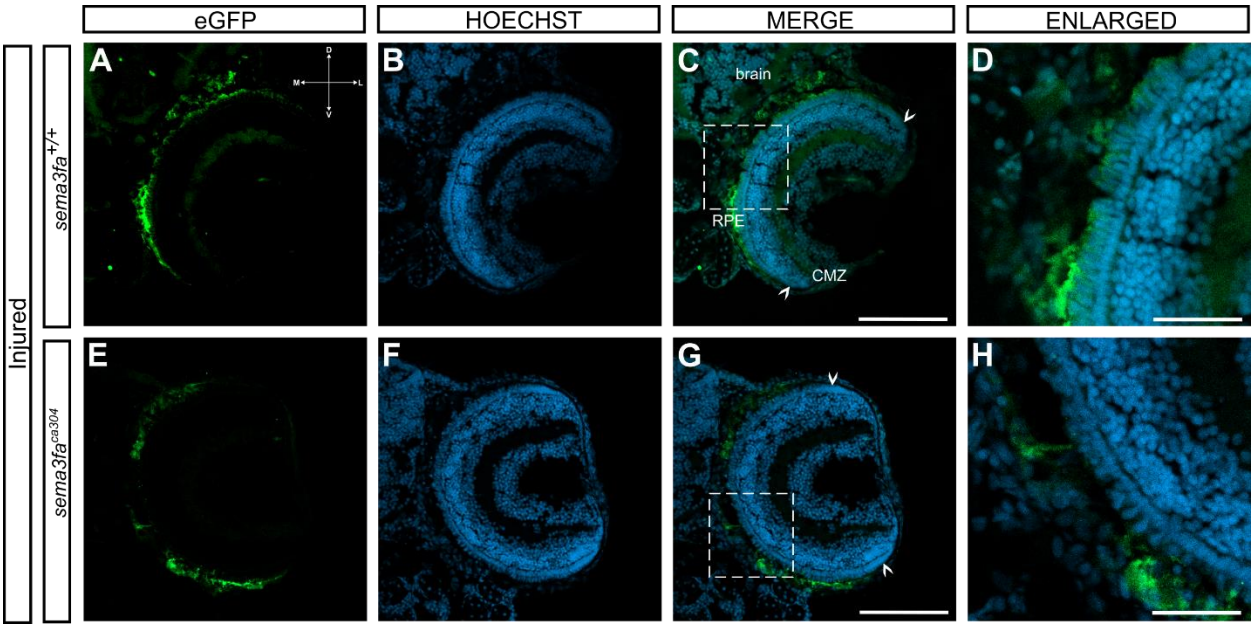

Figure 3.2 The extent of MTZ-induced RPE injury at 2 dpr appears to be similar in WT and sema3fa mutant larva.

Representative confocal images of transverse cryosections of 2 dpr MTZ-treated *sema3fa*$^{+/+}$ (A to D) and *sema3fa*^{ca304} (E to H) *Tg(rpe65a:NTR-GFP)* retinas, with chevrons indicating the observed GFP+ RPE borders at the edge of the ciliary marginal zone (CMZ). Gaps in the GFP fluorescence (green) are observed in both genotypes. Merge with Hoechst label shown (C, G). D and H show an enlargement of the boxed areas in C and G. Merge scale bar denotes 100 µm. Enlarged scale bar denotes 30 µm.

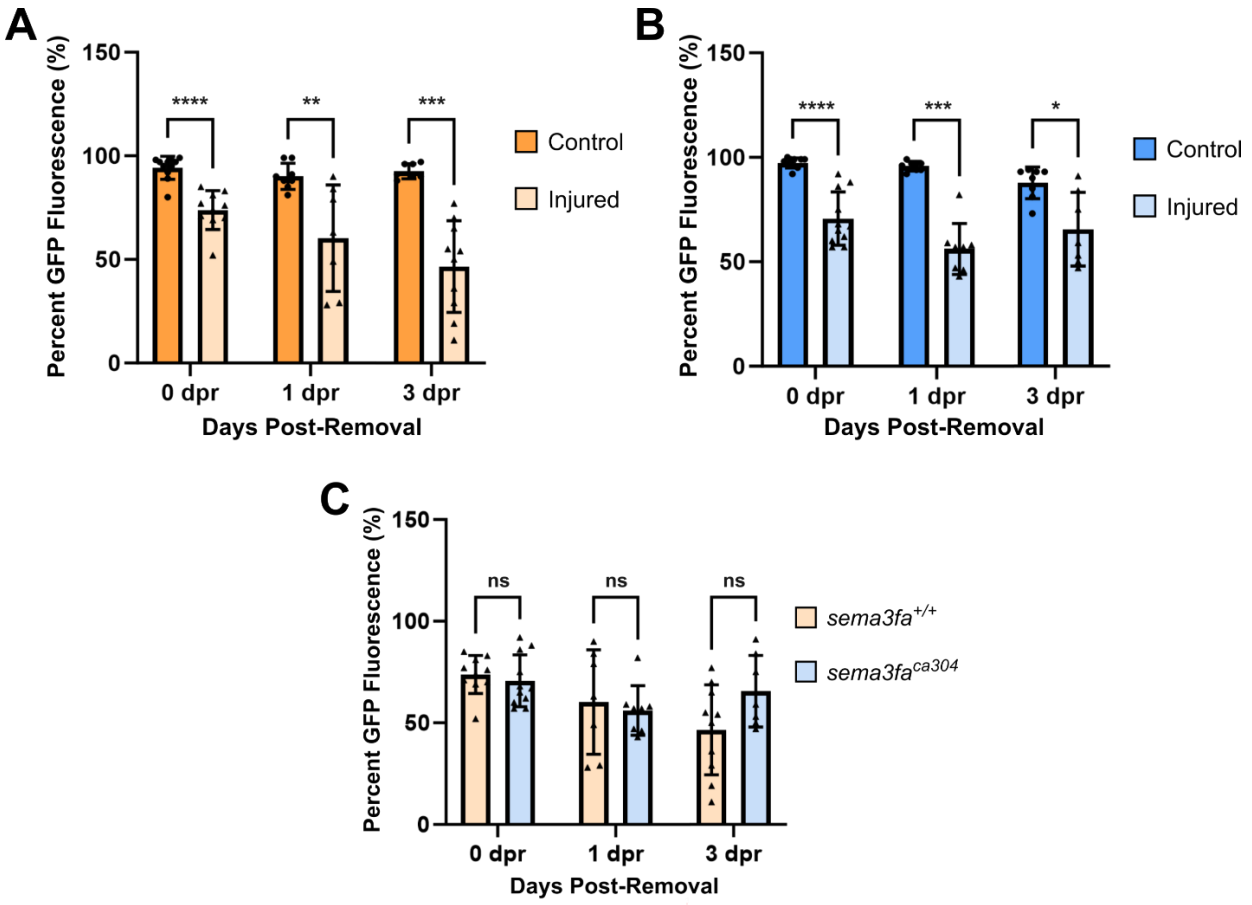

Figure 3.3 The extent and time course of MTZ-induced RPE injury appear to be similar in WT and sema3fa mutant larvae.

Normalized GFP+ RPE coverage in *sema3fa*$^{+/+}$ and *sema3fa*^{ca304} larvae on a *Tg(rpe65a:NTR-EGFP)* background at 0 dpr (6 dpf) to 3 dpr (9 dpf). For three retinal sections per embryo, the length of GFP+ RPE was measured and presented as a percentage of the total length of the GFP+ RPE (as per **Figure 2.3**). Each dot represents the average of values for the three sections per larva. The graph shows pooled data (n=7 to 11 embryos; N=3 independent experiments). Note that the control data is the same as represented in **Figure 3.1**. The GFP+ RPE coverage is significantly reduced in the MTZ-treated (injured) larvae as compared to control uninjured larvae of both genotypes at 0, 1, and 3 dpr (A, B). There was no statistically significant difference in the GFP+ RPE coverage in the MTZ-treated (injured) larvae between the two genotypes at 0, 1, and 3 dpr (C). These data suggest that the loss of *sema3fa* has no effect on the extent of RPE injury. Data show the mean and standard deviation. Significance was tested by using Mann-Whitney U tests. * $p \leq 0.05$ ** $p < 0.005$ *** $p < 0.0005$ **** $p < 0.0001$.

3.2.3 Loss of Sema3fa does not appear to impact the survival of developing RPE cells

To verify that the MTZ treatment induced apoptosis of RPE cells, and to determine if the extent of apoptosis was similar with and without Sema3fa, I counted dying cells over the time course of RPE injury in WT and *sema3fa* mutant retinas. Previously, it was shown that RPE cells in WT larvae on a *Tg(rpe65a:NTR-EGFP)* background undergo peak apoptosis, as measured by TUNEL staining, by 0 dpr after MTZ-mediated RPE injury (Hanovice et al., 2019). To identify dying cells I performed immunostaining for activated Caspase-3 (aCsp3) on central retinal sections. Caspase-3 is the most important of the effector ("executioner") subclass of caspases and upon activation, it signals the final pathway in the intrinsic apoptotic cascade (Cohen, 1997; Ponder & Boise, 2019). First, I compared the number of activated caspase-3 positive cells in WT and *sema3fa* mutant larvae on a *Tg(rpe65a:NTR-EGFP)* background at 0 dpr to 3 dpr to observe if loss of Sema3fa caused any difference in the apoptosis that occurs normally during development (**Figure 3.4**). I counted in a blinded manner the number of aCsp3-positive cells per section for three transverse, central retinal sections per larva. aCsp3+ cells were identified as rounded (crenated) reddish-orange fluorescent cells that were Hoechst+ and located in the GFP+ RPE layer (**Figure 3.4J**; arrowhead). To ensure that even if the aCsp3 count was zero for the RPE of a given retinal section the immunohistochemistry was successful, apoptotic cells were confirmed to be present in the adjacent olfactory epithelium and/or jaw (**Figure 3.4J**; arrow). These data (**Figure 3.4U**) revealed that the loss of Sema3fa appeared to not significantly impact the normal low levels of RPE apoptosis seen in developing WT larvae. As Sema3fa loss on its own does not appear to impact RPE cell survival, the non-MTZ treated fish could reasonably be used as controls for the MTZ-treated animals.

3.2.4 Loss of Sema3fa appears to delay and increase RPE apoptosis after MTZ-induced injury

I next assessed the number of aCsp3-positive cells in the RPE after NTR-MTZ-mediated injury to identify if loss of Sema3fa impacts the numbers of apoptotic RPE cells after injury. I applied 10 mM MTZ for 24 hours between 5 and 6 dpf and cryosectioned transverse sections of larval retinas at 0 dpr, 1 dpr and 3 dpr. I then conducted immunohistochemistry against aCsp3 and imaged and counted cells in the sections in a double blinded fashion (raw counts are found in the **Appendix**). Qualitatively, in both genotypes I observed decreased GFP+ RPE expression, confirming that the RPE was damaged by the MTZ treatment (**Figure 3.5**). Of note, aCsp3-positive cells in the RPE resided in regions of dim GFP expression, likely because cells undergoing apoptosis would show reduced expression of differentiated marker genes, including *rpe65a*, whose promoter was used to drive GFP expression. RPE cells that had died and were cleared would not have been counted in my analysis (**Figure 3.5E; J; O; T**). In certain sections, there were regions of bright orange fluorescence (**Figure 3.5K; N; O**), likely reflecting the fluorescence of eye-attached iridophores. Iridophores are pigment cells that act as multilayered guanine-based crystal reflectors that increase optical functionality in the zebrafish eye and are external to the retina and RPE, but at 4 dpr can be sufficiently dense to impair fluorescence microscopy due to their reflective properties (Avanesov & Malicki, 2010; Gur et al., 2018). Since I found the iridiophore reflective layer was external to the GFP fluorescing RPE cells, I was able to readily identify aCsp3+ cells within the RPE cell layer. Quantifying aCsp3-positive cells in WT larvae revealed a statistically significant increase in apoptotic cells in the MTZ-mediated injured RPE as compared to control, which began at 1 dpr and was sustained through 3 dpr (**Figure 3.6A**). The *sema3fa* mutants, however, did not appear to show a statistically significant increase in the number of apoptotic cells

in the RPE of injured larvae as compared to their controls until 3 dpr (**Figure 3.6B**). Potentially, these data suggest a delayed onset in RPE-specific apoptosis in the absence of Sema3fa. When I directly compared the number of apoptotic cells in the RPE layer of mutants as compared to their WT counterparts (**Figure 3.6C**), the mutants appeared to show significantly more apoptotic RPE cells at 3 dpr, but not at earlier time points. These data potentially point to delayed RPE apoptosis in the mutants and argue against a role for Sema3fa in promoting RPE survival.

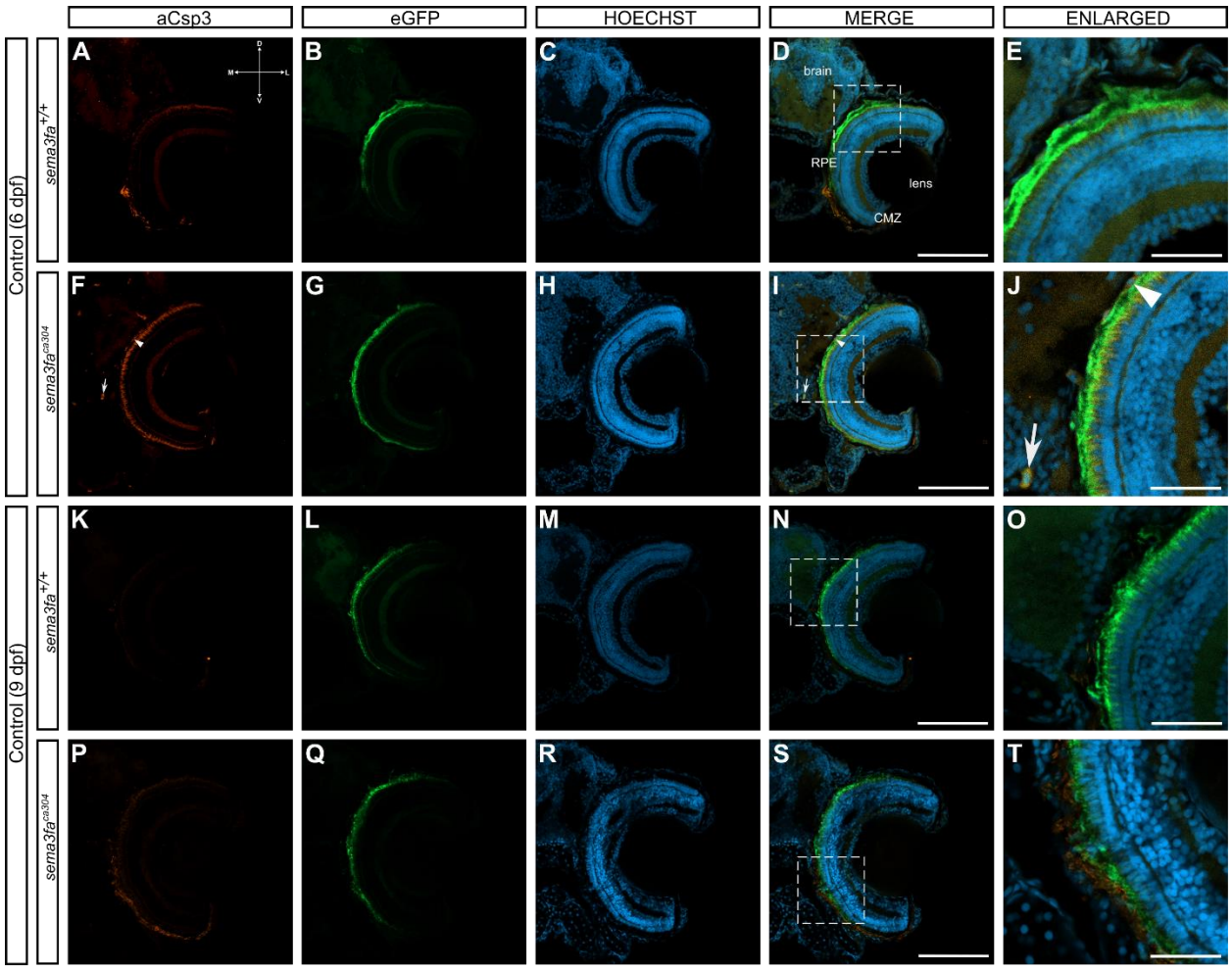
aCsp3
eGFP
HOECHST
MERGE
ENLARGED
Control (6 dpf)
Control (9 dpf)
sema3fa+/+
sema3faca304
A
B
C
D
E
F
G
H
I
J
K
L
M
N
O
P
Q
R
S
T
brain
RPE
lens
CMZ

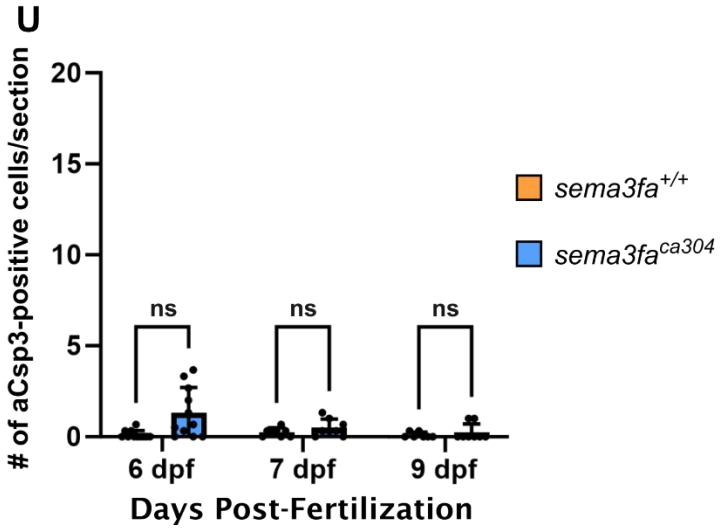
U
# of aCsp3-positive cells/section
20
15
10
5
0
ns
ns
ns
6 dpf
7 dpf
9 dpf
Days Post-Fertilization
sema3fa+/+
sema3faca304

Figure 3.4 Loss of Sema3fa does not appear to impact larval RPE survival.

Confocal images of activated Caspase-3 (aCsp3) immunolabeling of transverse cryosections of uninjured (control) 6 dpf *sema3fa*$^{+/+}$ (A to E) and *sema3fa*^{ca304} (F to J), and 9 dpf *sema3fa*$^{+/+}$ (K to O) and *sema3fa*^{ca304} (P to T) *Tg(rpe65a:NTR-EGFP)* retinas. J shows a positive aCsp3 cell in the jaw (arrow) and an example of a positive aCsp3 cell in the RPE (arrowhead). E, J, O, and T show enlargements of the respective boxed areas shown in D, I, N, and S. Merge scale bar denotes 100 µm. Enlarged scale bar denotes 30 µm. Apoptosis in the RPE, as quantified by counts of active Caspase 3 (aCsp3)-positive cells in the RPE layer in transverse retinal cryosections of uninjured *sema3fa*$^{+/+}$ and *sema3fa*^{ca304} larva on a *Tg(rpe65a:NTR-EGFP)* background from 6 dpf (0 dpr) to 9 dpf (3 dpr) (C). Note, these retinas serve as the controls for the MTZ treatments, whose data are shown in **Figure 3.6**. WT and *sema3fa*^{ca304} larvae display low numbers of apoptotic RPE cells from 6-9 dpf, with no significant difference between the two genotypes. The graph shows pooled data (n=7 to 11; N=3 independent experiments), with each point representing an average of aCsp3 counts from three retinal sections for an individual embryo. Data show the mean and standard deviation. Significance was tested by using Mann-Whitney U tests.

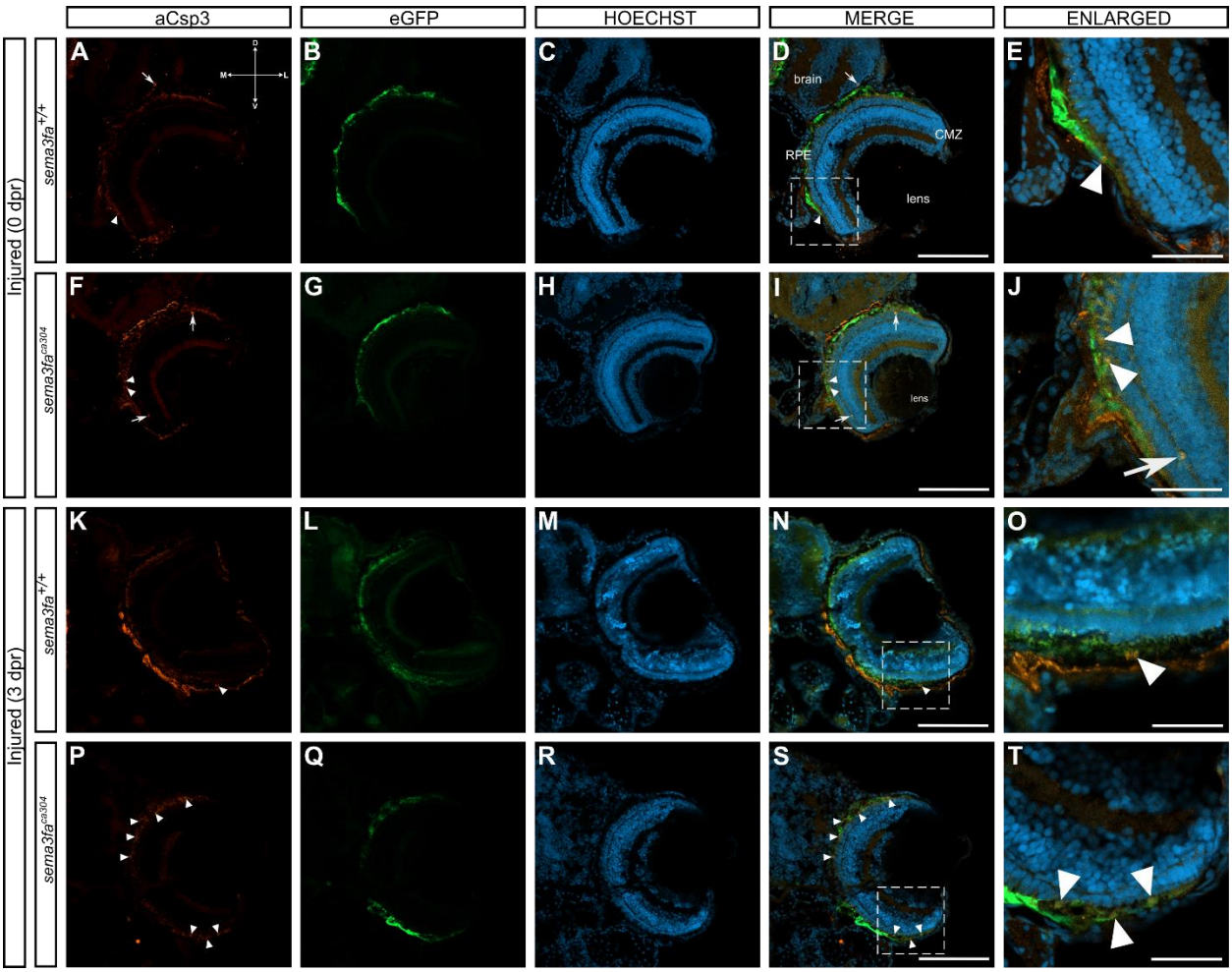

Figure 3.5 sema3fa mutants may show a delay and increase in RPE apoptosis after MTZ-induced RPE injury as compared to WT larvae.

Confocal images of transverse cryosections of 0 dpr *sema3fa*$^{+/+}$ (A to E) and *sema3fa*^{ca304} (F to J), and 3 dpr *sema3fa*$^{+/+}$ (K to O) and *sema3fa*^{ca304} (P to T) *Tg(rpe65a:NTR-GFP)* retinas after MTZ-treatment (injured). Arrowheads indicate activated caspase 3 (aCsp3)-positive cells in the RPE that are undergoing the process of apoptosis. Arrow in J shows aCsp3-positive cell within the outer nuclear layer (ONL). E, J, O, and T show an enlargement of the boxed areas in D, I, N, and S. Note only aCsp3+ cells located in the eGFP+ RPE layer were counted for the graphs in **Figure 3.6**. Merge scale bar denotes 100 µm. Enlarged scale bar denotes 30 µm.

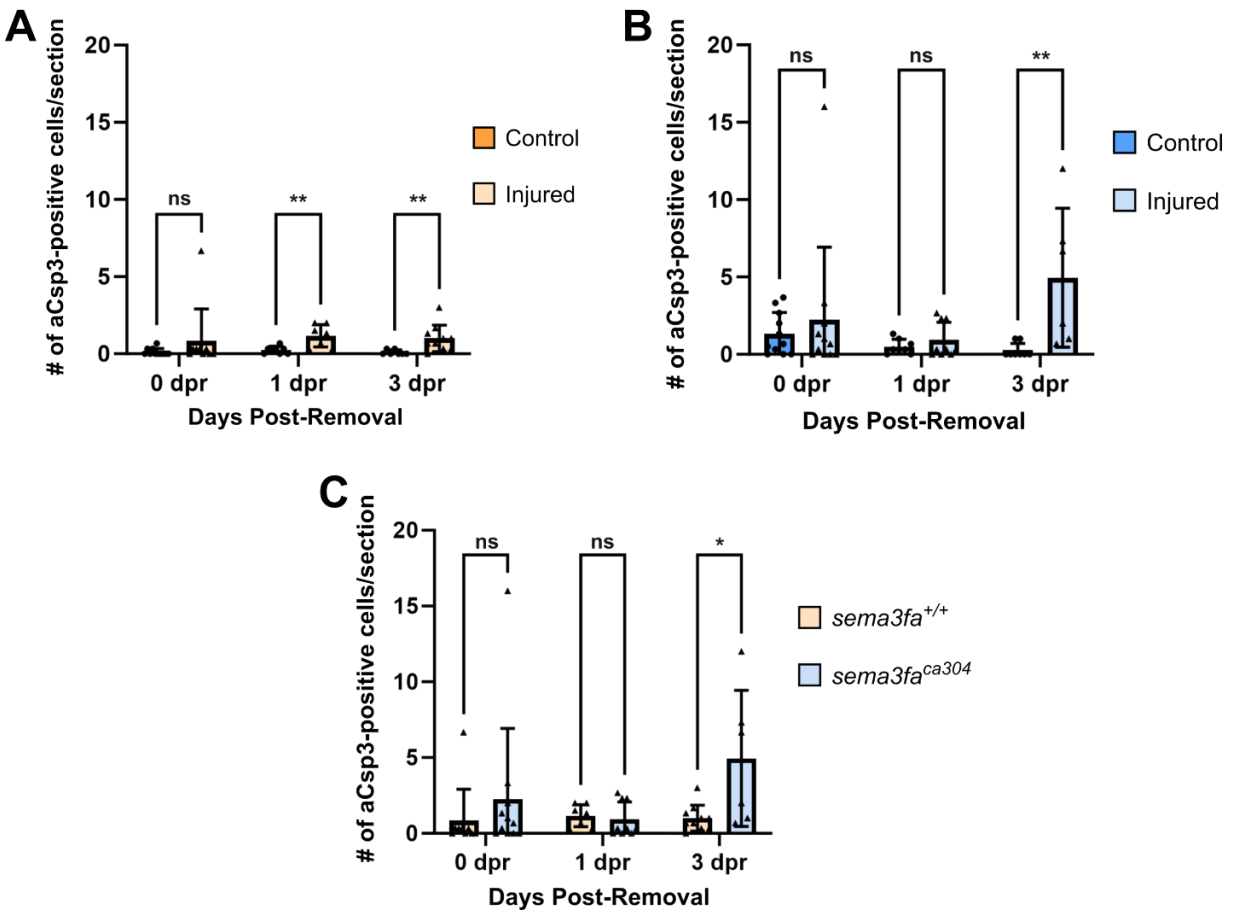

Figure 3.6 sema3fa mutants appear to show delayed and increased apoptosis after MTZ-induced RPE injury as compared to WT larvae.

Quantitation of cell death through counts of active Caspase 3 (aCsp3)-positive cells in the presumptive RPE layer in transverse retinal cryosections of *sema3fa*$^{+/+}$ (A) and *sema3fa*^{ca304} (B) larvae on a *Tg(rpe65a:NTR-EGFP)* background from 0 dpr (6 dpf) to 3 dpr (9 dpf). *sema3fa*$^{+/+}$ injured larvae show a statistically significant increase in apoptotic RPE cells by 1 dpr, which persists at 3 dpr (A). *sema3fa*^{ca304} injured RPE may display delayed apoptosis post-injury, with a statistically significant increase in apoptosis observed at 3 dpr (B). Comparison of aCsp3+ cell numbers in MTZ-injured WT and *sema3fa*^{ca304} larvae indicate a statistically significant higher numbers of apoptotic cells at 3 dpr in mutants as compared to WT. The graph shows pooled data (n=7 to 11 larvae; N=3 independent experiments), with each point representing an average of aCsp3 counts from three retinal sections for an individual embryo. Data show the mean and standard deviation. Significance was tested by using Mann-Whitney U tests. * $p \leq 0.05$ ** $p < 0.005$

3.2.5 Loss of Sema3fa does not appear to impact proliferation of the larval RPE

An indication that the RPE is regenerating post-injury is the proliferation of de-differentiated RPE cells. As a first indicator of whether the regenerative response depends on Sema3fa, I measured proliferation in the RPE layer in *sema3fa*$^{+/+}$ and *sema3fa*^{ca304} control and MTZ-treated larval retinas at 6, 8, and 10 dpf (**Figure 3.7**) by 5-ethynyl-2'-deoxyuridine (EdU) labeling of proliferating cells. EdU is a modified thymidine analogue that gets incorporated into newly synthesized DNA and fluorescently labels proliferating cells in S-phase of the cell cycle (Diermeier-Daucher et al., 2009). I fixed larvae after exposing them to a 4 hour, 400 µM EdU bath. I then conducted a Click-iT^{TM} EdU reaction on transverse retinal cryosections (Diermeier-Daucher et al., 2009). Labeling of progenitors in the ciliary marginal zone (CMZ), located at the periphery of the retina, provided a useful positive control to ensure the Click-iT^{TM} reaction was successful. The CMZ is a stem cell niche where retinal stem cells reside and divide asymmetrically (Wan et al., 2016). In both WT and *sema3fa* mutant retinas only a handful of RPE+ cells appeared to be EdU positive over the 6-10 dpf larval period (**Figure 3.7**). I counted the number of EdU-positive cells in the RPE for three retinal sections per larva (n=7 to 11 embryos per timepoint; data pooled from N=3 independent experimental replicates) (**Figure 3.7**). I found no statistically significant difference in the numbers of EdU+ RPE cells between WT and *sema3fa* mutant genotypes that were not injured, with the average number of EdU-positive cells being less than one cell per section (**Figure 3.7U**). Similar results were found previously with BrdU labeling of *Tg(rpe65a:NTR-EGFP)* 6-10 dpf RPE; at 6 dpf, the average number of EdU-positive cells was <1 cell per section, whereas at 8 and 10 dpf the average number of EdU-positive cells was zero (Hanovice et al., 2019). The low numbers reflect the fact that the RPE should be fully established by these timepoints, so that in the absence of injury, no proliferation is expected (Moreno-Marmol et al., 2018).

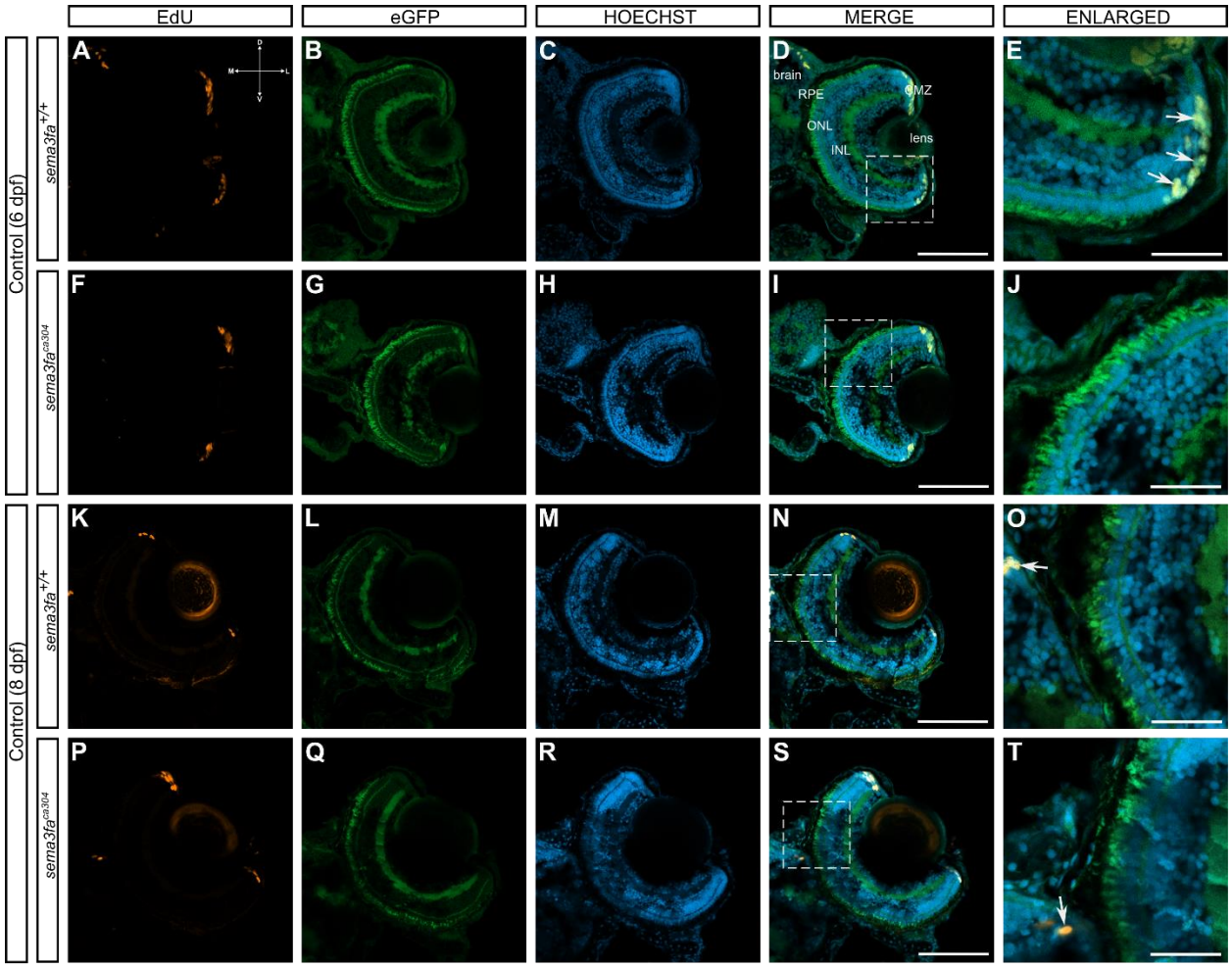
EdU
eGFP
HOECHST
MERGE
ENLARGED
Control (6 dpf)
Control (8 dpf)
sema3fa+/+
sema3faca304
A
B
C
D
E
F
G
H
I
J
K
L
M
N
O
P
Q
R
S
T
brain
RPE
CMZ
ONL
INL
lens

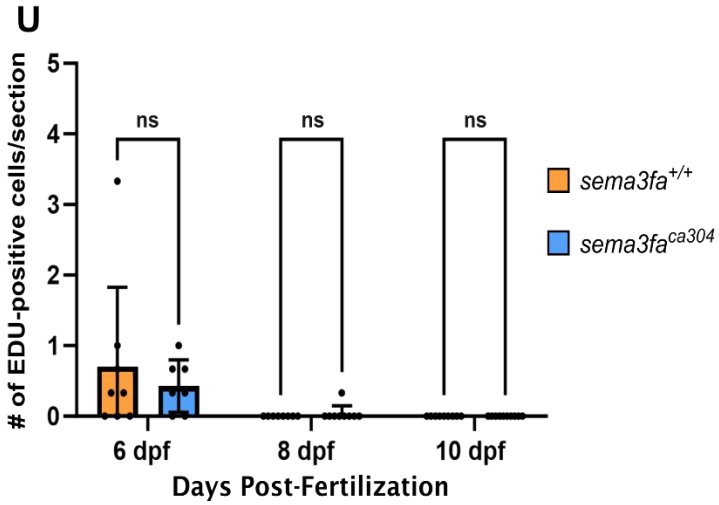
U
# of EDU-positive cells/section
0
1
2
3
4
5
ns
ns
ns
6 dpf
8 dpf
10 dpf
Days Post-Fertilization
sema3fa+/+
sema3faca304

Figure 3.7 Loss of Sema3fa does not appear to impact proliferation of the larval RPE.

Confocal images of transverse retinal cryosections of uninjured (control) *Tg(rpe65a:NTR-EGFP)* 6 dpf *sema3fa*$^{+/+}$ (A to E) and *sema3fa*^{ca304} (F to J), and 8 dpf *sema3fa*$^{+/+}$ (K to O) and *sema3fa*^{ca304} (P to T) larvae. Arrows indicate EdU-positive cells, and E shows EdU+ proliferating progenitors in the ciliary marginal zone (CMZ). E, J, O, and T show enlarged representations of the boxed areas in D, I, N, and S, respectively. Merge scale bar denotes 100 μm. Enlarged scale bar denotes 30 μm. Quantitation of proliferation through counts of EdU-positive cells in the RPE layer of transverse retinal cryosections of uninjured *sema3fa*$^{+/+}$ and *sema3fa*^{ca304} larva on a *Tg(rpe65a:NTR-EGFP)* background from 6 dpf (0 dpr) to 10 dpf (4 dpr) (C). Note, these retinas serve as the controls for the MTZ treatments. *sema3fa*$^{+/+}$ and *sema3fa*^{ca304} larvae display low numbers of proliferative RPE cells with no statistically significant difference seen between the two genotypes. The graph shows pooled data (n=7 to 11 larvae; N=3 independent experiments), with each point representing the average of EdU counts from three retinal sections for an individual larva. Data show the mean and standard deviation. Statistical significance was tested by using Mann-Whitney U tests.

3.2.6 Loss of Sema3fa may produce an earlier increase in proliferation in the RPE than seen in WT following MTZ-induced injury

I next asked if Sema3fa regulates the proliferative response post RPE injury. I bathed transgenic larvae in 10 mM MTZ for 24 hours from 5 to 6 dpf and allowed the fish to heal after removal from the MTZ. I then performed EdU labeling as described in Section **3.2.5** on transverse cryosections of the larvae at 0, 2, and 4 dpr. EdU-positive cells within the CMZ acted as internal positive controls. Note that the control data for WT and *sema3fa* mutant RPE was introduced above in Section **3.2.5**. Beginning from 0 dpr, both injured genotypes had EdU-positive cells in the RPE (**Figure 3.8A-J**) that were also present at 2 dpr (**Figure 3.8K-T**); arrowheads show RPE EdU-positive cells, while arrows denote EdU-positive cells in the ONL. The EdU-positive RPE cells were counted in a blinded fashion (**Figure 3.9**). Comparing WT and *sema3fa* mutant control and injured sections revealed for both genotypes a statistically significant increase in EdU-positive cells after injury that was present only at 2 dpr (**Figure 3.9A; B**), as was described previously (Hanovice et al., 2019). In comparing the WT and mutant injured larval data from 0 to 4 dpr, there are statistically significantly more EdU+ cells at 0 dpr in mutants as compared to WT, though by 2 dpr this difference seemed to have disappeared (**Figure 3.9C**). The early increase in mutant proliferation suggests that the loss of Sema3fa may allow for a more robust early proliferative response after MTZ-mediated injury.

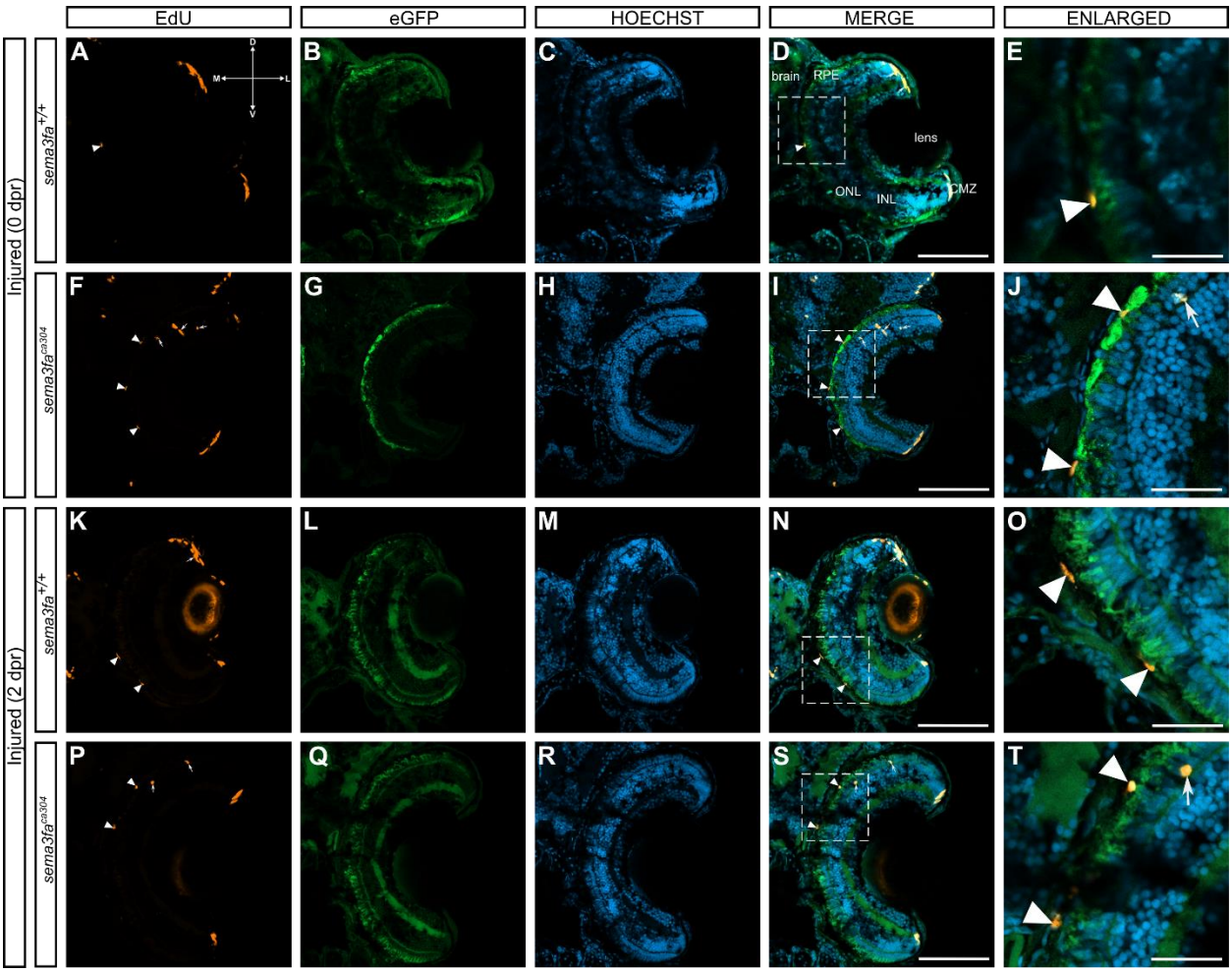

Figure 3.8 sema3fa mutants seem to show an earlier increase in proliferation after MTZ-induced RPE injury as compared to WT larvae.

Confocal images of transverse retinal cryosections of MTZ-treated (injured) *Tg(rpe65a:NTR-GFP)* in 0 dpr *sema3fa*$^{+/+}$ (A to E) and *sema3fa*^{ca304} (F to J), and in 2 dpr *sema3fa*$^{+/+}$ (K to O) and *sema3fa*^{ca304} (P to T) larvae. Arrowheads indicate EdU-positive cells in the RPE. Arrows in J and T shows EdU-positive cell within the ONL. E, J, O, and T are enlargements of the boxed areas in D, I, N, and S, respectively. Merge scale bar denotes 100 µm. Enlarged scale bar denotes 30 µm.

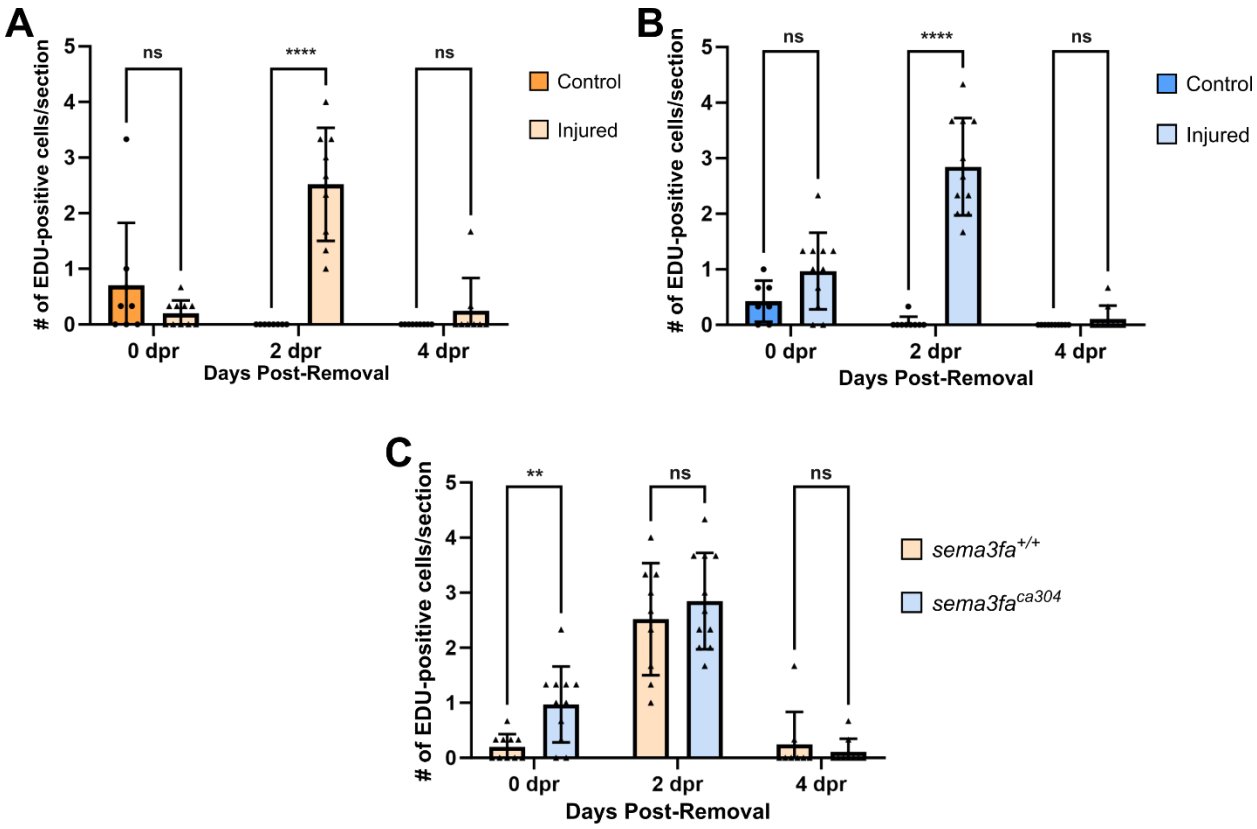

Figure 3.9 RPE proliferation post MTZ-induced RPE injury appears to be similar in WT and sema3fa mutant larvae, with potentially a more robust early response in mutants vs. WT.

Quantitation of RPE proliferation measured through counts of EdU-positive cells in the RPE layer of transverse retinal cryosections of *sema3fa*$^{+/+}$ (A) and *sema3fa*^{ca304} (B) larvae on a *Tg(rpe65a:NTR-EGFP)* background from 0 dpr (6 dpf) to 4 dpr (10 dpf). For both WT and mutants, a statistically significant increase in EdU-positive RPE cells of injured vs. control occurs at 2 dpr (A, B). When the proliferative response for injured WT RPE was compared to that of the mutant, statistically significantly more EdU+ cells were observed in the injured mutant larvae at 0 dpr, but this difference appeared to disappear by 2 dpr. The graph shows pooled data (n=7 to 11 larvae; N=3 independent experiments), with each point representing the average number of EdU-positive cells in the RPE layer from three retinal sections for an individual embryo. Data show the mean and standard deviation. Statistical significance was tested by using Mann-Whitney U tests. ** $p < 0.005$ **** $p < 0.0001$.

3.2.7 Some proliferation of cells in the ONL after MTZ-mediated RPE injury that may be stimulated by Sema3fa loss

When counting RPE+ EdU cells, I occasionally observed EdU+ cells in the inner and outer nuclear layers of the neural retina. Thus, I quantified proliferation in the neural retina after MTZ-mediated RPE injury, using the same sections I had used to quantify RPE proliferation (**Figure 3.7-Figure 3.9**), to observe if the loss of Sema3fa affected the proliferative response of the underlying photoreceptors. First, I quantified the number of EdU-positive cells in the ONL, which contains the cell bodies and outer segments of photoreceptors and resides between the RPE and the outer plexiform layer (OPL). Likely, proliferating cells in the ONL are photoreceptor progenitors that replace photoreceptors lost due to RPE ablation and subsequent loss of support to photoreceptor outer segments (Gardiner et al., 2016; Hanovice et al., 2019). Control WT and *sema3fa* mutants were not obviously different in their numbers of proliferating cells in the ONL over larval development (**Figure 3.10A**). In the MTZ-injuries, much like what I saw for the RPE proliferation, proliferation in the ONL seemed to peak at 2 dpr in both WT and mutant larvae (**Figure 3.10B; C**). When I directly compared proliferation in the ONL in injured *sema3fa* WT and mutants, the mutants displayed statistically significantly more proliferating cells at the peak of proliferation at 2 dpr, though this difference did not appear to be present at 4 dpr (**Figure 3.10D**).

Finally, I quantified the number of EdU-positive cells located in the inner nuclear layer (INL). These cells would likely reflect proliferating Müller glia (Webster et al., 2019). Control WT and *sema3fa* mutants did not exhibit statistically different numbers of proliferating cells in the INL over larval development (**Figure 3.11A**). After injury, the level of proliferation peaked at 2 dpr for the MTZ-treated larvae of both genotypes with respect to their corresponding controls (**Figure 3.11B; C**), with proliferation still significantly upregulated in WT at 4 dpr, but not in the mutants.

There seemed to be no statistically significant difference in the numbers of proliferating INL cells, however, between the WT and *sema3fa* mutants at any timepoint post-injury (**Figure 3.11D**).

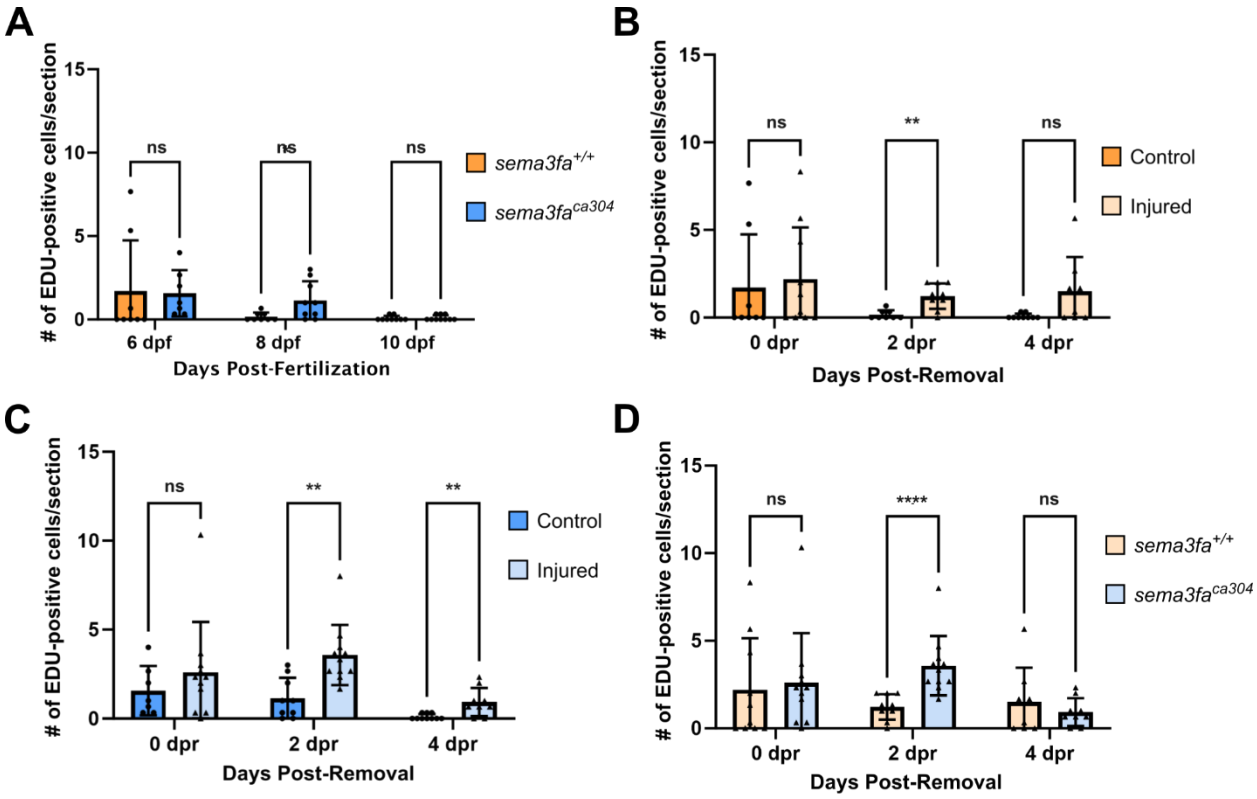

Figure 3.10 Loss of Sema3fa may impact the numbers of proliferative cells in the ONL after MTZ-treated RPE injury.

Proliferation in the ONL, as quantified through counts of EdU-positive cells in the ONL layer of transverse retinal cryosections of uninjured WT and mutants (A), *sema3fa*$^{+/+}$ injured (B), *sema3fa*^{ca304} injured (C), and WT and mutant injured (D) larvae on a *Tg(rpe65a:*NTR-EGFP) background from 0 dpr (6 dpf) to 4 dpr (10 dpf). Both *sema3fa*$^{+/+}$ and *sema3fa*^{ca304} display a small number of proliferative rod progenitors, which is not statistically significant different at any time point post-injury (A). Note, these retinas serve as the controls for the MTZ treatments. MTZ treatment increases the number of EdU-positive cells in the ONL to a statistically significant level in both genotypes at 2 dpr, but only in *sema3fa*^{ca304} at 4 dpr (B, C). Comparison of the number of EdU-positive cells in injured WT vs. mutant ONL shows statistically significantly more cells in the injured mutant vs. WT larvae at 2 dpr that apparently disappears by 4 dpr (D). The graphs show pooled data (n=7 to 11 larvae; N=3 independent experiments), with each point representing an average of EdU counts in the RPE from three retinal sections for an individual embryo. Data show the mean and standard deviation. Statistical significance was tested by using Mann-Whitney U tests. * $p \leq 0.05$ ** $p < 0.005$ **** $p < 0.0001$.

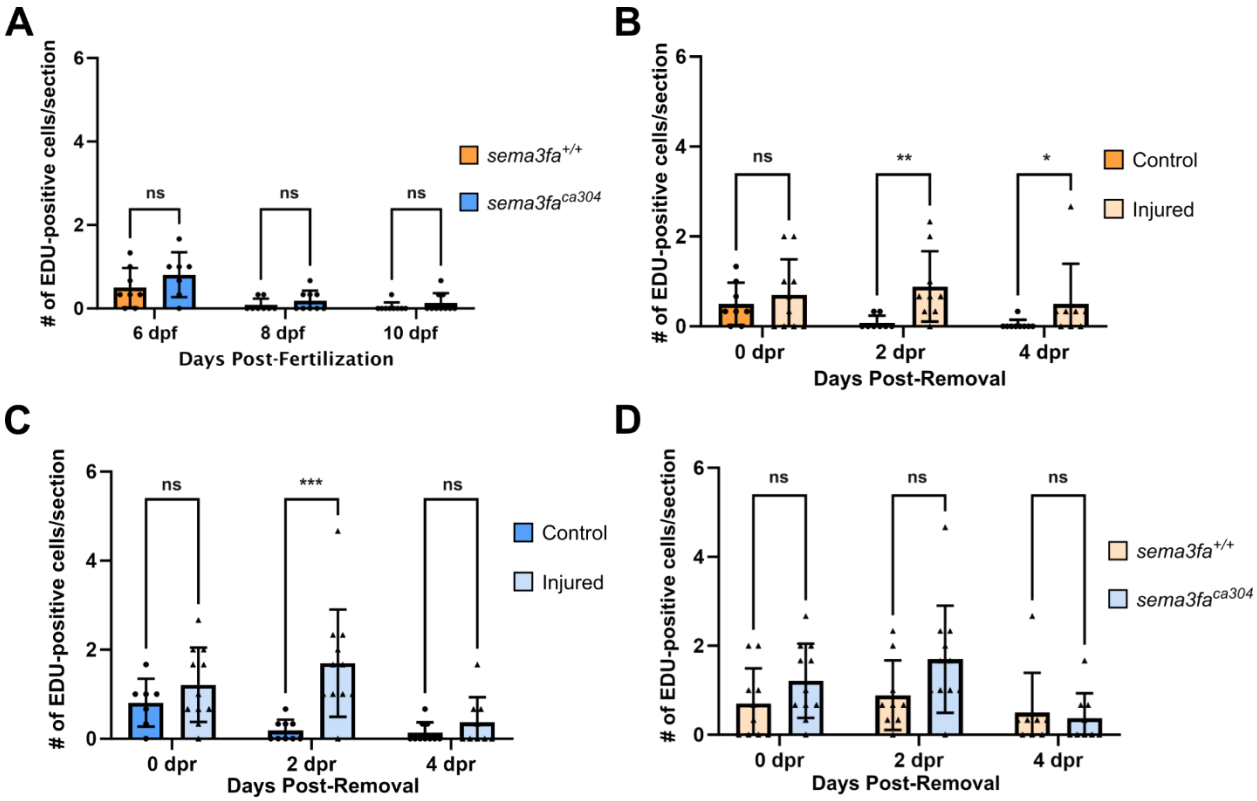

Figure 3.11 Loss of Sema3fa does not appear to impact proliferation of cells in the INL over larval development nor after MTZ-induced RPE injury.

Proliferation in the INL, as quantified through counts of EdU-positive cells in the INL layer of transverse cryosections of uninjured WT and mutant (A), *sema3fa*$^{+/+}$ injured (B), *sema3fa*^{ca304} injured (C), and WT and mutant injured (D) larvae on a *Tg(rpe65a:*NTR-EGFP) background from 0 dpr (6 dpf) to 4 dpr (10 dpf). Only a small number of EdU+ cells are present in the *sema3fa*$^{+/+}$ and *sema3fa*^{ca304} INL, with no significant difference between the two genotypes in the uninjured condition (A). Note, these retinas serve as the controls for the MTZ treatments. A significant increase in proliferation is observed in the injured WT larvae at 2 and 4 dpr (B), but only at 2 dpr for the mutant larvae (C). No significant difference in Edu+ cell counts in the INL is observed between the two genotypes (D). The graphs show pooled data (n=7 to 11 larvae; N=3 independent experiments), with each point representing an average of EdU counts in the INL from three retinal sections for an individual larva. Data show the mean and standard deviation. Statistical significance was tested by using Mann-Whiney U tests. * $p \leq 0.05$ ** $p < 0.005$ *** $p < 0.0005$.

3.3 Discussion

In addition to their role as axon guidance molecules, the functions of Sema3s in vertebrate biology are ever expanding (Alto & Terman, 2017). Sema3f's role as a potential anti-angiogenic molecule in the zebrafish retina has been elucidated, and Sema3f is expressed in the outer retina and RPE continuing into adulthood in zebrafish and mouse (Buehler et al., 2013; Callander et al., 2007; Halabi et al., 2021; Hehr et al., 2022; Sun et al., 2017). This RPE expression led me to explore Sema3fa's possible role in RPE regeneration in zebrafish (Hanovice et al., 2019). By using the transgenic MTZ-NTR injury model, to cause RPE-specific damage after timed application of 10 μM MTZ, I was able to compare the extent of RPE injury, apoptosis, and subsequent proliferation in both WT and *sema3fa* mutant larvae. My findings suggest that Sema3fa has no effect on the extent of injury, however RPE apoptosis may be delayed and increased in the absence of Sema3fa. Additionally, loss of Sema3fa may result in an initial increase in proliferation in the RPE as well as increased proliferation of photoreceptor progenitors of the outer nuclear layer. Although my findings suggest that Sema3fa may impact RPE apoptosis and regenerative proliferation, further research is needed to elucidate the pathways and mechanisms involved.

3.3.1 Sema3fa does not appear to impact larval RPE development

For the regeneration experiments, I first had to determine if the loss of Sema3fa in the *sema3fa*$^{ca304/ca304}$ mutants affected the RPE development in the larval zebrafish. SEMA3F is a known inhibitor of mTORC2, which regulates cell survival and proliferation in certain tissues (Nakayama et al., 2018; Saxton & Sabatini, 2017). Although loss of Sema3fa does not seem to regulate retinal cell survival in larval zebrafish (Halabi, 2019), it was important to know whether

there was a gross difference in the RPE in mutants vs. WT that would affect the interpretation of data obtained in the injury model.

In section **3.2.1**, I quantified the extent of RPE cell loss by measuring the length of the transgenic GFP expressed by RPE cells in the *Tg(rpe65a:NTR-EGFP)* background as a marker of overall RPE health, as only healthy RPE cells appear to activate the *rpe65a* promoter (Hanovice et al., 2019). I observed that loss of Sema3fa does not appear to impact the RPE coverage of the eye over larval development, from 6 to 9 dpf (**Figure 3.1**). Overexpressing SEMA3F in human retinal endothelial cells inhibits angiogenic sprouting (Buehler et al., 2013). Thus, I might have expected that knocking out its zebrafish paralogue, *sema3fa,* would promote aberrant choroidal angiogenesis, and possibly disruption of the RPE as seen by changes in the RPE-associated eGFP signal in the *sema3fa* mutants. While the McFarlane lab reported previously that a small degree of aberrant vascularization is present in the outer retina of adult and larval *sema3fa* mutants, the loss of Sema3fa does not appear to affect the development of zebrafish embryos and eyes, including the RPE (Halabi et al., 2021). Potentially, the extent of neovascularization is minimal, or RPE breaks are rapidly repaired. A final possibility is that while the gross anatomy of the RPE and the activity of the *rpe65a* promoter is not impacted by Sema3fa loss, some more subtle aspect of RPE anatomy and/or function is disrupted. In this case, it would be of interest to further characterize the anatomy of the RPE in the absence of Sema3fa via transmission electron microscopy (TEM) that would allow a clear view of RPE cell structure (without the obstruction of the melanin pigment granules) of control RPE cells in both WT and mutants. Note that this method was used to confirm MTZ-mediated RPE injury in larval zebrafish (Hanovice et al., 2019). Additionally, future experiments could focus on a role for Sema3fa in RPE function by using newly developed methods to measure RPE phagocytosis in control and RPE injured WT and mutants (Gao et al., 2023).

Nonetheless, in non-PTU treated embryos, the RPE is fully pigmented in *sema3fa* mutant fish, suggesting that at least some RPE function is intact. Similarly, my findings suggest Sema3fa loss has no gross impact on *rpe65a* expression, a gene involved in the visual cycle (Cai et al., 2009). In summary, my findings argue that (non-MTZ-treated) mutant larvae appear to show grossly normal RPE.

In section **3.2.3**, I used aCsp3 immunohistochemistry (IHC) to ask if Sema3fa was required for RPE survival in normal larval development. Developmental apoptosis in the zebrafish retina has been well characterized up until 96 hpf, with apoptosis ceasing by 48 hpf (Cole & Ross, 2001). Losing Sema3fa appears to have no impact on the low levels of developmental apoptosis of the RPE (**Figure 3.4**), which argues against a survival role for Sema3fa; in uninjured eyes from 5 to 7 dpf in both genotypes there were essentially zero apoptotic cells (<1 cell per section; **Figure 3.4**) (Hanovice et al., 2019). Since RPE apoptosis in WT fish has not previously been characterized beyond 7 dpf, my data show that low levels of apoptosis of the RPE seem to persist until at least 9 dpf.

In summary, my data support the idea that Sema3fa does not appear to influence the survival of RPE cells in normal development.

3.3.2 Sema3fa does not appear to impact the extent or time course of MTZ-induced RPE injury

In section **3.2.2**, I quantified the extent of RPE cell loss with MTZ-induced RPE injury by measuring the length of the transgenic GFP expressed by RPE cells in the *Tg(rpe65a:NTR-EGFP)* background that was remaining after injury. I observed a qualitative (**Figure 3.2**) as well as a

quantitative (**Figure 3.3**) decrease in GFP+ RPE following MTZ-induced injury. While Sema3fa is present in the larval RPE, it does not appear to play a significant role in protecting the RPE cells from injury, in that I observed statistically significant decreases in GFP coverage, as a marker of the RPE, in both WT and mutant injured retinas as compared to their uninjured controls (**Figure 3.3A; B**). This was true of all three timepoints measured. These data suggest that the RPE is similarly sensitive to MTZ treatment in both *sema3fa* WT and mutants, and that the injuries progress over the same time course. My data, where GFP+ RPE may continue to decrease from 0 to 3 dpr in both the WT and *sema3fa* mutants, also agree with the previous characterization of the MTZ-induced RPE injury model, where the RPE shows signs of injury from 0 dpr to 6 dpr (Hanovice et al., 2019). These data suggest the re-engineered *rpe65a:NTR* line works in a similar manner to the line developed by the Gross lab.

Previous literature described a qualitative decrease in RPE-associated GFP expression post-injury in an *rpe65a:NTR* model (Hanovice et al., 2019). Here, I developed an approach to quantify the extent of injury and recovery, which will be needed if we are to use the model to compare the ability of distinct molecular pathways to impact RPE injury and regeneration. My novel approach of quantifying overall RPE health in retinal sections, by calculating the percentage of RPE that is unimpacted by injury, appears to adequately identify RPE injury. The control non-MTZ treated eyes have close to 100% RPE coverage, while the injured larvae show a statistically significant reduction in RPE coverage as compared to controls (Hanovice et al., 2019). This method utilizes the transgenic GFP coverage as a measure of RPE health, so no additional, expensive equipment (like optical coherence tomography) is required. Additionally, this method accounts for the variable size of individual zebrafish eyes that arise, as well as any non-damage related gaps in the transgenic GFP expression (like tissue tears due to cryosectioning or the break

at the optic nerve exit from the eye). However, a caveat of this approach is that identifying the peripheral boundaries of the RPE is important. While I used consistent criteria to identify the boundaries, an alternate approach would be to use the entire pigmented RPE as "total length", including the peripheral RPE that wraps around to the lens; even with PTU treatment, residual pigment remains. The peripheral RPE, however, does not express *rpe65a,* and so would increase the "eGFP-free length" value even in the absence of injury, which might not be ideal.

3.3.3 Loss of Sema3fa may result in a delay and increase in RPE apoptosis after MTZ-induced RPE injury

In section **3.2.4**, I used aCsp3 IHC to ask if Sema3fa promotes RPE survival after RPE injury. I observed a delay in apoptosis in *sema3fa* mutants, with a statistically significant change in aCsp3-positive cells over control not becoming apparent until 3 dpr; as opposed to WT fish, where statistically significantly more aCsp3 cells in injured versus controls is first seen at 1 dpr (**Figure 3.6A; B**). Additionally, I observed what appears to be more aCsp3-positive RPE cells in the injured *sema3fa* mutants than injured WT at 3 dpr. Based on these data, I suggest tentatively that the loss of Sema3fa results in a delay and increase in RPE apoptosis after MTZ-induced RPE injury. Previous literature showed that in MTZ-injured WT fish the RPE injury is rapid, with apoptosis peaking at 0 dpr, and, while apoptosis decreases significantly by 1 dpr, the levels are still significantly above those seen in uninjured controls (Hanovice et al., 2019). The initial characterization of the MTZ-mediated RPE injury model by the Gross lab did not explore RPE apoptosis beyond 1 dpr. My data with the WT injured RPE suggests cells continue to die at least up to 3 dpr (**Figure 3.6A**). The mutant data suggest delayed, but ultimately robust, apoptosis of RPE cells in the absence of Sema3fa. One possible cell autonomous explanation for more apoptosis

is that Sema3fa may normally keep low the expression of the tumour suppressor gene and apoptosis effector gene, p53, to minimize apoptosis of larval RPE. This idea is based on the observation that normally Sema3F downregulates p53 expression in mouse hippocampal neurons (Shen & White, 2001; Yang et al., 2012). I hypothesize that in the *sema3fa*^{ca304} mutant, p53 is upregulated, allowing for more p53-mediated apoptosis to occur in response to the DNA damage caused by the MTZ-NTR injury. Another possible explanation for the increase in injury-induced apoptosis in mutants may relate to the known anti-angiogenic properties of Sema3fa. Overexpression of SEMA3F in human retinal endothelial cell spheroids significantly reduces angiogenesis (Buehler et al., 2013). Further, we found previously in zebrafish *sema3fa* mutants that there is some choroidal neovascularization of the outer retina (Halabi et al., 2021). Possibly in the injured mutants, with a damaged or dying RPE, and no Sema3fa coming from the remaining RPE or outer retina, choroid vessels inappropriately invade the outer retina. The result would be exacerbated disruption of RPE cells caused by the MTZ-NTR injury, which could lead to increased apoptosis. This would be a non-cell autonomous model of Sema3fa's role in the RPE. I could test this possibility by conducting fluorescent angiographies post-injury to determine how exactly Sema3fa regulates choroid neovascularization in the context of RPE injury.

While these two explanations may account for the increase in RPE apoptosis in mutants, they would not explain why RPE apoptosis appears to occur with a delay in mutants as compared to WT. An explanation for the delay could be that Sema3fa may normally limit the immune response associated with RPE injury that could hurt RPE regeneration. For instance, increased inflammation results in delayed and increased apoptosis in RPE and colon cells (Leach et al., 2021; Prieto et al., 2020; Wang et al., 2012). *In vivo* overexpression of SEMA3F in mouse multiple sclerosis models increases recruitment of macrophages (Aigrot et al., 2022), which are important

for clearing dying cells (Klöditz & Fadeel, 2019). Given that a decrease in macrophages can lead to increased inflammation, and subsequent delays and increase in apoptosis (Prieto et al., 2020; Wang et al., 2012), I hypothesize that Sema3fa may be involved in macrophage recruitment and in *sema3fa*$^{ca304/ca304}$ retinas a decrease in macrophage recruitment could similarly lead to increased inflammation and delayed apoptosis. To address this possibility, future experiments could compare macrophage activation in the RPE in WT and *sema3fa* mutants by measuring the production of cytokines, similar to previous studies (Leach et al., 2021).

One concern I have is that in the WT fish I saw no statistically significant difference in aCsp3+ cells between control and injured at 0 dpr (**Figure 3.6A**), which is where peak apoptosis is expected (Hanovice et al., 2019). One possible explanation is that Hanovice et al. used TUNEL (terminal deoxynucleotidyl transferase-mediated dUTP nick-end labeling) rather than aCsp3 to detect dying cells. TUNEL detects apoptotic DNA cleavage, but may also detect other forms of DNA damage, whereas aCsp3 is part of the specific, irreversible final apoptotic pathway (Wu et al., 2002). Additionally, the upregulation of aCsp3 peaks slightly after the peak of TUNEL within the injured rat retina (Wu et al., 2002). So, the contrast between previous literature and my study could be due to the less specific staining of TUNEL versus aCsp3. Furthermore, I observe significant loss in the GFP signal at 0 dpr, but no significant increase in aCsp3-positive cells, this may be because dying RPE cells contract and so lose expression of *rpe65a* but do not yet express aCsp3. Alternatively, aCsp3 is likely expressed only for a small window in time during apoptosis (2-4 hours), and so I could have missed dying cells that would have been detected by TUNEL (Hanovice et al., 2019). In summary, I suggest a few possible mechanisms by which Sema3fa may impact RPE apoptosis post MTZ-mediated injury that could be studied in the future.

3.3.4 Sema3fa does not appear to have a significant impact on the RPE proliferation regeneration response

In section **3.2.6**, I describe what appears to be a similarly sized peak in RPE proliferation post-injury for WT and mutants, but with statistically more EdU-positive cells in the *sema3fa* mutant at 0 dpr (**Figure 3.9**). Previous work on the dynamics of cell proliferation following MTZ-mediated RPE injury reveals peak cell proliferation as measured by BrdU labelling between 2 and 3 dpr (Hanovice et al., 2019). My data in the new *rpe65a:NTR* fish line agrees with these findings, with both injured WT and mutant larvae exhibiting peak EdU counts at 2 dpr (**Figure 3.9A; B**). Of note, Hanovice et al. applied the BrdU bath for a full 24 hours, which would capture all cells that moved through S-phase over that day-long period. Instead, I exposed my larvae to a 4-hour EdU bath, to provide an assessment of the proliferation occurring at a specific time point post-injury. Likely, the difference in the methods explains why Hanovice et al. observed 2 to 8 BrdU-positive cells per section, whereas I observe only 1 to 4 EdU-positive cells per section. Note that I also used EdU as it is less toxic to the live larvae and there is some debate that EdU is more reproducible and sensitive than BrdU (da Silva et al., 2017). Incubation time and EdU concentration can be adjusted for future experiments to allow for more time for EdU incorporation, and therefore more EdU-positive cells for stronger statistical power.

SEMA3F decreases proliferation of human kidney cells in culture through the inhibition of the PI3K-Akt-mTOR pathway, which is known to be essential for RPE regeneration in zebrafish (Hanovice et al., 2019; Nakayama et al., 2015). According to the literature, I might have expected loss of Sema3fa to result in more cell proliferation post-injury. This, however, does not appear to be the case with my data, as at the peak of RPE proliferation at 2 dpr there seems to be no significant difference between the numbers of EdU+ RPE cells in WT and mutants (**Figure 3.9C**).

Mutants do seem to show, however, initially more numbers of proliferative RPE cells per section at 0 dpr as compared to WT (**Figure 3.9C**). These data are hard to interpret, however, in that there is no statistically significant difference in EdU+ cell numbers between the control and injured mutants at 0 dpr in **Figure 3.9B**, and there appear to be similar numbers of EdU+ cells in WT and mutant uninjured controls at 0 dpr (**Figure 3.7U**). One possible explanation is that although the *sema3fa* mutants exhibit an increased proliferative response at 0 dpr, statistical significance is not reached due to limited statistical power. However, when comparing WT and mutants in the injured condition, a more noticeable difference emerges, thus achieving statistical significance. Additional experimental replicates may resolve this issue. Note that when I did my analyses, I did not consider whether there were differences (e.g dorsal vs. ventral, peripheral vs. central) in the spatial localization of the EdU+ RPE cells in the WT and mutants after injury. Future studies could consider the location of the EdU+ RPE cells to see if certain regions of the RPE contribute more to the regenerative response, and whether these regions differ in WT vs. *sema3fa* mutants.

Of note, the Click-iT^{TM} assay appeared to eliminate the GFP fluorescence from the transgene and caused increased autofluorescence in the retinal sections. I used the autofluorescence to visualize the interdigitation between the apical RPE microvilli and the outer segments of photoreceptors. As such, I did not quantitate the extent of RPE injury in the sections I used for the EdU assays.

The kinetics of retinal regeneration largely overlap those of RPE regeneration (Hanovice et al., 2019). To observe if the dynamics of retinal regeneration were affected by the loss of Sema3fa, I counted the number of EdU+ cells both within the ONL that contains the photoreceptors and photoreceptor progenitors (**Figure 3.10**), and the INL that contains the proliferative Muller glia (**Figure 3.11**). The number of EdU+ cells in both the ONL and INL appear to peak at 2 dpr

(**Figure 3.10**; **Figure 3.11**). These data agree with the initial analysis of the *rpe65a:NTR* model by Hanovice and colleagues that found peak BrdU proliferation occurs at 2 dpr in the central retina, although they do not distinguish between proliferative cells in the ONL and INL (Hanovice et al., 2019). I observed a statistically significant increase in proliferative cells within the ONL in the mutant injured larvae as compared to WT (**Figure 3.10D**). Proliferative cells in the ONL are photoreceptor progenitors (Hernández-Núñez et al., 2021), suggesting either that more photoreceptors die in the RPE injury model in mutants, or that the response of rod progenitors to RPE injury is normally repressed by Sema3fa. As for proliferating cells in the INL, I observed no statistical significance between WT and mutants post RPE injury (**Figure 3.11D**). The only proliferating cells in the INL of 5 dpf larval and adult retinas are Müller glia (Goldman, 2014; Hernández-Núñez et al., 2021; Powell et al., 2016). Müller glia produce rod progenitors at a low rate throughout the life of the fish, and become activated in response to injury, dedifferentiate and produce neurogenic progenitors (Bernardos et al., 2007; Hoang et al., 2022). My findings suggest that although Müller glia proliferate in response to RPE injury, Sema3fa may not be involved in this response.

3.3.5 Conclusions

Zebrafish RPE cells have an intrinsic ability to regenerate following injury in an MTZ-mediated transgenic RPE injury model. My work suggests that although Sema3fa does not appear to affect the extent of the RPE injury, as measured through *rpe65a* promoter-driven GFP fluorescence, there appears to be a delayed and increased apoptotic response in the RPE in the absence of Sema3fa. A loss of Sema3fa also appears to induce an earlier RPE proliferative response

than in WT, as well as more proliferation, presumably of rod progenitors, in the ONL post-injury, although more experiments are needed to support this conclusion. I suggest that Sema3fa may influence the immune response of RPE cells following MTZ-mediated RPE injury. By contributing to our understanding of Sema3fa, and its influence on RPE injury and subsequent regeneration, I hope to provide a greater understanding of the molecular mechanisms that underlie RPE regeneration, which will hopefully allow us to treat certain retinal diseases in humans in the future.

CHAPTER FOUR: Identification of Candidate Regulators of RPE Regeneration

4.1 Introduction

With the discovery of the intrinsic ability of zebrafish to regenerate large sections of their RPE after extensive RPE injury, research has begun to determine the cellular pathways that contribute to this regenerative capacity (Hanovice et al., 2019). Certain well-known signaling pathways appear to significantly impact RPE regeneration post MTZ-mediated injury. For example, pharmacological inhibition of Wnt signaling, by promoting destruction of β-catenin, impairs the recovery of pigmentation and mature RPE cells post-injury (Hanovice et al., 2019). Additionally, pharmacological and genetic inhibition of mTOR impairs RPE regeneration post-genetic ablation, with mTOR providing a possible means by which the immune response to injury participates in RPE regeneration (Lu et al., 2022). Except for these two examples, there is a large knowledge gap in our understanding of the mechanisms involved in RPE regeneration *in vivo* (Lu et al., 2023)**.**

To identify additional molecular candidates to explore for a role in RPE regeneration, I first generated a list of ten genes that I wished to study, based on three criteria: 1) the gene must be physiologically relevant. I explored the literature to identify genes involved in cell growth and/or division, mesenchymal-to-epithelial transition, and normal RPE development and function. 2) the gene should either be present in the zebrafish eye/RPE at 5 dpf, when I induce the MTZ injury, or upregulated post-injury. I collected this information by using a combination of the online Zebrafish Information Network (ZFIN) and multiple scRNA-seq databases, including an unpublished data set from the McFarlane lab (Bradford et al., 2022; Farnsworth et al., 2021; Storey & McFarlane, Unpublished). This latter set was collected using eyes dissected from 5 dpf *sema3fa*$^{+/+}$ larvae and

the transcriptomic data was visualized by a lab member using a dimensionality-reducing technique called Uniform Manifold Approximation and Projection (UMAP) (Storey & McFarlane, Unpublished). 3) Preferably the gene would have a commercially available pharmacological inhibitor for rapid functional analysis in the future.

In this chapter, I initiate an analysis of whether my 10 genes might prove to be useful candidates to explore in the future for a functional role in RPE regeneration, by determining if each gene is expressed in the WT RPE at 5 dpf and/or is up or down regulated after MTZ-induced RPE injury. Below I introduce my list of 10 candidate genes and in the Results, I explain why each was chosen. The candidate genes known to participate in RPE cell growth and/or division include: *bmp7b* (*bone morphogenetic protein 7b*), *caska* (*calcium-/calmodulin-dependent serine protein kinase a*), *foxm1* (*forkhead box protein m1*), *msnb* (*moesin b*), *trpm7* (transient receptor potential cation channel m7), and *vrk1* (*vaccinia-related kinase /serine/threonine kinase 1*). The other cohort of candidate genes are those involved in normal RPE function or development, which I might expect to be upregulated in response to RPE injury, to help heal the lesion. These genes are *rpe65a* (*retinoid isomerohydrolase*), *col4a6* (*collagen type IV, alpha 6*), *her4.1* (*hairy-related 4, tandem duplicate 1*), and *otx2b* (*orthodenticle homeobox 2b*). I selected each of the genes in this section based on the notion that perhaps similar mechanisms to RPE development are reengaged for differentiation post-injury.

To evaluate whether the expression of each the chosen candidate genes is correlated with RPE death and/or subsequent regeneration (de-differentiation, proliferation, migration, differentiation), I generated antisense riboprobes for each gene and performed fluorescent *in situ* hybridization (FISH). Initially, I attempted RNA wholemount *in situ* hybridization but encountered two problems: 1) the pigmentation in the RPE, even if embryos were exposed to PTU prior to the

onset of pigmentation, still made it difficult to see ISH label. 2) At 5 dpf, penetration of riboprobes into the larvae was hampered, and made labeling difficult. Instead, I performed FISH on retinal sections, which both allowed the use of fluorochromes to visualize RNA expression in the RPE and outer retina with less obstruction from pigment, and meant the probe had ready access to the RPE. In the chapter, I find that the cell growth/division group, consisting of candidate genes: *bmp7b, caska, foxm1, msnb, trpm7,* and *vrk1* all seemed to show some increase in FISH label post-injury. In the second group, consisting of candidate genes involved in normal RPE development/function, *rpe65a* and *her4.1* appeared to show some increase in FISH label post-injury, whereas *col4a6* and *otx2b* appeared to remain unchanged. These data point to potential new regulatory genes and pathways to be explored in RPE regeneration.

4.2 Results

For each candidate gene, I assessed expression in the annotated RPE clusters of our 5 dpf zebrafish eye single cell RNA-sequencing (scRNA-seq) data. Note the data of an MSc student in the lab (Sanjibani Sanyal, personal communication) suggests that the various clusters contain varying subtypes including: differentiated RPE cells of the central retina, differentiating RPE cells near the retinal periphery, and newly born or naïve RPE cells of the retinal periphery. Shown below for each gene is the expression (purple) in cells of the RPE clusters. I sought to confirm the scRNAseq data, and asked if the gene was dysregulated with RPE injury, by performing FISH on both 6 dpf control and 0 dpr (6 dpf) MTZ-injured larvae on the *Tg(rpe65a:NTR-EGFP)* background. Transverse retinal cryostat sections through the eyes were used for this analysis. Note that the protocol for FISH eradicated any eGFP fluorescence in this fish line.

4.2.1 Candidate genes involved in RPE cell growth and/or division

bone morphogenetic protein 7b (*bmp7b*) is a secreted ligand that binds to various TGF-beta receptors to activate SMAD transcription factors (Dong et al., 2022). This pathway is reported to both inhibit melanogenesis of zebrafish pigment cells, including the RPE, and impact retinal function (Dong et al., 2022). Zebrafish mutants for *bmp7b* show increased melanization of the skin and eyes, decreased larval growth, and defects in phototransduction (Dong et al., 2022). Additionally, in the chick optic cup, BMP signalling converts developing neural retinal cells into RPE cells (Steinfeld et al., 2017). According to a zebrafish scRNA-seq data set of 1 to 5 dpf embryos (Farnsworth et al., 2021), there is some *bmp7b* expression in annotated RPE, and a large amount in retinal progenitors. I thought this gene may be upregulated in response to RPE injury. Finally, Bmp7b binds to type II BMP receptors (BMPR2) and there are a few potent, selective inhibitors of this receptor (Dong et al., 2022; Modukuri et al., 2023). The McFarlane scRNA-seq data suggests little or no expression of *bmp7b* mRNA by 5 dpf RPE cells (**Figure 4.1A**). In 6 dpf uninjured larvae, while FISH label for *bmp7b* was present in the INL and CMZ, little or no expression was present in the RPE (n=8/9; N= 3; **Figure 4.1C-F**). This pattern of expression is represented schematically in **Figure 4.1B**. After being exposed to 10 mM MTZ for 24 hours, 0 dpr (6 dpf) injured larvae seemed to show an increase in the FISH label within the CMZ and outermost peripheral RPE (n=6/9; N=3; **Figure 4.1G-J**). To be able to localize FISH label with respect to the CMZ and peripheral RPE, I overlaid a brightfield (BF) image on top of the fluorescent image (**Figure 4.1F'; J'**). This allowed me to localize *bmp7b* mRNA with respect to the pigmented RPE and assess any change in expression in this area post RPE injury. There appeared to be no change in the *bmp7b* expression in the central RPE. Potentially, expression increased in the CMZ (**Figure**

4.1J', arrow), a known stem cell niche within the retina, and could include a subgroup of proliferative RPE cells at the periphery of the CMZ (George et al., 2021; Reinhardt et al., 2015).

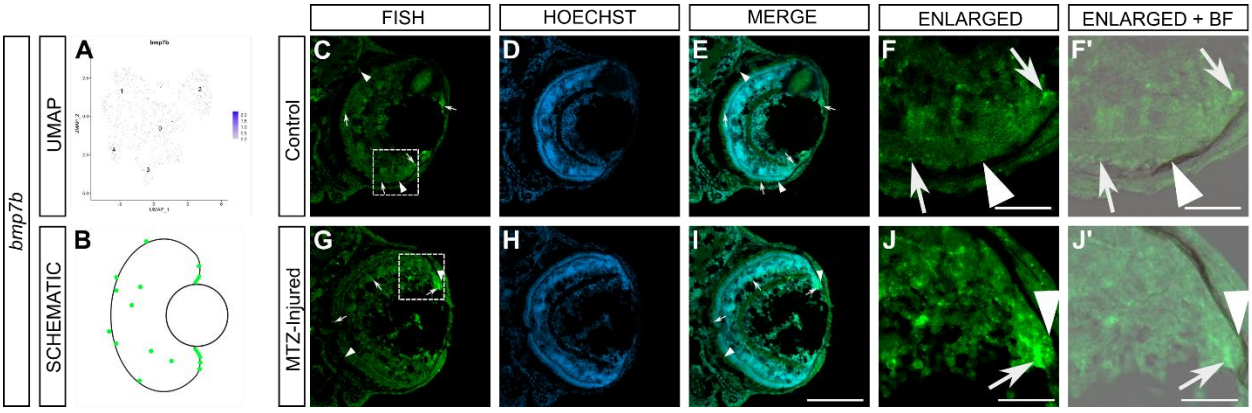

Figure 4.1 *bmp7b* expression seems to increase in the CMZ and peripheral RPE post-injury.

UMAP plot of scRNA-seq RPE data generated by the McFarlane lab from dissected eyes of 5 dpf larvae (A). Retinal schematic depicting where the gene is expressed by FISH in the healthy 6 dpf zebrafish retina (RPE, INL, CMZ) (B). Confocal images of a transverse section of control (uninjured) *sema3fa*$^{+/+}$ *Tg(rpe65a:NTR-EGFP)* 6 dpf retina showing *bmp7b* FISH (C), Hoechst label to denote nuclei (D), and merge (E). Scale bar denotes 100 µm. The boxed area in C is shown at a higher magnification in F to reveal FISH label in the RPE, INL, and CMZ (n=8/9; N=3). Brightfield (BF) image was overlaid with enlarged FISH image to visualize pigmented RPE near the CMZ (F'). Scale bar denotes 25 µm (F, F'). Confocal images of a transverse section of MTZ-injured *sema3fa*$^{+/+}$ *Tg(rpe65a:NTR-EGFP)* 0 dpr retina (6 dpf) showing *bmp7b* FISH (G), Hoechst label to denote nuclei (H), and merge (I). Scale bar denotes 100 µm. The boxed area in G is shown at a higher magnification in J to reveal increased FISH label in the CMZ and surrounding peripheral RPE (n=6/9; N=3). Brightfield (BF) image was overlaid with enlarged image to visualize pigmented RPE near the CMZ (J'). Scale bar denotes 25 µm (J, J'). Arrowheads depict RPE-localized FISH and arrows depict non-RPE-localized FISH.

Calcium-/calmodulin-dependent serine protein kinase a (*caska*) is a membrane-associated kinase. It is expressed in the mammalian nervous system, including in the developing optic vesicle where CASK is required for eye development (Hsueh, 2006; Kerr et al., 2019). Patients with a mutation in CASK suffer from several eye defects, including severe microcephaly, nystagmus, and strabismus (Cristofoli et al., 2018). I was further interested in CASK, in that in human tumours CASK functions in the Syndecan-1 signalling cascade, which is involved in epithelial to mesenchymal transition (EMT) (Menashe et al., 2010; Szatmári & Dobra, 2013). Additionally, Syndecan-1 binds to and activates pro-angiogenic factors like VEGF and promotes angiogenesis (Szatmári & Dobra, 2013). Although Syndecan-1 is not present in zebrafish (Lambaerts et al., 2012), its orthologs provide similar roles. According to ZFIN ISH data, *caska* mRNA is present in the optic vesicle from 19 hpf to at least 60 hpf (Thisse et al., 2004), and publicly available embryonic (1-5 dpf) scRNA-seq data indicate expression in the outer retina and RPE (Farnsworth et al., 2021). A known potent and selective inhibitor of CASK *in vitro* is the chemical probe NR162 (Russ et al., 2021).

My data agrees with previous ISH and embryonic scRNA-seq data, as I found *caska* was moderately expressed in the annotated RPE according to the McFarlane lab scRNA-seq data set (**Figure 4.2A**). In 6 dpf uninjured larvae, FISH label for *caska* was present in the ONL and INL (n=6/7; N=3; **Figure 4.2C-F**), as represented schematically in **Figure 4.2B**. After being exposed to 10 mM MTZ for 24 hours, 0 dpr (6 dpf) injured larvae seemed to show an increase in the FISH label within the central RPE (n=7/7; N=3; **Figure 4.2G-J**, arrowheads).

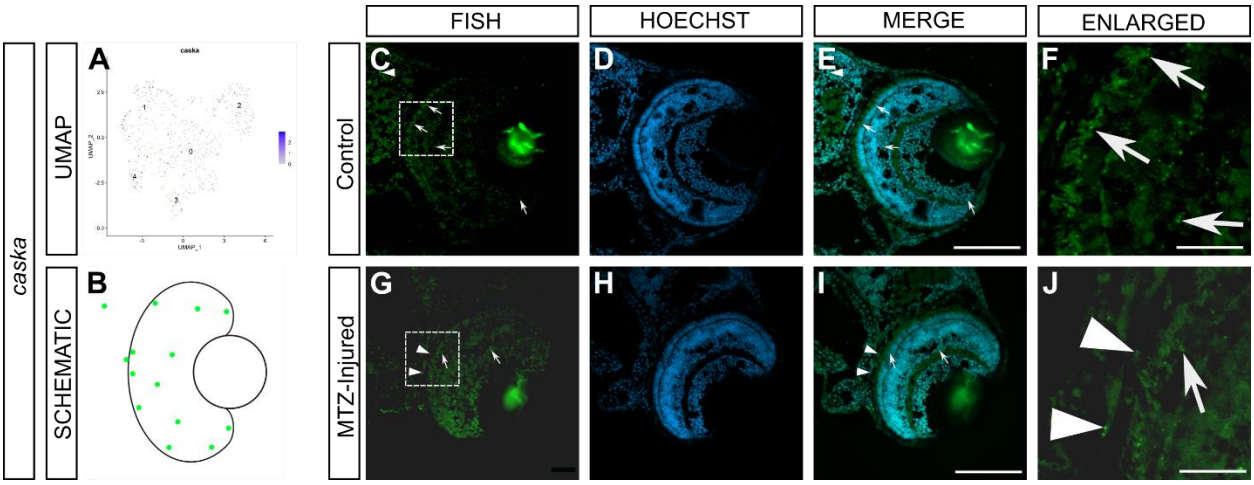

Figure 4.2 *caska* expression seems to increase in the RPE post-injury.

UMAP plot of scRNA-seq RPE data generated by the McFarlane lab from dissected eyes of 5 dpf larvae (A). Retinal schematic depicting where the gene is expressed by FISH in the healthy 6 dpf zebrafish retina (RPE, ONL, INL) (B). Confocal images of a transverse section of control (uninjured) *sema3fa*$^{+/+}$ *Tg(rpe65a:NTR-EGFP)* 6 dpf retina showing *caska* FISH (C), Hoechst label to denote nuclei (D), and merge (E). Scale bar denotes 100 µm. The boxed area in C is shown at a higher magnification in F to reveal FISH label in the ONL and INL (n=6/7; N=3). Scale bar denotes 25 µm (F). Confocal images of a transverse section of MTZ-injured *sema3fa*$^{+/+}$ *Tg(rpe65a:NTR-EGFP)* 0 dpr retina (6 dpf) showing *caska* FISH (G), Hoechst label to denote nuclei (H), and merge (I). Scale bar denotes 100 µm. The boxed area in G is shown at a higher magnification in J to reveal increased FISH label in the central RPE (n=7/7; N=3). Scale bar denotes 25 µm (J). Arrowheads depict RPE-localized FISH and arrows depict non-RPE-localized FISH.

Forkhead box protein m1 (*foxm1*) is a transcriptional activator. In zebrafish, *foxm1* is required for cardiomyocyte proliferation post-injury; *foxm1* expression increases post-injury, and *foxm1* mutants show decreased cardiomyocyte proliferation (Zuppo et al., 2023). I chose *foxm1* as a candidate because FOXM1 is responsible for mesenchymal-to-epithelial transition (MET) of human embryonic stem cell-derived RPE (Choudhary et al., 2015), and so could be involved in the reforming of an epithelial RPE layer after production of new RPE cells post-injury. *foxm1* has little expression in 1 to 5 dpf zebrafish larvae according to previously published embryonic scRNAseq data (Farnsworth et al., 2021). Nonetheless, *foxm1* may be upregulated post-injury, as its overexpression in human embryonic stem cell (hESC)-derived RPE results in an increase in MET and increased epithelial phenotypes (Choudhary et al., 2015). Thiostrepton is a known specific and direct inhibitor of the FOXM1 *in silico* and *in vitro* by binding directly to FOXM1 (Kongsema et al., 2019). *foxm1* showed little or no expression in the annotated RPE clusters of our zebrafish scRNAseq data (**Figure 4.3A**). In 6 dpf uninjured larvae, there was some FISH label for *foxm1* in the INL, RPE and the surrounding epithelial cells in the 6 dpf control larvae (n=4/4; N=1; **Figure 4.3C-F**, arrowhead), as represented in the schematic in **Figure 4.3B**. Interestingly after MTZ-mediated injury, there appeared to be an increase in FISH label in the ONL (n=4/4; N=1; **Figure 4.3G-J**). This suggests that *foxm1* is upregulated in the ONL post RPE injury.

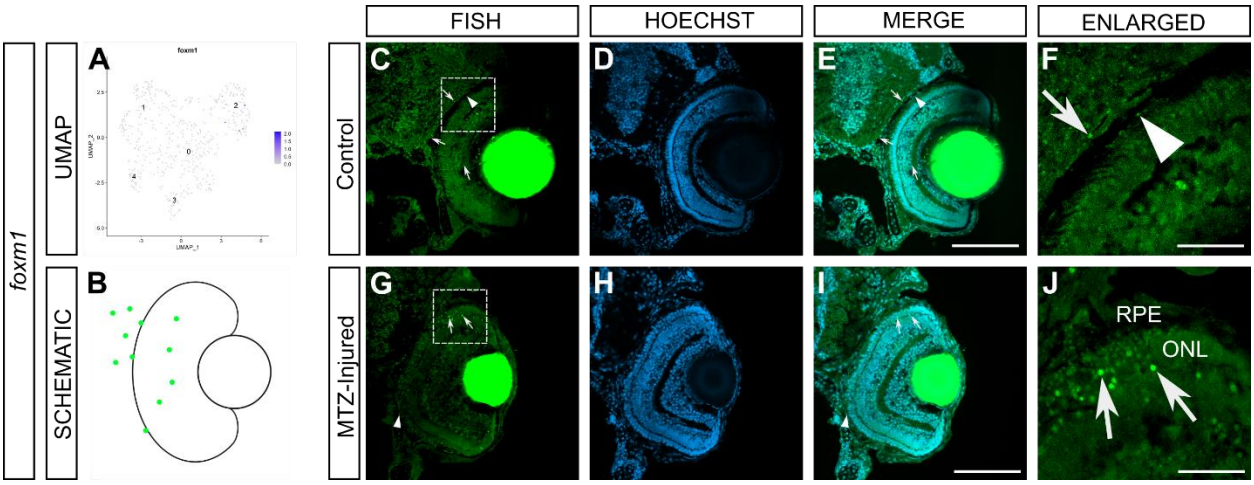

Figure 4.3 *foxm1* expression seems to increase in the ONL post-injury.

Overlay of *foxm1* expression on the UMAP plot of scRNA-seq RPE data generated by the McFarlane lab from dissected eyes of 5 dpf larvae (A). Retinal schematic depicting where the gene is expressed by FISH in the healthy 6 dpf zebrafish retina (RPE, INL, epithelium) (B). Confocal images of a transverse section of control (uninjured) *sema3fa*$^{+/+}$ *Tg(rpe65a:NTR-EGFP)* 6 dpf retina showing *foxm1* FISH (C), Hoechst label to denote nuclei (D), and merge (E). Scale bar denotes 100 µm. The boxed area in C is shown at a higher magnification in F to reveal FISH label in the RPE and epithelium (n=4/4; N=1). Scale bar denotes 25 µm (F). Confocal images of a transverse section of MTZ-injured *sema3fa*$^{+/+}$ *Tg(rpe65a:NTR-EGFP)* 0 dpr retina (6 dpf) showing *foxm1* FISH (G), Hoechst label to denote nuclei (H), and merge (I). Scale bar denotes 100 µm. The boxed area in G is shown at a higher magnification in J to reveal increased FISH label in the ONL (n=4/4; N=1). Scale bar denotes 25 µm (J). Arrowheads depict RPE-localized FISH and arrows depict non-RPE-localized FISH.

Moesin b (*msnb*) is part of the Ezrin-Radixin-Moesin (ERM) family that organizes membrane protein scaffolds to shape membranes (Karagiosis & Ready, 2004). In *Drosophila melanogaster,* moesin is required for retinal epithelium apical membrane organization and photoreceptor morphogenesis (Karagiosis & Ready, 2004). Phosphorylating moesin in 3-week-old rat retinas *in vitro* stimulates retinal pericyte migration and subsequent neovascularization, a similar pathology to human proliferative diabetic retinopathy (Zhang et al., 2020). The Moesin protein is also present in mouse RPE microvilli, although its impact on RPE development or regeneration remains unknown (Bonilha et al., 2004). I found high expression in the RPE cluster of a previously published scRNA-seq database of 1-5 dpf zebrafish larvae (Farnsworth et al., 2021). NSC668394 is a potent inhibitor of ERM phosphorylation that has been used *in vitro* and *in vivo* on juvenile immunocompromised mice (Proudfit et al., 2020). Another option for pharmacological inhibition is Polyphyllin VII (PP7), which is a novel, Moesin-specific inhibitor, acting on the Wnt/β-catenin pathway downstream of ERM in human multiple myeloma cell lines (H. Wang et al., 2022). Importantly, the Wnt/β-catenin pathway functions in RPE regeneration (Han et al., 2015; Hanovice et al., 2019). Our 5 dpf scRNA-seq RPE data suggested high *msnb* mRNA levels (**Figure 4.4A**), especially in RPE clusters that are suspected to be part of the central differentiated RPE (Sanjibani Sanyal, personal communication), and at lower levels in the cells of other RPE clusters. In retinal sections of 6 dpf control larvae, *msnb* FISH signal was present in the RPE (n=5/5; N=2) as denoted by arrowheads (**Figure 4.4C-F**), and represented schematically in **Figure 4.4B**. 24 hours after the onset of MTZ-mediated injury, there seemed to be increased expression of *msnb* in the central RPE (n=4/4; N=2; **Figure 4.4G-J**).

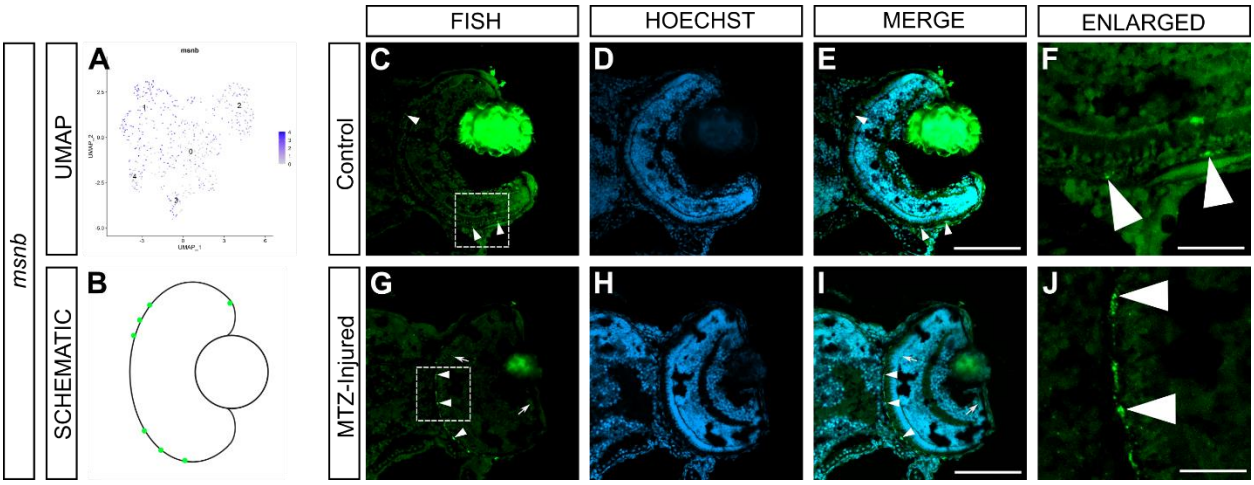

Figure 4.4 *msnb* expression seems to increase in the RPE post-injury.

UMAP plot of scRNA-seq RPE data generated by the McFarlane lab from dissected eyes of 5 dpf larvae (A). Retinal schematic depicting where the gene is expressed by FISH in the healthy 6 dpf zebrafish retina (RPE) (B). Confocal images of a transverse section of control (uninjured) *sema3fa*$^{+/+}$ *Tg(rpe65a:NTR-EGFP)* 6 dpf retina showing *msnb* FISH (C), Hoechst label to denote nuclei (D), and merge (E). Scale bar denotes 100 µm. The boxed area in C is shown at a higher magnification in F to reveal FISH label in the RPE (n=5/5; N=2). Scale bar denotes 25 µm (F). Confocal images of a transverse section of MTZ-injured *sema3fa*$^{+/+}$ *Tg(rpe65a:NTR-EGFP)* 0 dpr retina (6 dpf) showing *msnb* FISH (G), Hoechst label to denote nuclei (H), and merge (I). Scale bar denotes 100 µm. The boxed area in G is shown at a higher magnification in J to reveal increased FISH label in the RPE (n=4/4; N=2). Scale bar denotes 25 µm (J). Arrowheads depict RPE-localized FISH and arrows depict non-RPE-localized FISH.

Transient receptor potential cation channel m7 (*trpm7*) is an ion channel. TRPM7 can also act as a serine/threonine protein kinase to control the PI3K-Akt pathway responsible for cell growth, migration, and invasion of bladder cancer tumors *in vitro* (Lee et al., 2020). The PI3K-Akt-mTOR pathway *is* essential for RPE regeneration (Lu et al., 2022), raising the possibility that Trpm7 functions in zebrafish RPE regeneration. Indeed, *in vitro trpm7* protects rat RPE cells from apoptosis (Hu & Xu, 2021). The zebrafish embryonic scRNA-seq data indicates that some RPE expression is present at 1 to 5 dpf (Farnsworth et al., 2021), so it would be of interest to see if *trpm7* influences RPE regeneration (Lu et al., 2022). Pharmacological inhibition can be achieved by application of free Mg^{2+} and Mg·ATP which decreases functional TRPM7 channel activity in zebrafish cell lines (Jansen et al., 2016).

I found a small number of cells in RPE clusters 0, 1, and 2 from the McFarlane scRNA-seq data that appeared to express *trpm7* (**Figure 4.5A**). I observed strong FISH expression in the 6 dpf control retina in the peripheral RPE (arrowheads) as well as in the ONL, INL and CMZ (arrows), as represented schematically (n=5/5; N= 2; **Figure 4.5B; C-F**). Post MTZ-mediated RPE injury, the 0 dpr larvae appeared to show an increase in *trpm7* FISH expression, specifically in the periphery of the RPE, close to the CMZ as well as in the ONL (n=6/6; N=2; **Figure 4.5G-J**). *trpm7* also appeared to be upregulated in Müller glia post-injury (**Figure 4.5G-I**). To be able to localize FISH label with respect to the CMZ and peripheral RPE, I overlaid the brightfield (BF) image on top of the FISH image (**Figure 4.5F'; J'**). This allowed me to localize *trpm7* mRNA relative to the pigmented RPE and assess any change in expression in this area post RPE injury. There appeared to be an increase in FISH label colocalized with RPE pigmentation in **Figure 4.5J'**, suggesting an upregulation of *trpm7* in peripheral RPE post MTZ-mediated RPE injury. There also

appeared to be an increase in FISH label in the peripheral ONL post-injury (top arrow; **Figure 4.5J; J'**).

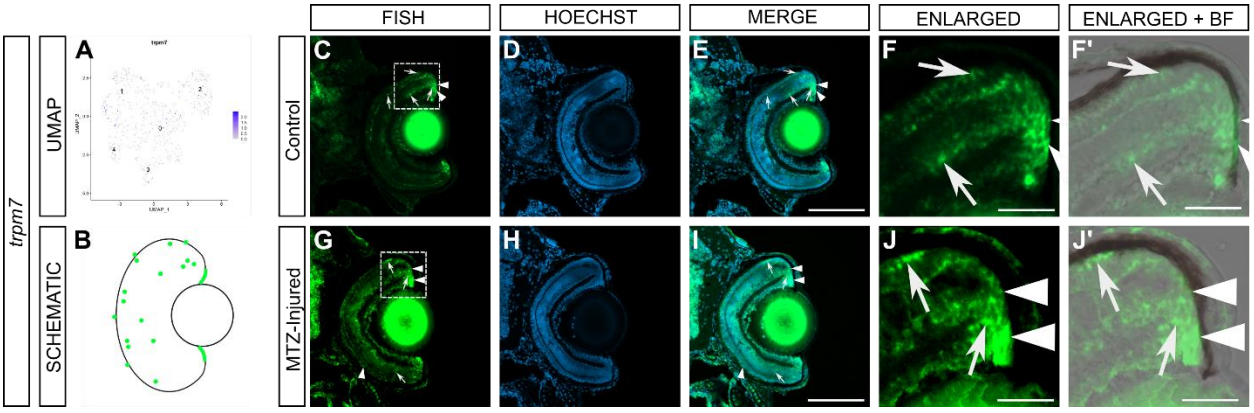

Figure 4.5 *trpm7* expression seems to increase in ONL and peripheral RPE post-injury.

UMAP plot of scRNA-seq RPE data generated by the McFarlane lab from dissected eyes of 5 dpf larvae (A). Retinal schematic depicting where the gene is expressed by FISH in the healthy 6 dpf zebrafish retina (RPE, ONL, INL, and CMZ) (B). Confocal images of a transverse section of control (uninjured) *sema3fa*$^{+/+}$ *Tg(rpe65a:NTR-EGFP)* 6 dpf retina showing *trpm7* FISH (C), Hoechst label to denote nuclei (D), and merge (E). Scale bar denotes 100 µm. The boxed area in C is shown at a higher magnification in F to reveal FISH label in the RPE, ONL, and INL (n=5/5; N=2). Brightfield (BF) image was overlaid with enlarged FISH image to visualize pigmented RPE near the CMZ (F'). Scale bar denotes 25 µm (F, F'). Confocal images of a transverse section of MTZ-injured *sema3fa*$^{+/+}$ *Tg(rpe65a:NTR-EGFP)* 0 dpr retina (6 dpf) showing *trpm7* FISH (G), Hoechst label to denote nuclei (H), and merge (I). Scale bar denotes 100 µm. The boxed area in G is shown at a higher magnification in J to reveal increased FISH label in the CMZ and RPE proximal to the CMZ (n=6/6; N=2). Brightfield (BF) image was overlaid with enlarged image to visualize pigmented RPE near the CMZ (J'). Scale bar denotes 25 µm (J, J'). Arrowheads depict RPE-localized FISH and arrows depict non-RPE-localized FISH.

vrk1 (*Vaccinia-related kinase/ serine/threonine kinase 1*) is a kinase involved in cell proliferation, nuclear envelope formation and heterochromatin formation (Carrasco Apolinario et al., 2023). *vrk1* has a potential role in neuronal proliferation in 6-month-old $Vrk1^{GT3/GT3}$ hypomorphic mouse mutants as reported in _____ (Valbuena et al., 2011; Vinograd-Byk et al., 2018). Upregulation of VRK1 induces proliferation of human uveal melanoma cell lines (Landreville et al., 2011), which suggests Vrk1 could impact zebrafish pigment cell proliferation. *vrk1* has moderate expression within the RPE at 1 to 5 dpf according to previously published zebrafish embryonic scRNA-seq data, and may be upregulated in response to injury, as seen in human uveal melanoma cell lines (Farnsworth et al., 2021; Landreville et al., 2011). A novel inhibitor, VRK-IN-1 blocks VRK1 phosphorylation of histone H3 and p53 targets in human cell lines (Monte-Serrano & Lazo, 2023). *vrk1* appeared to be expressed by only a handful of 5 dpf RPE cells in the McFarlane scRNA-seq dataset (**Figure 4.6A**). In 6 dpf control larvae, I observed FISH label in a handful of RPE and INL cells, as well as in the brain, which is represented schematically (n=5/5; N=1; **Figure 4.6B; C-F**). Injured larvae at 0 dpr appeared to have increased FISH label in both the central RPE and ONL (n=3/3; N=1; **Figure 4.6G-J**).

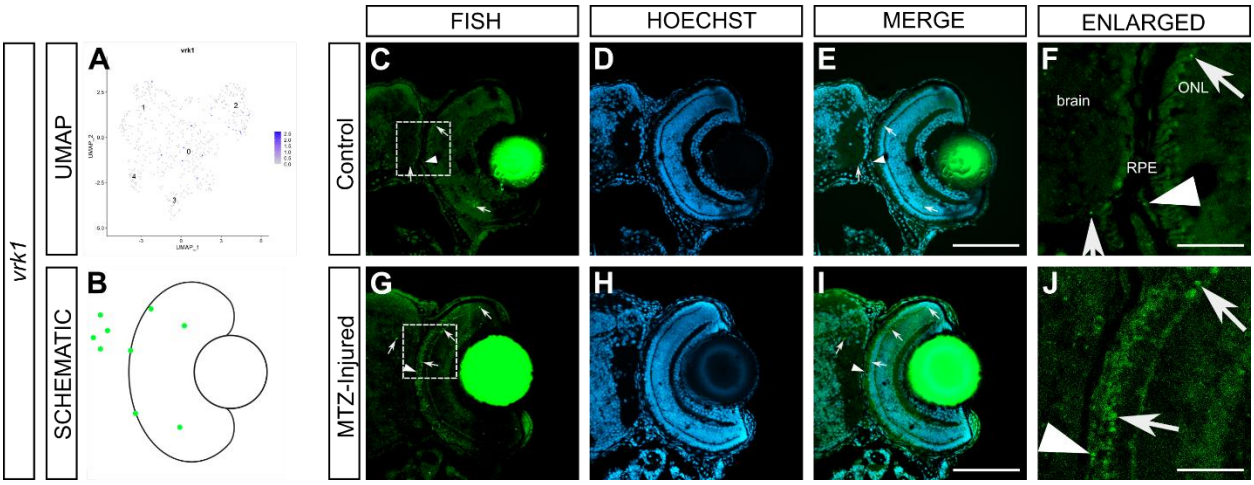

Figure 4.6 *vrk1* expression seems to increase in the RPE and ONL post-injury.

UMAP plot of scRNA-seq RPE data generated by the McFarlane lab from dissected eyes of 5 dpf larvae (A). Retinal schematic depicting where the gene is expressed by FISH in the healthy 6 dpf zebrafish retina (RPE, INL, and brain) (B). Confocal images of a transverse section of control (uninjured) *sema3fa*$^{+/+}$ *Tg(rpe65a:NTR-EGFP)* 6 dpf retina showing *vrk1* FISH (C), Hoechst label to denote nuclei (D), and merge (E). Scale bar denotes 100 µm. The boxed area in C is shown at a higher magnification in F to reveal FISH label in the RPE and brain (n=5/5; N=1). Scale bar denotes 25 µm (F). Confocal images of a transverse section of MTZ-injured *sema3fa*$^{+/+}$ *Tg(rpe65a:NTR-EGFP)* 0 dpr retina (6 dpf) showing *vrk1* FISH (G), Hoechst label to denote nuclei (H), and merge (I). Scale bar denotes 100 µm. The boxed area in G is shown at a higher magnification in J to reveal increased FISH label in the ONL and RPE (n=3/3; N=1). Scale bar denotes 25 µm (J). Arrowheads depict RPE-localized FISH and arrows depict non-RPE-localized FISH.

4.2.2 Candidate genes involved in normal RPE function or development

First, I wanted to observe expression of *rpe65a* as a marker of zebrafish RPE cells; hence why its promotor was used for the *Tg(rpe65a:NTR-EGFP)* background in Chapter Three. RPE65a (*retinoid isomerohydrolase*) is critical in the visual cycle and normal function of the RPE, and is the key isomerase in converting the all-*trans*-retinyl ester to 11-*cis*-retinol. Potentially, RPE regeneration requires this functional role of RPE cells and *rpe65a* is expressed highly by embryonic (1-5 dpf) RPE according to the Farnsworth scRNA-seq database (Cai et al., 2009; Farnsworth et al., 2021). There are a few non-retinoid inhibitors of RPE65 *in vivo,* including CU239 and RPE65-61 (Shin et al., 2018; Y. Wang et al., 2022).

I compared *rpe65a* mRNA expression by FISH in retinal sections with the transgenic expression of Chapter 3, and asked if its expression changed in response to RPE injury. According to the McFarlane RPE scRNA-seq data, *rpe65a* mRNA is expressed in the most differentiated RPE cells (**Figure 4.7A**). In uninjured/control 6 dpf larvae, FISH signal is localized to the central RPE (n=4/4; N=1; **Figure 4.7C-F**, arrowheads). This RPE expression is represented schematically (**Figure 4.7B**). With RPE injury, at 0 dpr *rpe65a* expression appears to be increased (n=3/3; N=1), with qualitatively larger sections of the RPE having the fluorescent label (**Figure 4.7G-J**).

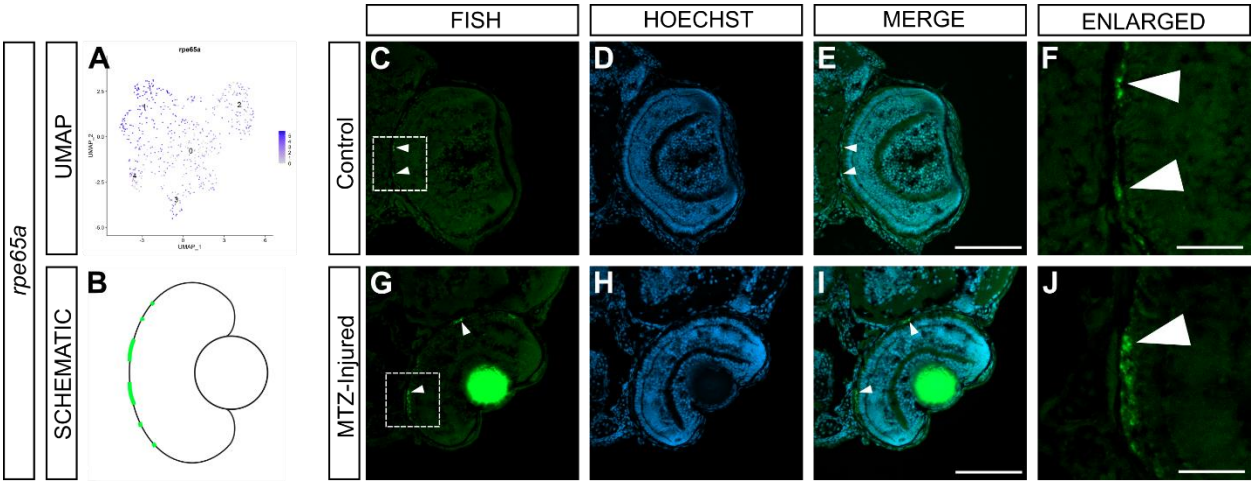

Figure 4.7 *rpe65a* expression seems to increase in the RPE post-injury.

UMAP plot of scRNA-seq RPE data generated by the McFarlane lab from dissected eyes of 5 dpf larvae (A). Retinal schematic depicting where the gene is expressed by fluorescent *in situ* hybridization (FISH) in the healthy 6 dpf zebrafish retina (RPE) (B). Confocal images of a transverse section of control (uninjured) *sema3fa*$^{+/+}$ *Tg(rpe65a:NTR-EGFP)* 6 dpf retina showing *rpe65a* FISH (C), Hoechst label to denote nuclei (D), and merge (E). Scale bar denotes 100 µm. The boxed area in C is shown at a higher magnification in F to reveal FISH label in the RPE (n=4/4; N=1). Scale bar denotes 25 µm (F). Confocal images of a transverse section of MTZ-injured *sema3fa*$^{+/+}$ *Tg(rpe65a:NTR-EGFP)* 0 dpr retina (6 dpf) showing *rpe65a* FISH (G), Hoechst label to denote nuclei (H), and merge (I). Scale bar denotes 100 µm. The boxed area in G is shown at a higher magnification in J to reveal increased FISH label in the RPE (n=3/3; N=1). Scale bar denotes 25 µm (J). Arrowheads depict RPE-localized FISH.

Collagen, type IV, alpha 6 (*col4a6*) encodes one of the six subunits of type IV collagen, the major structural component of basement membranes in neural cells and most ocular cells (Bai et al., 2009; Takeuchi et al., 2015). *col4a6* contributes to axon formation in zebrafish granule cells and retinal ganglion cells (Takeuchi et al., 2015). According to various scRNA-seq databases, *COL4A6* is down regulated with age in human RPE, and is moderately expressed in annotated RPE of embryonic (1 to 5 dpf) zebrafish scRNAseq data (Butler et al., 2021; Farnsworth et al., 2021). There is some speculation as to the impact of COL4A6 on the RPE, but one idea is that COL4A6 contributes to the phagolyosome function of the RPE and that this slows with age, contributing to an increased risk of AMD (Butler et al., 2021). Although COL4A6 does not have a pharmacological inhibitor, it was a key candidate, so warrants potentially using a CRISPR-Cas9-mediated F0 loss-of-function approach, which has been successfully employed in a similar screen (Lu et al., 2023).

I found *col4a6* was moderately expressed in the RPE of the McFarlane scRNA-seq data; predominantly in cluster 1, and to a lesser extent, 0 and 2 (**Figure 4.8A**). In 6 dpf uninjured larvae, FISH label for *col4a6* was present in the epithelium and at lower levels in the RPE (n=4/5; N=2; **Figure 4.8C-F**). This pattern of expression is represented schematically in **Figure 4.8B**. After being exposed to 10 mM MTZ for 24 hours, 0 dpr (6 dpf) injured larvae still expressed *col4a6* in the epithelium (arrows), but the levels appeared decreased in the RPE (arrowhead; n=5/5; N=2; **Figure 4.8G-J**). The faint FISH label, however, prevents definitive conclusions to be made.

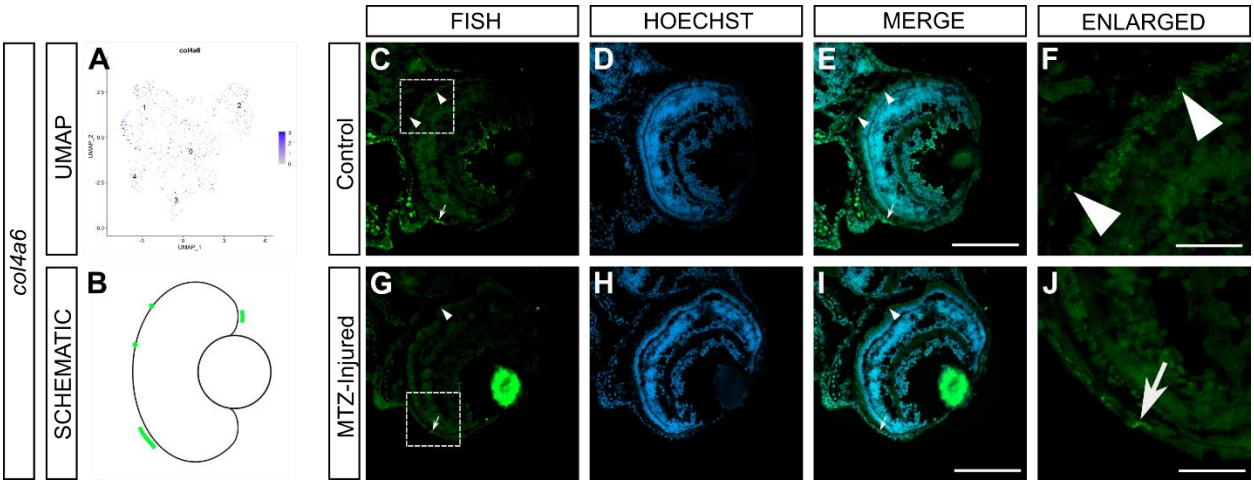

Figure 4.8 *col4a6* expression appears to be unchanged post-injury.

UMAP plot of scRNA-seq RPE data generated by the McFarlane lab from dissected eyes of 5 dpf larvae (A). Retinal schematic depicting where the gene is expressed by FISH in the healthy 6 dpf zebrafish retina (RPE, epithelium) (B). Confocal images of a transverse section of control (uninjured) *sema3fa*$^{+/+}$ *Tg(rpe65a:NTR-EGFP)* 6 dpf retina showing *col4a6* FISH (C), Hoechst label to denote nuclei (D), and merge (E). Scale bar denotes 100 µm. The boxed area in C is shown at a higher magnification in F to reveal FISH label in the RPE and epithelium (n=4/5; N=2). Scale bar denotes 25 µm (F). Confocal images of a transverse section of MTZ-injured *sema3fa*$^{+/+}$ *Tg(rpe65a:NTR-EGFP)* 0 dpr retina (6 dpf) showing *col4a6* FISH (G), Hoechst label to denote nuclei (H), and merge (I). Scale bar denotes 100 µm. The boxed area in G is shown at a higher magnification in J to reveal similar FISH label in the epithelium (n=5/5; N=2). Scale bar denotes 25 µm (J). Arrowheads depict RPE-localized FISH and arrows depict non-RPE-localized FISH.

her4.1 (*hairy-related 4, tandem duplicate 1*) is a transcription factor that regulates cell differentiation in the neural plate, and is required for Notch-mediated signaling in zebrafish neurogenesis, beginning as early as the 5-somite stage (Takke et al., 1999; Yeo et al., 2007). In the larval zebrafish, *her4.1* is upregulated in Müller glia in response to retinal damage (Mitra et al., 2018). According to ISH data, *her4.1* is found in 48 hpf zebrafish in the outer retina and is sequestered to the CMZ by 70 hpf (Taylor et al., 2015), which may become activated in response to RPE injury (Hanovice et al., 2019). I became interested in Her4.1 when a student in the McFarlane lab identified, using our scRNA-seq data, *her4.1* expression in a subset of 5 dpf RPE. Although there is no publicly available *her4.1* pharmacological inhibitor for zebrafish, RO4929097 is effective in inhibiting Notch signaling in 6-month-old zebrafish (Fogerty et al., 2022).

I found with the McFarlane scRNA-seq data that *her4.1* is selectively expressed in cluster 2 (**Figure 4.9A**). In 6 dpf uninjured larvae, FISH label for *her4.1* was present in the INL and CMZ, and potentially in the most peripheral RPE adjacent to the CMZ (n=4/4; N= 1; **Figure 4.9C-F,** arrowhead in F). This pattern of expression is represented schematically in **Figure 4.9B**. After being exposed to 10 mM MTZ for 24 hours, 0 dpr (6 dpf) injured larvae seemed to show an increase in the FISH label within the CMZ and outermost peripheral RPE (n=3/3; N=1; **Figure 4.9G-J**). To be able to localize FISH label with respect to the CMZ and peripheral RPE, I overlaid the brightfield (BF) image on top of the FISH image (**Figure 4.9F'; J'**). This allowed me to localize *her4.1* mRNA relative to the pigmented RPE and assess any change in expression in this area post RPE injury. I observed an increase in peripheral RPE FISH label, but there appeared to be no change in the *her4.1* expression in the central RPE (**Figure 4.9F'; J'**).

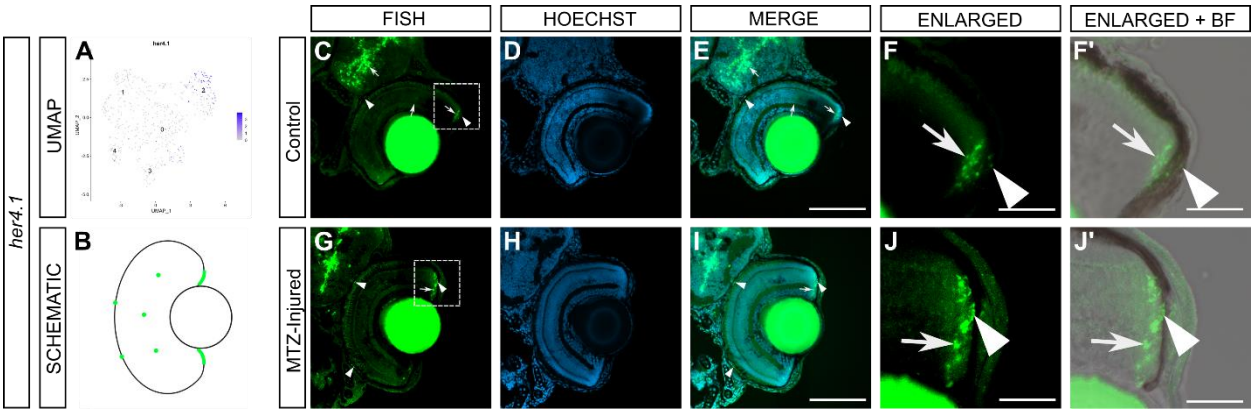

Figure 4.9 *her4.1* expression seems to increase in peripheral RPE post-injury.

UMAP plot of scRNA-seq RPE data generated by the McFarlane lab from dissected eyes of 5 dpf larvae (A). Retinal schematic depicting where the gene is expressed by FISH in the healthy 6 dpf zebrafish retina (RPE, INL, CMZ, and brain) (B). Confocal images of a transverse section of control (uninjured) *sema3fa*$^{+/+}$ *Tg(rpe65a:NTR-EGFP)* 6 dpf retina showing *her4.1* FISH (C), Hoechst label to denote nuclei (D), and merge (E). Scale bar denotes 100 µm. The boxed area in C is shown at a higher magnification in F to reveal FISH label in the RPE and brain (n=4/4; N=1). Brightfield (BF) image was overlaid with enlarged FISH image to visualize pigmented RPE near the CMZ (F'). Scale bar denotes 25 µm (F, F'). Confocal images of a transverse section of MTZ-injured *sema3fa*$^{+/+}$ *Tg(rpe65a:NTR-EGFP)* 0 dpr retina (6 dpf) showing *her4.1* FISH (G), Hoechst label to denote nuclei (H), and merge (I). Scale bar denotes 100 µm. The boxed area in G is shown at a higher magnification in J to reveal similar FISH label in the RPE and INL (n=3/3; N=1). Brightfield (BF) image was overlaid with enlarged image to visualize pigmented RPE near the CMZ (J'). Scale bar denotes 25 µm (J). Arrowheads depict RPE-localized FISH and arrows depict non-RPE-localized FISH.

orthodenticle homeobox 2b (*otx2b*) is a key transcription factor in RPE development in vertebrates, first being expressed in the developing optic vesicles and eventually restricted to differentiating RPE (Lane & Lister, 2012). Otx2b also has an important role in early (35 hpf) RPE pigmentation in embryonic zebrafish RPE. OTX2 is one of the first specification genes to be expressed in mouse and chick RPE, and *otx2b* expression is maintained in the 72 hpf zebrafish RPE (Lane & Lister, 2012; Nadauld et al., 2006). To inhibit *otx2b,* I suggest using all-trans retinoic acid (ATRA), which pharmacologically knocks down OTX2 expression, resulting in repressed proliferation of retinoblastoma cells *in vivo* (Li et al., 2015).

I found moderate expression of *otx2b* in the 5 dpf McFarlane scRNA-seq RPE cluster, predominantly in in clusters 1 and 2 (**Figure 4.10A**). In 6 dpf uninjured larvae, FISH label for *otx2b* was present in the CMZ and to a lesser extent the INL and RPE (n=11/12; N=3; **Figure 4.10C-F**). This pattern of expression is represented schematically in **Figure 4.10B**. After being exposed to 10 mM MTZ for 24 hours, 0 dpr (6 dpf) injured larvae still appeared to show FISH label in the CMZ, INL, and RPE (n=11/12; N=3; **Figure 4.10G-J**). There seemed to be no discernable change in CMZ or RPE FISH label (neither central nor peripheral) post-injury.

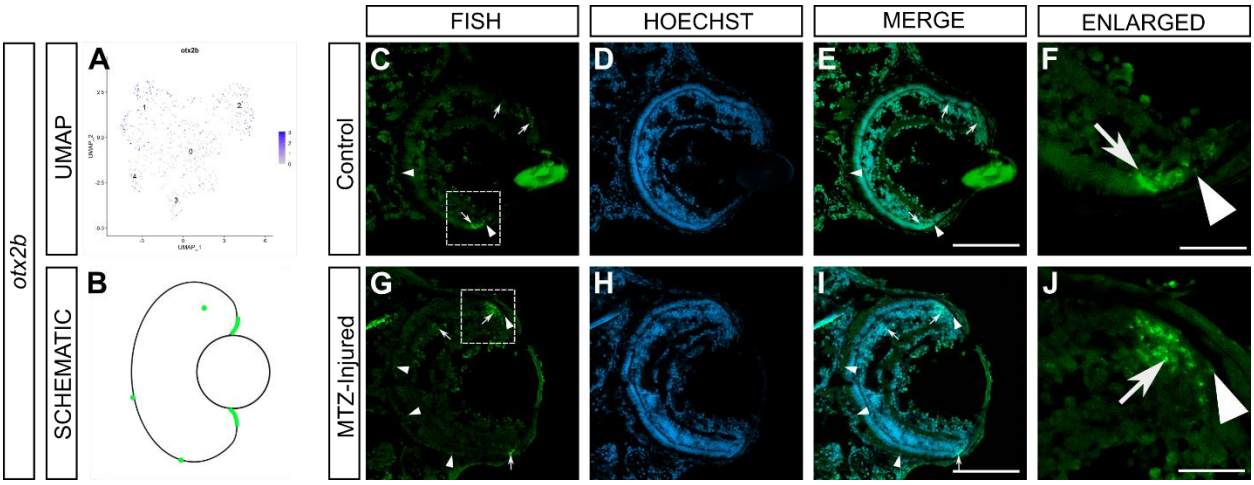

Figure 4.10 *otx2b* expression appears to be unchanged post-injury.

UMAP plot of scRNA-seq RPE data generated by the McFarlane lab from dissected eyes of 5 dpf larvae (A). Retinal schematic depicting where the gene is expressed by FISH in the healthy 6 dpf zebrafish retina CMZ and to a lesser extent, the INL and RPE (B). Confocal images of a transverse section of control (uninjured) *sema3fa*$^{+/+}$ *Tg(rpe65a:NTR-EGFP)* 6 dpf retina showing *otx2b* FISH (C), Hoechst label to denote nuclei (D), and merge (E). Scale bar denotes 100 µm. The boxed area in C is shown at a higher magnification in F to reveal FISH label in the CMZ (n=11/12; N=3). Scale bar denotes 25 µm (F). Confocal images of a transverse section of MTZ-injured *sema3fa*$^{+/+}$ *Tg(rpe65a:NTR-EGFP)* 0 dpr retina (6 dpf) showing *otx2b* FISH (G), Hoechst label to denote nuclei (H), and merge (I). Scale bar denotes 100 µm. The boxed area in G is shown at a higher magnification in J to reveal similar FISH label in the CMZ (n=11/12; N=3). Scale bar denotes 25 µm (J). Arrowheads depict RPE-localized FISH and arrows depict non-RPE-localized FISH.

4.3 Discussion

In this chapter, I developed a list of ten candidate genes for which I observed their mRNA expression pre- and post-MTZ-mediated injury. The criteria for these genes were that 1) they must be physiologically relevant, 2) the gene should either be present in the zebrafish eye/RPE by 5 dpf or upregulated post-injury, and 3) preferably, the gene would have a commercially available pharmacological inhibitor. I separated the ten candidate genes into two groups, where the genes encode: 1) Proteins that are known to participate in cell growth and/or division that could be recruited in response to RPE injury, and 2) Proteins involved in normal RPE development/function and could be upregulated in response to RPE injury. In the cell growth/division group, *bmp7b, caska, foxm1, msnb, trpm7,* and *vrk1* all seemed to show some increase in FISH label post-injury. In the second group, normal RPE development/function, only mRNAs for *rpe65a* and *her4.1* appeared to increase post-injury, whereas *col4a6* and *otx2b* mRNAs appeared to remain unchanged.

4.3.1 Candidate genes involved in RPE cell growth and/or division appear to be upregulated post-injury

All the candidate genes from the cell growth/division group appear to be upregulated post-RPE-injury. *bmp7b* FISH label appears to increase in the CMZ and peripheral RPE post-injury (**Figure 4.1**). The CMZ, a stem cell niche within the retina, contains both neural retinal progenitors and at its periphery, proliferative RPE cells (George et al., 2021; Reinhardt et al., 2015). Potentially, in response to injury *bmp7b* is upregulated within the CMZ to trigger retinal stem cell and progenitor proliferation to replace the photoreceptors that are lost due to RPE ablation.

Similarly, *bmp7b* may be upregulated in the RPE progenitors of the CMZ to regulate progenitor proliferation and stimulate production of new RPE cells.

Next, *caska* FISH label appears to show a marginal increase in the central RPE post-injury (**Figure 4.2**) that may point to a role for Caska in RPE regeneration. The fact that *caska* is expressed in the developing optic vesicle and contributes to neural development (Hsueh, 2006) support a role for Caska in progenitors in larval eyes. Caska acts as a transcriptional activator and regulates Notch signaling (D'Souza et al., 2010; Fogerty et al., 2022), suggesting that Notch receptors and their Delta/Jagged ligands may influence RPE regeneration in zebrafish.

Both genes involved in mesenchymal-epithelial transition (MET), *foxm1* and *msnb*, seem to be upregulated post-injury. However, *foxm1* FISH label appears to increase in the ONL post RPE injury (**Figure 4.3**), but not in the RPE. Since *foxm1* is known to be required for zebrafish cardiomyocyte proliferation (Zuppo et al., 2023), this new expression could be in photoreceptor progenitors that proliferate in response to the degradation of the underlying photoreceptors when they lose support from the ablated RPE (Hanovice et al., 2019). Foxm1, however, may play no direct role in RPE regeneration.

The other MET-involved gene, *msnb*, appears to be the most robustly upregulated gene in the RPE post-injury of any of my 10 candidate genes; *msnb* FISH label appears to increase in the central RPE post-injury (**Figure 4.4**). It is unlikely that the increased *msnb* label is in the choroid vasculature as there is no evidence of *msnb* expression in vascular clusters in scRNA-seq databases (Farnsworth et al., 2021). MSNB is a component of the ERM protein complex responsible for organizing protein scaffolds to shape membranes (Karagiosis & Ready, 2004). Thus, increased Msnb could contribute to restructuring of membrane protein scaffolding in still-differentiating nascent RPE cells that migrate centrally in response to lesions in the RPE layer. In the future, I

would suggest localizing *msnb* mRNA with EdU to observe if proliferating RPE cells have increased *msnb* expression. While EMT, the opposite process to MET, is well characterized in cancer research, many processes and signalling pathways in MET remain unknown (Sipos & Galamb, 2012). RPE cells undergo EMT in human retinal diseases such as AMD and PVR, which is accompanied by dysregulation of TGF-β and Wnt pathways among others (Zhou et al., 2020). Since the Wnt pathway ensures efficient regeneration of zebrafish RPE post-injury (Hanovice et al., 2019), I would be interested in the future to explore the mechanisms of MET in zebrafish RPE regeneration, with Msnb providing a potential tool to do so. Future experiments could focus on inhibiting *msnb* pharmacologically with NSC668394 (Proudfit et al., 2020) in the *rpe65:NTR* injury model to observe if RPE regeneration is impacted. Additionally, FISH labeling alongside EdU labeling could reveal if *msnb* is upregulated in proliferating RPE cells.

The final two cell growth/division candidate genes both appear to have increased FISH label in the ONL and RPE post-injury. *trpm7* mRNA appears increased in the peripheral ONL and RPE, near the CMZ (**Figure 4.5**). This area of the zebrafish retina, the boundary between the CMZ and RPE, has not been very well characterized and it is proposed that regenerating RPE cells may arise from the CMZ (Hanovice et al., 2019). Future research could address if *trpm7* is implicated in potential CMZ-derived RPE progenitor differentiation and/or migration by employing lineage tracing to observe if proliferating RPE, which is known to fill in lesions in a peripheral to central fashion (Hanovice et al., 2019), arises from the CMZ or peripheral RPE. Although, attempts at conducting lineage tracing in zebrafish RPE has yet to be successful (Hanovice et al., 2019).

vrk1 mRNA also seems increased in the RPE and ONL after RPE injury, although located more centrally in the retina (**Figure 4.6**). The potential upregulation of *vrk1* in the outer retina, including in the RPE, is not unsurprising considering the role of Vrk1 in creating complexes with

histones, transcription factors and proteins in response to DNA damage (Campillo-Marcos & Lazo, 2018). DNA crosslinking should occur in the RPE when MTZ is applied in the presence of *rpe65a*-driven NTR. In all, genes responsible for cell division/growth appear to be upregulated in the outer retina and RPE post-injury.

4.3.2 Certain genes involved in normal RPE function and/or development appear to be upregulated post RPE injury

To observe if certain functional or developmental pathways become recruited in response to RPE injury, I looked at a few candidate genes that are present in the uninjured differentiated or developing RPE. Two of the four candidates did not appear to show any qualitative change in FISH label post-injury, including *col4a6*, a basement membrane collagen component. Although I find *col416* expression in the epithelium, RPE expression is sparse, with no obvious up- or downregulation of the FISH label post-injury **Figure 4.8**). The weak *col4a6* FISH label, however, makes conclusions difficult to make. Even though I used PTU to diminish pigment in the RPE for more ready viewing of fluorescence, there was still sufficient melanin pigment to sometimes obscure FISH label. But if the lack of *col4a6* upregulation post-injury is true, then possibly a key extracellular matrix protein may not be an important regulator of RPE regeneration.

mRNA for the developmental transcription factor, *otx2b,* is prominent in the CMZ, with some additional FISH label in the RPE and INL, but with no apparent change post-injury (**Figure 4.10**). Otx2b, in conjunction with Otx1a, is required during normal zebrafish RPE development, with knockouts resulting in major structural and functional defects, including loss of ventral RPE tissue and pathologic rotation of the entire eye (Lane & Lister, 2012). No qualitative expression change of *otx2b* suggests that some key RPE developmental pathways may not be recruited in

response to RPE injury. Other developmental genes and pathways, however, may still participate in RPE regeneration.

Two candidate genes that appear upregulated in the RPE post-injury are *her4.1* and *rpe65a*. *her4.1* FISH label appears to increase in the main CMZ and distal-most peripheral CMZ (**Figure 4.9**), where it colocalizes with peripheral RPE pigmentation. RPE-located peripheral CMZ stem cells are thought to give rise to both RPE and other retinal cells (Miles & Tropepe, 2021), and *her4.1* may be a key gene that participates. Her4 is normally a downstream effector of Notch signaling which increases in the central retina in response to photoreceptor damage (Wilson et al., 2016), so it would be of interest to observe if a similar regenerative response occurs in response to RPE damage. Pharmacological or CRISPR-mediated knockdown of *her4.1* in the future would reveal the importance of this gene in RPE regeneration.

Finally, since *rpe65a* is a prominent marker gene and essential for normal RPE visual cycle function, I sought to observe its expression in response to regeneration. *rpe65a* mRNA is apparently increased in the central retinal RPE post-injury (**Figure 4.7**). This observation differs from what I saw in section **3.2.2**, where *rpe65a*-driven eGFP expression decreases in the RPE in response to injury. One possible explanation may be that with the reporter line I measured the "extent" of a cytoplasmic protein marker (eGFP), while with FISH I viewed mRNA localization. Additionally, healthy RPE cells and injured ones likely exhibit distinct morphologies. While, eGFP will capture the entire morphology of a cell, FISH label is dictated by where the mRNA is present. mRNA in a round, spheroid injured RPE cell will be more readily captured in a single cryostat section than the mRNA of a healthy, flattened, control RPE cell that may be distributed over a greater area. Finally, with injured or dying cells, mRNA may be present but the cells fail to make the associated proteins, including eGFP. To determine whether *rpe65a* levels change upon injury,

I could use quantitative RT-PCR (RT-qPCR) to measure changes in gene expression post-injury. One caveat of RT-qPCR is that if the gene is not RPE-specific, small changes in gene expression may not be accurately measured and may not appear significant due to the small number of RPE cells within the eye. For an RPE-specific gene such as *rpe65a,* however, RT-qPCR would be an appropriate future experiment. It would be valuable to further study the dynamics of *rpe65a* expression post-injury as RPE65 mutations cause inherited retinal dystrophy in humans (Russell et al., 2017; Sodi et al., 2021). Potentially, overexpression of *rpe65a* could lead to improved RPE regeneration in zebrafish.

In summary, some proteins required for normal RPE development and function may be upregulated in the outer retina and RPE post RPE injury.

4.3.3 Conclusions

In all, most of the ten candidate genes were potentially upregulated in response to the MTZ-mediated RPE injury. Most of these genes were from the cell growth or division subgroup (except for *her4.1* and *rpe65a*). Potentially, there are different subpopulation/subtypes of RPE cells, as supported by the distinct clusters observed in the scRNA-seq data, which may have varying capabilities to de-differentiate and proliferate to produce new RPE to fill in the lesions caused by MTZ-mediated RPE injury. The function of candidate genes of particular interest could be explored by pharmacological or genetic inhibition using the *rpe65a:NTR* zebrafish ablation model. Additionally, to strengthen the data I have collected, I would suggest increasing the number of replicates, using a sense control probe to rule out any non-specific binding, and returning to whole mount ISH to reduce issues related to visualizing FISH in flattened RPE in cross-section. In all, my data point to potential new regulatory genes and pathways to be explored in RPE regeneration.

Table 1 Primers designed for Chapter Four candidate genes for in situ hybridization

Gene	Forward Primer (5' → 3')	T7 + Reverse Primer (5' → 3')	PCR Size
bmp7b	GAGGCGCCATCACAGAGAAT	TAATACGACTCACTATAGGGTTACAGGCCTGC TTCTGGTC	522 bp
caska	CTGGCTGAAGAGAGACCGCT	TAATACGACTCACTATAGGGTGTCTCCGTTCG TGCTTTCT	596 bp
col4a6	GCCATTAACCGAGGCTCACT	TAATACGACTCACTATAGGGGTGGACCAACAT CCCCCTTT	739 bp
foxm1	GGTGGTGGTGATCCCGAAAT	TAATACGACTCACTATAGGGCGGGGTCACCCA AAGGCTTAT	640 bp
her4.1	AGTTCATCAAGCAGCAGCCC	TAATACGACTCACTATAGGGGTAAGAGTACAG GCAATTCTTCTCC	424 bp
msnb	TTCAGTCCAGTACAACTGGTAAAC	TAATACGACTCACTATAGGGAAGCATCAACAC CCAACCAC	609 bp
otx2b	GCTTCACGGTTTGAAGAAAAGG	TAATACGACTCACTATAGGGCTGCTGTTGGCG ACACTTTG	548 bp
rpe65a	**(Halabi, 2019)		
trpm7	GATACACGCACGCATTGGTC	TAATACGACTCACTATAGGGAACTCCACACGGT CCATCAC	540 bp
vrk1	CTGAGGGAGTGCCAAAGGAG	TAATACGACTCACTATAGGGTTTTCTTCACCG CTGGCTCA	630 bp

CHAPTER FIVE: GENERAL DISCUSSION

In this thesis, I begin to explore potential pathways that influence RPE regeneration in zebrafish. In Chapter Three, I present evidence of Sema3fa involvement in RPE regeneration. First, I develop an approach to quantify RPE cell loss by measuring the normalized "existing" GFP-expressing RPE in the absence or presence of MTZ-mediated RPE injury on a *Tg(rpe65a:NTR-EGFP)* background. By using this method, I present evidence to suggest that the loss of Sema3fa does not significantly impact larval RPE development nor the extent of MTZ-induced RPE injury. Next, I present evidence that loss of Sema3fa may result in delayed and increased apoptosis in the RPE after injury. Further, I suggest that loss of Sema3fa may induce an initial increase in proliferation in the RPE and increased proliferation in the photoreceptor-residing outer nuclear layer. This Chapter provides data to suggest a role for a secreted Sema, Sema3f, in RPE regeneration following a timed metronidazole-mediated injury. In Chapter Four, I collect a list of ten candidate genes, which satisfy three criteria, that may be involved in RPE regeneration. These ten genes fall into two separate groups: genes involved in cell growth and/or division, and genes involved in normal RPE development/function. By generating FISH expression data for these genes in the absence and presence of the RPE injury, I suggest that eight of the ten genes exhibit increased expression in the zebrafish retina post-injury. Note, that all the candidate genes from the cell growth/division subgroup appear upregulated in response to RPE injury. These data suggest some genes/pathways that could be involved in RPE regeneration in zebrafish and that could warrant further investigation. In Chapter Five, I discuss my findings and how they fill knowledge gaps in the current literature and describe future experiments that can be done to further augment findings from my work.

5.1 Sema3fa as a regulator of RPE injury and regeneration

I was successful in replicating the injury model of the re-engineered *Tg(rpe65a:NTR-EGFP)* in both *sema3fa*$^{+/+}$ and *sema3fa*$^{ca304/ca304}$ zebrafish lines. This injury model is new to the McFarlane lab and I got it working reliably. Previous work with RPE regeneration had not described a quick and effective method of quantifying the level of RPE injury, and in this thesis I suggest a simple method to be able to quantify the extent of MTZ-mediated injury. By using this method, Sema3fa did not appear to impact the extent of RPE injury qualitatively nor quantitatively. I hypothesize that this secreted extrinsic signal may influence the immune response of the RPE cells following injury. There appears to be a delay and increase in the number of apoptotic cells in the absence of Sema3fa. I suggest that this result may relate to an increase in inflammation in the *sema3fa* mutants relative to WT, which is a critical regulator of RPE injury and subsequent regeneration (Leach et al., 2021; Prieto et al., 2020; Wang et al., 2012).

A loss of Sema3fa also appears to induce an earlier RPE proliferative response than in WT, as well as more proliferation, presumably of rod progenitors, in the ONL post-injury, although this may be a false positive due to the low number of EdU-positive cells in the ONL. In general, I found few aCsp3+ and EdU+ cells in my samples. The low numbers could be due to the narrow time frame of cell dynamics captured by aCsp3 and EdU labeling; aCsp3 immunolabeling captures cells in the final stages of apoptosis, a time frame of only 2 to 4 hours, while my EdU labeling approach captured cells in S-phase over a similar 4-hour window. Potentially I could use TUNEL to measure apoptosis as it is could identify more dying cells, and use a longer EdU pulse to allow for a longer period of thymidine analog incorporation and the identification of more proliferating cells.

The modest differences I found between the *sema3fa* WT and mutants with respect apoptosis and proliferation could reflect redundancy and/or compensation by another class 3 Sema. For instance, SEMA3A and SEMA3F work in combination to inhibit tumor angiogenesis *in vitro* (Guttmann-Raviv et al., 2007). Alternatively, Sema3aa, whose mRNA is expressed by cells of the zebrafish ONL (Callander et al., 2007), could be upregulated and compensate for the loss of Sema3fa. Perhaps, a double loss-of-function mutant of both *sema3fa* and *sema3aa* would have a more obvious phenotype in RPE injury and regeneration.

Because Sema3fa was originally known as an axon guidance cue (Sahay et al., 2003), it would be of interest to observe if Sema3fa promotes RPE migration during the regenerative process. It is suggested that RPE cells proliferate at the periphery of the RPE injury and that still-differentiating RPE cells migrate from the periphery to central injury sites to fill the lesion (Hanovice et al., 2019). To address a role for Sema3fa in RPE migration I could perform *in vivo* time lapse microscopy of RPE cells in both WT and *sema3fa* mutants following injury at 6 dpr, when proliferating cells become more evident in the central RPE (Hanovice et al., 2019). If Sema3fa is involved in RPE migration following injury, then I predict that in the *sema3fa* mutants proliferative cells would be disrupted in their migration and less efficient in filling the RPE lesion. I only tested a role for Sema3fa in RPE regeneration up to 4 dpr and so likely would have missed any role for Sema3fa in RPE migration. More longitudinal studies can be conducted in the future, as RPE injury does not fully heal in zebrafish until 1 to 2 weeks post-removal from MTZ (Hanovice et al., 2019).

There are many different RPE injury models, each with its own strengths and weaknesses. For example, sodium iodate injections induce oxidative stress in RPE cells resulting in cell death, however, injury responses vary, and the injury may not be entirely specific to RPE (George et al.,

2021). Laser photocoagulation injures both the RPE and retina instantly and robustly but does not simulate the degradation of RPE as seen in pathologies like AMD (George et al., 2021). "Genetic ablation" like that in the NTR-MTZ injury zebrafish model appears to cause RPE-specific acute damage, with secondary degradation of the underlying photoreceptors, a phenotype that emulates AMD (George et al., 2021). I believe that this latter injury method is the most effective because it most closely represents the pathology of AMD and that more research needs to be done to be able to accurately characterize the extent, time course and mechanisms of RPE injury and subsequent regeneration. In this thesis, I attempt to add to this scientific discussion. Although Sema3fa does appear to have some influence on the apoptotic response following RPE injury, it does not appear to be critical to RPE injury or regeneration over the first 4 days post-injury, and as such, other candidate genes should be considered for future research. My work in Chapter 4 starts to identify candidate RPE genes. By contributing to our understanding of Sema3fa, and its influence on RPE injury and subsequent regeneration, I hope to provide a greater understanding of the molecular mechanisms that underlie RPE regeneration, which will hopefully allow us to treat certain retinal diseases in humans in the future.

5.2 Candidate regulators of RPE regeneration

I find that mRNAs for *bmp7b, caska, foxm1, her4.1, msnb, rpe65a, trpm7,* and *vrk1* all exhibit some increase in the retina or RPE following MTZ-mediated RPE injury. Most of these genes (with the exception of *her4.1* and *rpe65a*) are known to regulate cell growth/proliferation, which is consistent with the need for RPE cells to divide and differentiate after injury to fill in the lesion site. In the RPE development/function subgroup, two of the four candidates did not seem to exhibit any change in expression post-injury (*col4a6* and *otx2b*). This latter observation suggests

that the expression of some developmentally important genes does not appear to be upregulated when new RPE cells are generated after RPE injury. Thus, new, non-development signaling pathways may be activated in response to RPE injury. An example of another developmental candidate gene would be vimentin (*vim*), a wound healing gene that encodes an intermediate filament protein; *vim* functions in zebrafish retina and nervous system development, and is upregulated in response to brain injury in rats (Cerdà et al., 1998; Malik et al., 2011). It is also found in developing human RPE *in vitro,* but not *in vivo* (Hunt & Davis, 1990). Additionally, ephrin receptor b 3b (*ephb3b*) is found in the developing zebrafish retina (including RPE) and liver, and appears to be upregulated following retinal injury in rat glaucoma models (Cayuso et al., 2016; Liu et al., 2018; Wagle et al., 2004). By studying how other developmentally important genes respond following RPE injury, we can test the extent to which RPE regeneration either does or does not mimic development.

The RPE in the regeneration model can be divided into four spatial zones: peripheral, differentiated, transition zone, and injury site (Hanovice et al., 2019). The injury itself was characterized as having three temporal phases: early (1 dpr), peak (3 dpr), and late (6 dpr) (Leach et al., 2021), with complete regeneration of the RPE occurring by 2 weeks post-injury (Hanovice et al., 2019). In the early phase or near the injury site, we would expect upregulation of inflammatory genes. Then as the inflammation abates, proliferation, migration, and differentiation occur, but the exact timeline of these events remains unclear. A better understanding of the cellular events of the complete regeneration process is needed if we are to understand the molecular basis of RPE regeneration. Note that I only performed my expression analysis at one time point, 6 dpf/0 dpr, which is directly after removal of larvae from the MTZ and at the peak of apoptosis. Perhaps some of my candidate genes show little or modest regulation because they participate in later

events in the regenerative process, and so FISH might exhibit more robust changes at later time points post-injury. For instance, *claudin7b* (*cldn7b*), a gene that encodes a multifunctional protein that maintains apical tight junction barrier integrity and epithelial cell polarity in zebrafish, is only required in late-phase RPE regeneration (Lu et al., 2023). In the future I could address this problem by comparing the expression of candidate genes at multiple time points, to capture the involvement of different genes responsible at distinct points in the injury and subsequent repair process.

scRNA-seq data is a valuable approach for observing transcriptomics of specific cell types, and is quickly becoming a fundamental tool in molecular and genetic research. A caveat of this tool, however, is that for cells that have small numbers within a tissue, such as the RPE monolayer, there is a small sample size of cells for annotation and transcriptomic analysis. A small sample size cannot accurately represent the entire RPE population and account for the probability of variety and small transcriptomic changes. Unfortunately, RPE data is often excluded from retinal scRNA-seq data sets, because researchers often remove the RPE when surgically removing eyes for mRNA isolation. One possible solution would be to dissect out the RPE layer after enucleation to perform scRNA-seq on the RPE layer only. However, this approach would require delicate microdissection of RPE from many eyes to obtain enough RPE cells for a significant scRNA-seq sample size. Another possibility to isolate zebrafish RPE cells would be fluorescence-activated cell sorting (FACS) using the Higdon model, which would sort and retain eGFP-positive RPE cells from the transgenic fish (Higdon et al., 2013). Cell sorting would allow for specific RPE cell capture, but would not account for potential subtypes of RPE cells that do not express *rpe65a*, like the CMZ-associated peripheral RPE, thus disregarding a potential important regenerative niche. Neither solution is perfect, with manual dissection being time-consuming and potentially non-specific and FACS being too specific and potentially omitting important RPE subgroups. With either method I

could perform scRNA-seq on RPE cells isolated from control and injured RPE, to identify differentially expressed genes. I would choose to do two timepoints: 1 dpr and 6 dpr. This is because these timepoints are representative of early and late stage RPE regeneration. I would be able to compare both the upregulation of genes in injured RPE to the control, uninjured RPE, and at the different timepoints to observe temporal differences in gene regulation following RPE injury.

Of the genes that I studied in this thesis, the two most interesting to me were *msnb* and *trpm7*. I provide FISH evidence to suggest that *msnb* has increased expression in the central RPE post-injury. I chose *msnb* because it has robust expression in the RPE from a previously published zebrafish embryonic scRNA-seq dataset (Farnsworth et al., 2021). Additionally, MSNB is involved in MET, which may occur in RPE regeneration, but is not yet well characterized (Sipos & Galamb, 2012; Zhou et al., 2020). EMT of RPE cells is also observed, and occurs due to aging, loss of tight junctions, misfolded protein accumulation and inflammation: the epithelial cell phenotype of the RPE becomes dysfunctional and leads to RPE cells adopting a mesenchymal phenotype (Zhou et al., 2020). This process occurs in AMD and PVR, two diseases that involve dysfunction of the normal RPE phenotype (Zhou et al., 2020). It would then be of interest to study if zebrafish use MET pathways to generate a functional RPE layer post-injury, and if Msnb among others, is involved in this transition. One possibility is to generate a conditional *msnb* knock-out fish line, with *msnb* being conditionally knocked out in RPE cells following heat shock regulated expression of a guide RNA. Heat-shock-induced gene ablation has been successful to temporally inactivate tyrosinase in zebrafish (Le et al., 2007; Wu & Wang, 2020), so a similar technique could potentially be used to temporally inactivate *msnb* following RPE injury. Clarifying the role of MET-involved genes in RPE regeneration may begin to provide targets for future experiments in animal models to better understand diseases such as AMD and PVR.

Another interesting gene is *trpm7.* In this thesis, I provide evidence to suggest that *trpm7* has increased expression in the ONL and the peripheral RPE post-injury. I chose *trpm7* because of its known involvement in the PI3K-Akt-mTOR pathway, which is required for RPE regeneration (Lee et al., 2020; Lu et al., 2022). *trpm7* has not been yet studied in the context of RPE regeneration. Peripheral RPE, where *trpm7* expression seems to increase after injury, is an understudied region of the RPE (Miles & Tropepe, 2021). I suggest that this outer section of the RPE, next to the CMZ, may contain RPE progenitors that in zebrafish produce new RPE cells as the eye grows through the lifespan of the fish, and can also proliferate in response to RPE injury. This CMZ-associated area is pigmented, which suggests that it is part of the RPE and not the CMZ, and RPE regeneration is known to occur in a peripheral to central fashion (Hanovice et al., 2019). My data with *trpm7* supports the idea that certain RPE clusters in our 5 dpf scRNA-seq data relate to RPE progenitors, an idea a MSc student in the lab is exploring. If the peripheral RPE is in fact a niche for readily proliferating RPE cells, then this would add to our knowledge on RPE regeneration in the zebrafish retina. To further explore this idea, I could employ an mCherry *trpm7* reporter line bred onto the MTZ line to follow *trpm7*-expressing cells and their progeny following RPE injury to observe if peripheral RPE expressing *trpm7* proliferates to fill in lesions. By using a laser-induced gene operator heat-shock system that has been developed to precisely label a single cell and its progeny in the zebrafish brain (He et al., 2020), future experiments could explore not only *trpm7*-expressing daughter cells in the RPE, but also other genes that may impact RPE regeneration.

If I were to repeat my candidate screen, I would maintain the same three criteria for selection. I would, however, be more specific for RPE injury in the zebrafish model when I defined the genes that I intended to screen. I could do so by first conducting bulk RNA-seq on surgically

or FACS isolated zebrafish RPE that underwent control and MTZ-induced RPE injury to identify upregulated genes post-injury, and build off pathways already implicated in RPE regeneration. For example, I would look at other genes involved in the Wnt and mTOR pathways, as these are known to be essential for RPE regeneration (Hanovice et al., 2019; Lu et al., 2022), to uncover which of the specific genes within these pathways are most influential in RPE regeneration. Additionally, the immune response appears to be a critical regulator of RPE regeneration in zebrafish, with RPE expressing immune-related genes post-injury (Leach et al., 2021). I would further explore some immune-related genes that influence macrophage/microglia cell response such as: *cxcl18b, il11b, il34,* and *saa* (Leach et al., 2021). These genes have been identified via bulk RNA-seq to be upregulated in the zebrafish RPE post MTZ-mediated injury, but their expression has not yet been spatially characterized in the injured RPE. I am satisfied with my three criteria established for candidate genes and I believe that FISH was the most appropriate approach to quickly identify if these candidate genes were present in the RPE or upregulated post-injury. I was able to identify 8 of my 10 candidate genes as having some kind of upregulation following injury, with *msnb* and *trpm7* having the most potential for future research.

5.3 Significance

I present in this thesis data to suggest a role for Sema3f involvement in RPE regeneration in zebrafish. Specifically, my data suggest Sema3f promotes RPE cell survival after injury and limits the proliferative response; loss of Sema3fa appears to result in a delay and increase in apoptosis as well as induce an initial increase in proliferation in the RPE post-injury. In addition to the reported anti-angiogenic role of Sema3fa in maintaining an avascular outer retina (Halabi et al., 2021), a possible interesting role of Sema3fa to explore in the future is as a suppressor of

immune responses post-injury; increased inflammation that might be present with Sema3fa loss would result in delayed and increased apoptosis, as it does in RPE and colon cells (Leach et al., 2021; Prieto et al., 2020; Wang et al., 2012).

Second, I provide an initial assessment of the involvement of additional pathways in zebrafish RPE regeneration. These pathways impact cell growth and/or proliferation or normal RPE function/development and are expressed within the RPE. Genes that may show changes in expression post-injury *bmp7b, caska*, *foxm1, her4.1, msnb, rpe65a, trpm7,* and *vrk1*. Future work could include using loss-of-function approaches in the RPE injury model to determine potential roles of these genes in RPE regeneration.

My data further supports the growing literature of Sema signalling in non-guidance-related functions as well as the genes and mechanisms involved in intrinsic RPE regeneration in zebrafish. In the long-term, this work may impact gene therapies for patients suffering from retinal degenerative diseases.

REFERENCES

Aigrot, M. S., Barthelemy, C., Moyon, S., Dufayet-Chaffaud, G., Izagirre-Urizar, L., Gillet-Legrand, B., . . . Tepavčević, V. (2022). Genetically modified macrophages accelerate myelin repair. *EMBO Mol Med*, *14*(8), e14759. https://doi.org/10.15252/emmm.202114759

Alto, L. T., & Terman, J. R. (2017). Semaphorins and their Signaling Mechanisms. *Methods Mol Biol*, *1493*, 1-25. https://doi.org/10.1007/978-1-4939-6448-2_1

Avanesov, A., & Malicki, J. (2010). Analysis of the retina in the zebrafish model. *Methods Cell Biol*, *100*, 153-204. https://doi.org/10.1016/B978-0-12-384892-5.00006-2

Bai, X., Dilworth, D. J., Weng, Y. C., & Gould, D. B. (2009). Developmental distribution of collagen IV isoforms and relevance to ocular diseases. *Matrix Biol*, *28*(4), 194-201. https://doi.org/10.1016/j.matbio.2009.02.004

Bernardos, R. L., Barthel, L. K., Meyers, J. R., & Raymond, P. A. (2007). Late-stage neuronal progenitors in the retina are radial Müller glia that function as retinal stem cells. *J Neurosci*, *27*(26), 7028-7040. https://doi.org/10.1523/JNEUROSCI.1624-07.2007

Bonilha, V. L. (2014). Retinal pigment epithelium (RPE) cytoskeleton in vivo and in vitro. *Exp Eye Res*, *126*, 38-45. https://doi.org/10.1016/j.exer.2013.09.015

Bonilha, V. L., Bhattacharya, S. K., West, K. A., Sun, J., Crabb, J. W., Rayborn, M. E., & Hollyfield, J. G. (2004). Proteomic characterization of isolated retinal pigment epithelium microvilli. *Mol Cell Proteomics*, *3*(11), 1119-1127. https://doi.org/10.1074/mcp.M400106-MCP200

Bradford, Y., Van Slyke, C., Ruzicka, L., Singer, A., Eagle, A., Fashena, D., . . . Westerfield, M. (2022). Zebrafish information network, the knowledgebase for Danio rerio research [Article]. *Genetics*, *220*(4). https://doi.org/10.1093/genetics/iyac016

Brend, T., & Holley, S. A. (2009). Zebrafish whole mount high-resolution double fluorescent in situ hybridization. *J Vis Exp*(25). https://doi.org/10.3791/1229

Buehler, A., Sitaras, N., Favret, S., Bucher, F., Berger, S., Pielen, A., . . . Stahl, A. (2013). Semaphorin 3F forms an anti-angiogenic barrier in outer retina. *FEBS Lett*, *587*(11), 1650-1655. https://doi.org/10.1016/j.febslet.2013.04.008

Butler, J. M., Supharattanasitthi, W., Yang, Y. C., & Paraoan, L. (2021). RNA-seq analysis of ageing human retinal pigment epithelium: Unexpected up-regulation of visual cycle gene transcription. *J Cell Mol Med*, *25*(12), 5572-5585. https://doi.org/10.1111/jcmm.16569

Cai, X., Conley, S. M., & Naash, M. I. (2009). RPE65: role in the visual cycle, human retinal disease, and gene therapy. *Ophthalmic Genet*, *30*(2), 57-62. https://doi.org/10.1080/13816810802626399

Callander, D. C., Lamont, R. E., Childs, S. J., & McFarlane, S. (2007). Expression of multiple class three semaphorins in the retina and along the path of zebrafish retinal axons. *Dev Dyn*, *236*(10), 2918-2924. https://doi.org/10.1002/dvdy.21315

Campillo-Marcos, I., & Lazo, P. A. (2018). Implication of the VRK1 chromatin kinase in the signaling responses to DNA damage: a therapeutic target? *Cell Mol Life Sci*, *75*(13), 2375-2388. https://doi.org/10.1007/s00018-018-2811-2

Carrasco Apolinario, M. E., Umeda, R., Teranishi, H., Shan, M., Phurpa, Sebastian, W. A., . . . Hanada, R. (2023). Behavioral and neurological effects of Vrk1 deficiency in zebrafish. *Biochem Biophys Res Commun*, *675*, 10-18. https://doi.org/10.1016/j.bbrc.2023.07.005

Cayuso, J., Dzementsei, A., Fischer, J. C., Karemore, G., Caviglia, S., Bartholdson, J., . . . Ober, E. A. (2016). EphrinB1/EphB3b Coordinate Bidirectional Epithelial-Mesenchymal Interactions Controlling Liver Morphogenesis and Laterality. *Dev Cell*, *39*(3), 316-328. https://doi.org/10.1016/j.devcel.2016.10.009

Cechmanek, P. B., & McFarlane, S. (2017). Retinal pigment epithelium expansion around the neural retina occurs in two separate phases with distinct mechanisms. *Dev Dyn*, *246*(8), 598-609. https://doi.org/10.1002/dvdy.24525

Cerdà, J., Conrad, M., Markl, J., Brand, M., & Herrmann, H. (1998). Zebrafish vimentin: molecular characterization, assembly properties and developmental expression. *Eur J Cell Biol*, *77*(3), 175-187. https://doi.org/10.1016/S0171-9335(98)80105-2

Charan, J., & Kantharia, N. D. (2013). How to calculate sample size in animal studies? *J Pharmacol Pharmacother*, *4*(4), 303-306. https://doi.org/10.4103/0976-500X.119726

Chhetri, J., Jacobson, G., & Gueven, N. (2014). Zebrafish--on the move towards ophthalmological research. *Eye (Lond)*, *28*(4), 367-380. https://doi.org/10.1038/eye.2014.19

Chiba, C. (2014). The retinal pigment epithelium: an important player of retinal disorders and regeneration. *Exp Eye Res*, *123*, 107-114. https://doi.org/10.1016/j.exer.2013.07.009

Choudhary, P., Dodsworth, B. T., Sidders, B., Gutteridge, A., Michaelides, C., Duckworth, J. K., . . . Benn, C. L. (2015). A FOXM1 Dependent Mesenchymal-Epithelial Transition in Retinal Pigment Epithelium Cells. *PLoS One*, *10*(6), e0130379. https://doi.org/10.1371/journal.pone.0130379

Christie, S. M., Hao, J., Tracy, E., Buck, M., Yu, J. S., & Smith, A. W. (2021). Interactions between semaphorins and plexin-neuropilin receptor complexes in the membranes of live cells. *J Biol Chem*, *297*(2), 100965. https://doi.org/10.1016/j.jbc.2021.100965

Cohen, G. M. (1997). Caspases: the executioners of apoptosis. *Biochem J*, *326 (Pt 1)*(Pt 1), 1-16. https://doi.org/10.1042/bj3260001

Cole, L. K., & Ross, L. S. (2001). Apoptosis in the developing zebrafish embryo. *Dev Biol*, *240*(1), 123-142. https://doi.org/10.1006/dbio.2001.0432

Cristofoli, F., Devriendt, K., Davis, E., Van Esch, H., & Vermeesch, J. (2018). Novel CASK mutations in cases with syndromic microcephaly [Article]. *Human Mutation*, *39*(7), 993-1001. https://doi.org/10.1002/humu.23536

Curado, S., Anderson, R. M., Jungblut, B., Mumm, J., Schroeter, E., & Stainier, D. Y. (2007). Conditional targeted cell ablation in zebrafish: a new tool for regeneration studies. *Dev Dyn*, *236*(4), 1025-1035. https://doi.org/10.1002/dvdy.21100

Curado, S., Stainier, D. Y., & Anderson, R. M. (2008). Nitroreductase-mediated cell/tissue ablation in zebrafish: a spatially and temporally controlled ablation method with applications in developmental and regeneration studies. *Nat Protoc*, *3*(6), 948-954. https://doi.org/10.1038/nprot.2008.58

D'Souza, B., Meloty-Kapella, L., & Weinmaster, G. (2010). Canonical and non-canonical Notch ligands. *Curr Top Dev Biol*, *92*, 73-129. https://doi.org/10.1016/S0070-2153(10)92003-6

da Silva, M. S., Muñoz, P. A. M., Armelin, H. A., & Elias, M. C. (2017). Differences in the Detection of BrdU/EdU Incorporation Assays Alter the Calculation for G1, S, and G2 Phases of the Cell Cycle in Trypanosomatids. *J Eukaryot Microbiol*, *64*(6), 756-770. https://doi.org/10.1111/jeu.12408

Dias, M. F., Joo, K., Kemp, J. A., Fialho, S. L., da Silva Cunha, A., Woo, S. J., & Kwon, Y. J. (2018). Molecular genetics and emerging therapies for retinitis pigmentosa: Basic

research and clinical perspectives. *Prog Retin Eye Res*, *63*, 107-131. https://doi.org/10.1016/j.preteyeres.2017.10.004
Diermeier-Daucher, S., Clarke, S. T., Hill, D., Vollmann-Zwerenz, A., Bradford, J. A., & Brockhoff, G. (2009). Cell type specific applicability of 5-ethynyl-2'-deoxyuridine (EdU) for dynamic proliferation assessment in flow cytometry. *Cytometry A*, *75*(6), 535-546. https://doi.org/10.1002/cyto.a.20712
Dong, X. R., Wan, S. M., Zhou, J. J., Nie, C. H., Chen, Y. L., Diao, J. H., & Gao, Z. X. (2022). Functional Differentiation of BMP7 Genes in Zebrafish: . *Front Cell Dev Biol*, *10*, 838721. https://doi.org/10.3389/fcell.2022.838721
Euler, T., Haverkamp, S., Schubert, T., & Baden, T. (2014). Retinal bipolar cells: elementary building blocks of vision. *Nat Rev Neurosci*, *15*(8), 507-519. https://doi.org/10.1038/nrn3783
Farnsworth, D. R., Posner, M., & Miller, A. C. (2021). Single cell transcriptomics of the developing zebrafish lens and identification of putative controllers of lens development. *Exp Eye Res*, *206*, 108535. https://doi.org/10.1016/j.exer.2021.108535
Fogerty, J., Song, P., Boyd, P., Grabinski, S. E., Hoang, T., Reich, A., . . . Perkins, B. D. (2022). Notch Inhibition Promotes Regeneration and Immunosuppression Supports Cone Survival in a Zebrafish Model of Inherited Retinal Dystrophy. *J Neurosci*, *42*(26), 5144-5158. https://doi.org/10.1523/JNEUROSCI.0244-22.2022
Ford, K. M., Saint-Geniez, M., Walshe, T., Zahr, A., & D'Amore, P. A. (2011). Expression and role of VEGF in the adult retinal pigment epithelium. *Invest Ophthalmol Vis Sci*, *52*(13), 9478-9487. https://doi.org/10.1167/iovs.11-8353
Frick, K. D., Gower, E. W., Kempen, J. H., & Wolff, J. L. (2007). Economic impact of visual impairment and blindness in the United States. *Arch Ophthalmol*, *125*(4), 544-550. https://doi.org/10.1001/archopht.125.4.544
Fuhrmann, S. (2010). Eye morphogenesis and patterning of the optic vesicle. *Curr Top Dev Biol*, *93*, 61-84. https://doi.org/10.1016/B978-0-12-385044-7.00003-5
Fuhrmann, S., Zou, C., & Levine, E. M. (2014). Retinal pigment epithelium development, plasticity, and tissue homeostasis. *Exp Eye Res*, *123*, 141-150. https://doi.org/10.1016/j.exer.2013.09.003
Gao, F., Tom, E., Lieffrig, S. A., Finnemann, S. C., & Skowronska-Krawczyk, D. (2023). A novel quantification method for retinal pigment epithelium phagocytosis using a very-long-chain polyunsaturated fatty acids-based strategy. *Front Mol Neurosci*, *16*, 1279457. https://doi.org/10.3389/fnmol.2023.1279457
Gardiner, K. L., Downs, L., Berta-Antalics, A. I., Santana, E., Aguirre, G. D., & Genini, S. (2016). Photoreceptor proliferation and dysregulation of cell cycle genes in early onset inherited retinal degenerations. *BMC Genomics*, *17*, 221. https://doi.org/10.1186/s12864-016-2477-9
George, S. M., Lu, F., Rao, M., Leach, L. L., & Gross, J. M. (2021). The retinal pigment epithelium: Development, injury responses, and regenerative potential in mammalian and non-mammalian systems. *Prog Retin Eye Res*, *85*, 100969. https://doi.org/10.1016/j.preteyeres.2021.100969
Gheorghe, A., Mahdi, L., & Musat, O. (2015). AGE-RELATED MACULAR DEGENERATION. *Rom J Ophthalmol*, *59*(2), 74-77.
Goldman, D. (2014). Müller glial cell reprogramming and retina regeneration. *Nat Rev Neurosci*, *15*(7), 431-442. https://doi.org/10.1038/nrn3723

Golestaneh, N., Chu, Y., Xiao, Y. Y., Stoleru, G. L., & Theos, A. C. (2017). Dysfunctional autophagy in RPE, a contributing factor in age-related macular degeneration. *Cell Death Dis*, *8*(1), e2537. https://doi.org/10.1038/cddis.2016.453

Gur, D., Nicolas, J. D., Brumfeld, V., Bar-Elli, O., Oron, D., & Levkowitz, G. (2018). The Dual Functional Reflecting Iris of the Zebrafish. *Adv Sci (Weinh)*, *5*(8), 1800338. https://doi.org/10.1002/advs.201800338

Guttmann-Raviv, N., Shraga-Heled, N., Varshavsky, A., Guimaraes-Sternberg, C., Kessler, O., & Neufeld, G. (2007). Semaphorin-3A and semaphorin-3F work together to repel endothelial cells and to inhibit their survival by induction of apoptosis. *J Biol Chem*, *282*(36), 26294-26305. https://doi.org/10.1074/jbc.M609711200

Halabi, R. (2019). *Semaphorin3f as a Spatial Regulator of Embryogenesis* University of Calgary]. Calgary, AB.

Halabi, R., Watterston, C., Hehr, C. L., Mori-Kreiner, R., Childs, S. J., & McFarlane, S. (2021). Semaphorin 3fa Controls Ocular Vascularization From the Embryo Through to the Adult. *Invest Ophthalmol Vis Sci*, *62*(2), 21. https://doi.org/10.1167/iovs.62.2.21

Han, J. W., Lyu, J., Park, Y. J., Jang, S. Y., & Park, T. K. (2015). Wnt/β-Catenin Signaling Mediates Regeneration of Retinal Pigment Epithelium After Laser Photocoagulation in Mouse Eye. *Invest Ophthalmol Vis Sci*, *56*(13), 8314-8324. https://doi.org/10.1167/iovs.15-18359

Hanovice, N. J., Leach, L. L., Slater, K., Gabriel, A. E., Romanovicz, D., Shao, E., . . . Gross, J. M. (2019). Regeneration of the zebrafish retinal pigment epithelium after widespread genetic ablation. *PLoS Genet*, *15*(1), e1007939. https://doi.org/10.1371/journal.pgen.1007939

He, S., Tian, Y., Feng, S., Wu, Y., Shen, X., Chen, K., . . . Qu, J. Y. (2020). In vivo single-cell lineage tracing in zebrafish using high-resolution infrared laser-mediated gene induction microscopy. *Elife*, *9*. https://doi.org/10.7554/eLife.52024

Hehr, C. L., Halabi, R., & McFarlane, S. (2022). Spatial regulation of amacrine cell genesis by Semaphorin 3f. *Dev Biol*, *491*, 66-81. https://doi.org/10.1016/j.ydbio.2022.08.008

Hernández-Núñez, I., Quelle-Regaldie, A., Sánchez, L., Adrio, F., Candal, E., & Barreiro-Iglesias, A. (2021). Decline in Constitutive Proliferative Activity in the Zebrafish Retina with Ageing. *Int J Mol Sci*, *22*(21). https://doi.org/10.3390/ijms222111715

Higdon, C. W., Mitra, R. D., & Johnson, S. L. (2013). Gene expression analysis of zebrafish melanocytes, iridophores, and retinal pigmented epithelium reveals indicators of biological function and developmental origin. *PLoS One*, *8*(7), e67801. https://doi.org/10.1371/journal.pone.0067801

Hoang, T., Kim, D. W., Appel, H., Pannullo, N. A., Leavey, P., Ozawa, M., . . . Blackshaw, S. (2022). Genetic loss of function of Ptbp1 does not induce glia-to-neuron conversion in retina. *Cell Rep*, *39*(11), 110849. https://doi.org/10.1016/j.celrep.2022.110849

Hsueh, Y. P. (2006). The role of the MAGUK protein CASK in neural development and synaptic function. *Curr Med Chem*, *13*(16), 1915-1927. https://doi.org/10.2174/092986706777585040

Hu, L., & Xu, G. (2021). Potential Protective Role of TRPM7 and Involvement of PKC/ERK Pathway in Blue Light-Induced Apoptosis in Retinal Pigment Epithelium Cells in Vitro. *Asia Pac J Ophthalmol (Phila)*, *10*(6), 572-578. https://doi.org/10.1097/APO.0000000000000447

Hunt, R. C., & Davis, A. A. (1990). Altered expression of keratin and vimentin in human retinal pigment epithelial cells in vivo and in vitro. *J Cell Physiol*, *145*(2), 187-199. https://doi.org/10.1002/jcp.1041450202
Idrees, S., Sridhar, J., & Kuriyan, A. E. (2019). Proliferative Vitreoretinopathy: A Review. *Int Ophthalmol Clin*, *59*(1), 221-240. https://doi.org/10.1097/IIO.0000000000000258
Jackson, G. R., Owsley, C., & Curcio, C. A. (2002). Photoreceptor degeneration and dysfunction in aging and age-related maculopathy. *Ageing Res Rev*, *1*(3), 381-396. https://doi.org/10.1016/s1568-1637(02)00007-7
Jackson, R. E., & Eickholt, B. J. (2009). Semaphorin signalling. *Curr Biol*, *19*(13), R504-507. https://doi.org/10.1016/j.cub.2009.04.055
Jansen, C., Sahni, J., Suzuki, S., Horgen, F. D., Penner, R., & Fleig, A. (2016). The coiled-coil domain of zebrafish TRPM7 regulates Mg·nucleotide sensitivity. *Sci Rep*, *6*, 33459. https://doi.org/10.1038/srep33459
Javed, A., & Cayouette, M. (2017). Temporal Progression of Retinal Progenitor Cell Identity: Implications in Cell Replacement Therapies. *Front Neural Circuits*, *11*, 105. https://doi.org/10.3389/fncir.2017.00105
Kampik, D., Basche, M., Luhmann, U. F. O., Nishiguchi, K. M., Williams, J. A. E., Greenwood, J., . . . Ali, R. R. (2017). In situ regeneration of retinal pigment epithelium by gene transfer of E2F2: a potential strategy for treatment of macular degenerations. *Gene Ther*, *24*(12), 810-818. https://doi.org/10.1038/gt.2017.89
Karagiosis, S., & Ready, D. (2004). Moesin contributes an essential structural role in Drosophila photoreceptor morphogenesis [Article]. *Development*, *131*(4), 725-732. https://doi.org/10.1242/dev.00976
Kerr, A., Patel, P. A., LaConte, L. E. W., Liang, C., Chen, C. K., Shah, V., . . . Mukherjee, K. (2019). Non-Cell Autonomous Roles for CASK in Optic Nerve Hypoplasia. *Invest Ophthalmol Vis Sci*, *60*(10), 3584-3594. https://doi.org/10.1167/iovs.19-27197
Klöditz, K., & Fadeel, B. (2019). Three cell deaths and a funeral: macrophage clearance of cells undergoing distinct modes of cell death. *Cell Death Discov*, *5*, 65. https://doi.org/10.1038/s41420-019-0146-x
Komiya, Y., & Habas, R. (2008). Wnt signal transduction pathways. *Organogenesis*, *4*(2), 68-75. https://doi.org/10.4161/org.4.2.5851
Kongsema, M., Wongkhieo, S., Khongkow, M., Lam, E. W., Boonnoy, P., Vongsangnak, W., & Wong-Ekkabut, J. (2019). Molecular mechanism of Forkhead box M1 inhibition by thiostrepton in breast cancer cells. *Oncol Rep*, *42*(3), 953-962. https://doi.org/10.3892/or.2019.7225
Kovach, J. L., Schwartz, S. G., Flynn, H. W., & Scott, I. U. (2012). Anti-VEGF Treatment Strategies for Wet AMD. *J Ophthalmol*, *2012*, 786870. https://doi.org/10.1155/2012/786870
Kwon, W., & Freeman, S. A. (2020). Phagocytosis by the Retinal Pigment Epithelium: Recognition, Resolution, Recycling. *Front Immunol*, *11*, 604205. https://doi.org/10.3389/fimmu.2020.604205
Lagnado, L. (1998). Retinal processing: amacrine cells keep it short and sweet. *Curr Biol*, *8*(17), R598-600. https://doi.org/10.1016/s0960-9822(98)70385-9
Lambaerts, K., Van Dyck, S., Mortier, E., Ivarsson, Y., Degeest, G., Luyten, A., . . . Zimmermann, P. (2012). Syntenin, a syndecan adaptor and an Arf6 phosphatidylinositol 4,5-bisphosphate effector, is essential for epiboly and gastrulation cell movements in

zebrafish [Article]. *Journal of Cell Science*, *125*(5), 1129-1140. https://doi.org/10.1242/jcs.089987

Landreville, S., Lupien, C. B., Vigneault, F., Gaudreault, M., Mathieu, M., Rousseau, A. P., . . . Salesse, C. (2011). Identification of differentially expressed genes in uveal melanoma using suppressive subtractive hybridization. *Mol Vis*, *17*, 1324-1333.

Lane, B. M., & Lister, J. A. (2012). Otx but not Mitf transcription factors are required for zebrafish retinal pigment epithelium development. *PLoS One*, *7*(11), e49357. https://doi.org/10.1371/journal.pone.0049357

Le, X., Langenau, D. M., Keefe, M. D., Kutok, J. L., Neuberg, D. S., & Zon, L. I. (2007). Heat shock-inducible Cre/Lox approaches to induce diverse types of tumors and hyperplasia in transgenic zebrafish. *Proc Natl Acad Sci U S A*, *104*(22), 9410-9415. https://doi.org/10.1073/pnas.0611302104

Leach, L. L., Hanovice, N. J., George, S. M., Gabriel, A. E., & Gross, J. M. (2021). The immune response is a critical regulator of zebrafish retinal pigment epithelium regeneration. *Proc Natl Acad Sci U S A*, *118*(21). https://doi.org/10.1073/pnas.2017198118

Lee, E. H., Chun, S. Y., Kim, B., Yoon, B. H., Lee, J. N., Kim, B. S., . . . Ha, Y. S. (2020). Knockdown of TRPM7 prevents tumor growth, migration, and invasion through the Src, Akt, and JNK pathway in bladder cancer. *BMC Urol*, *20*(1), 145. https://doi.org/10.1186/s12894-020-00714-2

Lejoyeux, R., Benillouche, J., Ong, J., Errera, M. H., Rossi, E. A., Singh, S. R., . . . Chhablani, J. (2022). Choriocapillaris: Fundamentals and advancements. *Prog Retin Eye Res*, *87*, 100997. https://doi.org/10.1016/j.preteyeres.2021.100997

Li, J., Di, C., Jing, J., Di, Q., Nakhla, J., & Adamson, D. C. (2015). OTX2 is a therapeutic target for retinoblastoma and may function as a common factor between C-MYC, CRX, and phosphorylated RB pathways. *Int J Oncol*, *47*(5), 1703-1710. https://doi.org/10.3892/ijo.2015.3179

Li, Z., Ptak, D., Zhang, L., Walls, E. K., Zhong, W., & Leung, Y. F. (2012). Phenylthiourea specifically reduces zebrafish eye size. *PLoS One*, *7*(6), e40132. https://doi.org/10.1371/journal.pone.0040132

Liu, S. T., Zhong, S. M., Li, X. Y., Gao, F., Li, F., Zhang, M. L., . . . Wang, Z. (2018). EphrinB/EphB forward signaling in Müller cells causes apoptosis of retinal ganglion cells by increasing tumor necrosis factor alpha production in rat experimental glaucomatous model. *Acta Neuropathol Commun*, *6*(1), 111. https://doi.org/10.1186/s40478-018-0618-x

Lu, F., Leach, L. L., & Gross, J. M. (2022). mTOR activity is essential for retinal pigment epithelium regeneration in zebrafish. *PLoS Genet*, *18*(3), e1009628. https://doi.org/10.1371/journal.pgen.1009628

Lu, F., Leach, L. L., & Gross, J. M. (2023). A CRISPR-Cas9-mediated F0 screen to identify pro-regenerative genes in the zebrafish retinal pigment epithelium. *Sci Rep*, *13*(1), 3142. https://doi.org/10.1038/s41598-023-29046-5

Malik, S. Z., Motamedi, S., Royo, N. C., LeBold, D., & Watson, D. J. (2011). Identification of potentially neuroprotective genes upregulated by neurotrophin treatment of CA3 neurons in the injured brain. *J Neurotrauma*, *28*(3), 415-430. https://doi.org/10.1089/neu.2010.1487

Marmorstein, A. D. (2001). The polarity of the retinal pigment epithelium. *Traffic*, *2*(12), 867-872. https://doi.org/10.1034/j.1600-0854.2001.21202.x

Marques, A. P., Ramke, J., Cairns, J., Butt, T., Zhang, J. H., Muirhead, D., . . . Burton, M. J. (2021). Global economic productivity losses from vision impairment and blindness. *EClinicalMedicine*, *35*, 100852. https://doi.org/10.1016/j.eclinm.2021.100852

Masland, R. H. (2001). The fundamental plan of the retina. *Nat Neurosci*, *4*(9), 877-886. https://doi.org/10.1038/nn0901-877

Mazzoni, F., Safa, H., & Finnemann, S. C. (2014). Understanding photoreceptor outer segment phagocytosis: use and utility of RPE cells in culture. *Exp Eye Res*, *126*, 51-60. https://doi.org/10.1016/j.exer.2014.01.010

Mead, B., & Tomarev, S. (2016). Evaluating retinal ganglion cell loss and dysfunction. *Exp Eye Res*, *151*, 96-106. https://doi.org/10.1016/j.exer.2016.08.006

Meeker, N. D., Hutchinson, S. A., Ho, L., & Trede, N. S. (2007). Method for isolation of PCR-ready genomic DNA from zebrafish tissues. *Biotechniques*, *43*(5), 610, 612, 614. https://doi.org/10.2144/000112619

Menashe, I., Maeder, D., Garcia-Closas, M., Figueroa, J., Bhattacharjee, S., Rotunno, M., . . . Chatterjee, N. (2010). Pathway Analysis of Breast Cancer Genome-Wide Association Study Highlights Three Pathways and One Canonical Signaling Cascade [Article]. *Cancer Research*, *70*(11), 4453-4459. https://doi.org/10.1158/0008-5472.CAN-09-4502

Miles, A., & Tropepe, V. (2021). Retinal Stem Cell 'Retirement Plans': Growth, Regulation and Species Adaptations in the Retinal Ciliary Marginal Zone. *Int J Mol Sci*, *22*(12). https://doi.org/10.3390/ijms22126528

Mitra, S., Sharma, P., Kaur, S., Khursheed, M. A., Gupta, S., Ahuja, R., . . . Ramachandran, R. (2018). Histone Deacetylase-Mediated Müller Glia Reprogramming through Her4.1-Lin28a Axis Is Essential for Retina Regeneration in Zebrafish. *iScience*, *7*, 68-84. https://doi.org/10.1016/j.isci.2018.08.008

Modukuri, R. K., Monsivais, D., Li, F., Palaniappan, M., Bohren, K. M., Tan, Z., . . . Matzuk, M. M. (2023). Discovery of Highly Potent and BMPR2-Selective Kinase Inhibitors Using DNA-Encoded Chemical Library Screening. *J Med Chem*, *66*(3), 2143-2160. https://doi.org/10.1021/acs.jmedchem.2c01886

Molday, R. S., & Moritz, O. L. (2015). Photoreceptors at a glance. *J Cell Sci*, *128*(22), 4039-4045. https://doi.org/10.1242/jcs.175687

Moniz, L., Andrews, C., & Pereira, J. (2022). Canadian patient experience with age-related macular degeneration. *Investigative Ophthalmology & Visual Science*, *63*(7), 4226 – A0154.

Monte-Serrano, E., & Lazo, P. A. (2023). VRK1 Kinase Activity Modulating Histone H4K16 Acetylation Inhibited by SIRT2 and VRK-IN-1. *Int J Mol Sci*, *24*(5). https://doi.org/10.3390/ijms24054912

Moreno-Marmol, T., Cavodeassi, F., & Bovolenta, P. (2018). Setting Eyes on the Retinal Pigment Epithelium. *Front Cell Dev Biol*, *6*, 145. https://doi.org/10.3389/fcell.2018.00145

Mori-Kreiner, R. (2020a). *Semaphorin3f in the maturation of the*

outer retina University of Calgary]. Calgary, AB. https://prism.ucalgary.ca/server/api/core/bitstreams/e0d4d419-dc69-46c5-b1ee-356fc88b6e2f/content

Mori-Kreiner, R. (2020b). *Semaphorin3f in the maturation of the outer retina* University of Calgary]. Calgary, AB. https://prism.ucalgary.ca/server/api/core/bitstreams/e0d4d419-dc69-46c5-b1ee-356fc88b6e2f/content

Nadauld, L. D., Chidester, S., Shelton, D. N., Rai, K., Broadbent, T., Sandoval, I. T., . . . Jones, D. A. (2006). Dual roles for adenomatous polyposis coli in regulating retinoic acid biosynthesis and Wnt during ocular development. *Proc Natl Acad Sci U S A*, *103*(36), 13409-13414. https://doi.org/10.1073/pnas.0601634103

Nakayama, H., Bruneau, S., Kochupurakkal, N., Coma, S., Briscoe, D. M., & Klagsbrun, M. (2015). Regulation of mTOR Signaling by Semaphorin 3F-Neuropilin 2 Interactions In Vitro and In Vivo. *Sci Rep*, *5*, 11789. https://doi.org/10.1038/srep11789

Nakayama, H., Kusumoto, C., Nakahara, M., Fujiwara, A., & Higashiyama, S. (2018). Semaphorin 3F and Netrin-1: The Novel Function as a Regulator of Tumor Microenvironment. *Front Physiol*, *9*, 1662. https://doi.org/10.3389/fphys.2018.01662

Nawrot, M., West, K., Huang, J., Possin, D. E., Bretscher, A., Crabb, J. W., & Saari, J. C. (2004). Cellular retinaldehyde-binding protein interacts with ERM-binding phosphoprotein 50 in retinal pigment epithelium. *Invest Ophthalmol Vis Sci*, *45*(2), 393-401. https://doi.org/10.1167/iovs.03-0989

Osaba, M., Doro, J., Liberal, M., Lagunas, J., Kuo, I. C., & Reviglio, V. E. (2019). Relationship Between Legal Blindness and Depression. *Med Hypothesis Discov Innov Ophthalmol*, *8*(4), 306-311.

Pasterkamp, R. J., & Verhaagen, J. (2001). Emerging roles for semaphorins in neural regeneration. *Brain Res Brain Res Rev*, *35*(1), 36-54. https://doi.org/10.1016/s0165-0173(00)00050-3

Polato, F., & Becerra, S. P. (2016). Pigment Epithelium-Derived Factor, a Protective Factor for Photoreceptors in Vivo. *Adv Exp Med Biol*, *854*, 699-706. https://doi.org/10.1007/978-3-319-17121-0_93

Ponder, K. G., & Boise, L. H. (2019). The prodomain of caspase-3 regulates its own removal and caspase activation. *Cell Death Discov*, *5*, 56. https://doi.org/10.1038/s41420-019-0142-1

Powell, C., Cornblath, E., Elsaeidi, F., Wan, J., & Goldman, D. (2016). Zebrafish Müller glia-derived progenitors are multipotent, exhibit proliferative biases and regenerate excess neurons. *Sci Rep*, *6*, 24851. https://doi.org/10.1038/srep24851

Prieto, K., Lozano, M. P., Urueña, C., Alméciga-Díaz, C. J., Fiorentino, S., & Barreto, A. (2020). The delay in cell death caused by the induction of autophagy by P2Et extract is essential for the generation of immunogenic signals in melanoma cells. *Apoptosis*, *25*(11-12), 875-888. https://doi.org/10.1007/s10495-020-01643-z

Proudfit, A., Bhunia, N., Pore, D., Parker, Y., Lindner, D., & Gupta, N. (2020). Pharmacologic Inhibition of Ezrin-Radixin-Moesin Phosphorylation is a Novel Therapeutic Strategy in Rhabdomyosarcoma. *Sarcoma*, *2020*, 9010496. https://doi.org/10.1155/2020/9010496

Rein, D. B., Wittenborn, J. S., Zhang, X., Honeycutt, A. A., Lesesne, S. B., Saaddine, J., & Group, V. H. C.-E. S. (2009). Forecasting age-related macular degeneration through the year 2050: the potential impact of new treatments. *Arch Ophthalmol*, *127*(4), 533-540. https://doi.org/10.1001/archophthalmol.2009.58

Reinhardt, R., Centanin, L., Tavhelidse, T., Inoue, D., Wittbrodt, B., Concordet, J. P., . . . Wittbrodt, J. (2015). Sox2, Tlx, Gli3, and Her9 converge on Rx2 to define retinal stem cells in vivo. *EMBO J*, *34*(11), 1572-1588. https://doi.org/10.15252/embj.201490706

Russ, N., Schroder, M., Berger, B., Mandel, S., Aydogan, Y., Mauer, S., . . . Knapp, S. (2021). Design and Development of a Chemical Probe for Pseudokinase Ca2+/calmodulin-Dependent Ser/Thr Kinase [Article]. *Journal of Medicinal Chemistry*, *64*(19), 14358-14376. https://doi.org/10.1021/acs.jmedchem.1c00845

Russell, S., Bennett, J., Wellman, J., Chung, D., Yu, Z., Tillman, A., . . . Maguire, A. (2017). Efficacy and safety of voretigene neparvovec (AAV2-hRPE65v2) in patients with RPE65-mediated inherited retinal dystrophy: a randomised, controlled, open-label, phase 3 trial [Article]. *Lancet*, *390*(10097), 849-860. https://doi.org/10.1016/S0140-6736(17)31868-8

Sahay, A., Molliver, M. E., Ginty, D. D., & Kolodkin, A. L. (2003). Semaphorin 3F is critical for development of limbic system circuitry and is required in neurons for selective CNS axon guidance events. *J Neurosci*, *23*(17), 6671-6680. https://doi.org/10.1523/JNEUROSCI.23-17-06671.2003

Saxton, R. A., & Sabatini, D. M. (2017). mTOR Signaling in Growth, Metabolism, and Disease. *Cell*, *169*(2), 361-371. https://doi.org/10.1016/j.cell.2017.03.035

Schindelin, J., Arganda-Carreras, I., Frise, E., Kaynig, V., Longair, M., Pietzsch, T., . . . Cardona, A. (2012). Fiji: an open-source platform for biological-image analysis. *Nat Methods*, *9*(7), 676-682. https://doi.org/10.1038/nmeth.2019

Schultz, N. M., Bhardwaj, S., Barclay, C., Gaspar, L., & Schwartz, J. (2021). Global Burden of Dry Age-Related Macular Degeneration: A Targeted Literature Review. *Clin Ther*, *43*(10), 1792-1818. https://doi.org/10.1016/j.clinthera.2021.08.011

Shen, Y., & White, E. (2001). p53-dependent apoptosis pathways. *Adv Cancer Res*, *82*, 55-84. https://doi.org/10.1016/s0065-230x(01)82002-9

Shin, Y., Moiseyev, G., Petrukhin, K., Cioffi, C. L., Muthuraman, P., Takahashi, Y., & Ma, J. X. (2018). A novel RPE65 inhibitor CU239 suppresses visual cycle and prevents retinal degeneration. *Biochim Biophys Acta Mol Basis Dis*, *1864*(7), 2420-2429. https://doi.org/10.1016/j.bbadis.2018.04.014

Sipos, F., & Galamb, O. (2012). Epithelial-to-mesenchymal and mesenchymal-to-epithelial transitions in the colon. *World J Gastroenterol*, *18*(7), 601-608. https://doi.org/10.3748/wjg.v18.i7.601

Sodi, A., Banfi, S., Testa, F., Della Corte, M., Passerini, I., Pelo, E., . . . Group, I. I. W. (2021). RPE65-associated inherited retinal diseases: consensus recommendations for eligibility to gene therapy. *Orphanet J Rare Dis*, *16*(1), 257. https://doi.org/10.1186/s13023-021-01868-4

Soker, S., Takashima, S., Miao, H. Q., Neufeld, G., & Klagsbrun, M. (1998). Neuropilin-1 is expressed by endothelial and tumor cells as an isoform-specific receptor for vascular endothelial growth factor. *Cell*, *92*(6), 735-745. https://doi.org/10.1016/s0092-8674(00)81402-6

Steinfeld, J., Steinfeld, I., Bausch, A., Coronato, N., Hampel, M. L., Depner, H., . . . Vogel-Höpker, A. (2017). BMP-induced reprogramming of the neural retina into retinal pigment epithelium requires Wnt signalling. *Biol Open*, *6*(7), 979-992. https://doi.org/10.1242/bio.018739

Storey, S., & McFarlane, S. (Unpublished). *Muller Glia Heterogeneity: The Diversity and Function of Subtypes*. University of Calgary.

Strauss, O. (2005). The retinal pigment epithelium in visual function. *Physiol Rev*, *85*(3), 845-881. https://doi.org/10.1152/physrev.00021.2004

Sun, Y., Liegl, R., Gong, Y., Bühler, A., Cakir, B., Meng, S. S., . . . Stahl, A. (2017). Sema3f Protects Against Subretinal Neovascularization In Vivo. *EBioMedicine*, *18*, 281-287. https://doi.org/10.1016/j.ebiom.2017.03.026

Szatmári, T., & Dobra, K. (2013). The role of syndecan-1 in cellular signaling and its effects on heparan sulfate biosynthesis in mesenchymal tumors. *Front Oncol*, *3*, 310. https://doi.org/10.3389/fonc.2013.00310

Takeuchi, M., Yamaguchi, S., Yonemura, S., Kakiguchi, K., Sato, Y., Higashiyama, T., . . . Hibi, M. (2015). Type IV Collagen Controls the Axogenesis of Cerebellar Granule Cells by Regulating Basement Membrane Integrity in Zebrafish. *PLoS Genet*, *11*(10), e1005587. https://doi.org/10.1371/journal.pgen.1005587

Takke, C., Dornseifer, P., v Weizsäcker, E., & Campos-Ortega, J. A. (1999). her4, a zebrafish homologue of the Drosophila neurogenic gene E(spl), is a target of NOTCH signalling. *Development*, *126*(9), 1811-1821. https://doi.org/10.1242/dev.126.9.1811

Taylor, S. M., Alvarez-Delfin, K., Saade, C. J., Thomas, J. L., Thummel, R., Fadool, J. M., & Hitchcock, P. F. (2015). The bHLH Transcription Factor NeuroD Governs Photoreceptor Genesis and Regeneration Through Delta-Notch Signaling. *Invest Ophthalmol Vis Sci*, *56*(12), 7496-7515. https://doi.org/10.1167/iovs.15-17616

Thisse, B., Heyer, V., Lux, A., Alunni, V., Degrave, A., Seiliez, I., . . . Thisse, C. (2004). Spatial and temporal expression of the zebrafish genome by large-scale in situ hybridization screening [Review]. *Zebrafish:2nd Edition Genetics Genomics and Informatics*, *77*, 505-519.

Tran, T. S., Kolodkin, A. L., & Bharadwaj, R. (2007). Semaphorin regulation of cellular morphology. *Annu Rev Cell Dev Biol*, *23*, 263-292. https://doi.org/10.1146/annurev.cellbio.22.010605.093554

Uribe, R. A., & Gross, J. M. (2007). Immunohistochemistry on cryosections from embryonic and adult zebrafish eyes. *CSH Protoc*, *2007*, pdb.prot4779. https://doi.org/10.1101/pdb.prot4779

Valbuena, A., Sanz-García, M., López-Sánchez, I., Vega, F. M., & Lazo, P. A. (2011). Roles of VRK1 as a new player in the control of biological processes required for cell division. *Cell Signal*, *23*(8), 1267-1272. https://doi.org/10.1016/j.cellsig.2011.04.002

Vinograd-Byk, H., Renbaum, P., & Levy-Lahad, E. (2018). Vrk1 partial Knockdown in Mice Results in Reduced Brain Weight and Mild Motor Dysfunction, and Indicates Neuronal VRK1 Target Pathways. *Sci Rep*, *8*(1), 11265. https://doi.org/10.1038/s41598-018-29215-x

Wagle, M., Grunewald, B., Subburaju, S., Barzaghi, C., Le Guyader, S., Chan, J., & Jesuthasan, S. (2004). EphrinB2a in the zebrafish retinotectal system. *J Neurobiol*, *59*(1), 57-65. https://doi.org/10.1002/neu.10340

Wan, Y., Almeida, A. D., Rulands, S., Chalour, N., Muresan, L., Wu, Y., . . . Harris, W. A. (2016). The ciliary marginal zone of the zebrafish retina: clonal and time-lapse analysis of a continuously growing tissue. *Development*, *143*(7), 1099-1107. https://doi.org/10.1242/dev.133314

Wang, H., Xiao, X., Li, Z., Luo, S., Hu, L., Yi, H., . . . Liu, J. (2022). Polyphyllin VII, a novel moesin inhibitor, suppresses cell growth and overcomes bortezomib resistance in multiple myeloma. *Cancer Lett*, *537*, 215647. https://doi.org/10.1016/j.canlet.2022.215647

Wang, Y., Ma, X., Muthuraman, P., Raja, A., Jayaraman, A., Petrukhin, K., . . . Moiseyev, G. (2022). The novel visual cycle inhibitor (±)-RPE65-61 protects retinal photoreceptors from light-induced degeneration. *PLoS One*, *17*(10), e0269437. https://doi.org/10.1371/journal.pone.0269437

Wang, Y., Shen, D., Wang, V. M., Yu, C. R., Wang, R. X., Tuo, J., & Chan, C. C. (2012). Enhanced apoptosis in retinal pigment epithelium under inflammatory stimuli and oxidative stress. *Apoptosis*, *17*(11), 1144-1155. https://doi.org/10.1007/s10495-012-0750-1

Webster, M. K., Barnett, B. J., Stanchfield, M. L., Paris, J. R., Webster, S. E., Cooley-Themm, C. A., . . . Linn, C. L. (2019). Stimulation of Retinal Pigment Epithelium With an α7 nAChR Agonist Leads to Müller Glia Dependent Neurogenesis in the Adult Mammalian Retina. *Invest Ophthalmol Vis Sci*, *60*(2), 570-579. https://doi.org/10.1167/iovs.18-25722

Wilson, S. G., Wen, W., Pillai-Kastoori, L., & Morris, A. C. (2016). Tracking the fate of her4 expressing cells in the regenerating retina using her4:Kaede zebrafish. *Exp Eye Res*, *145*, 75-87. https://doi.org/10.1016/j.exer.2015.11.002

Wu, J., Gorman, A., Zhou, X., Sandra, C., & Chen, E. (2002). Involvement of caspase-3 in photoreceptor cell apoptosis induced by in vivo blue light exposure. *Invest Ophthalmol Vis Sci*, *43*(10), 3349-3354.

Wu, Y. C., & Wang, I. J. (2020). Heat-shock-induced tyrosinase gene ablation with CRISPR in zebrafish. *Mol Genet Genomics*, *295*(4), 911-922. https://doi.org/10.1007/s00438-020-01681-x

Xia, J., Swiercz, J. M., Bañón-Rodríguez, I., Matković, I., Federico, G., Sun, T., . . . Worzfeld, T. (2015). Semaphorin-Plexin Signaling Controls Mitotic Spindle Orientation during Epithelial Morphogenesis and Repair. *Dev Cell*, *33*(3), 299-313. https://doi.org/10.1016/j.devcel.2015.02.001

Yang, G., Qu, X., Zhang, J., Zhao, W., & Wang, H. (2012). Sema3F downregulates p53 expression leading to axonal growth cone collapse in primary hippocampal neurons. *Int J Clin Exp Pathol*, *5*(7), 634-641.

Yang, J. H., Le, W. D., Basinger, S. F., Wu, S. M., & Yang, C. Y. (2005). Mechanisms of apoptosis in human retinal pigment epithelium induced by TNF-alpha in conditions of heavy metal ion deficiency. *Invest Ophthalmol Vis Sci*, *46*(3), 1039-1046. https://doi.org/10.1167/iovs.04-0325

Yang, S., Zhou, J., & Li, D. (2021). Functions and Diseases of the Retinal Pigment Epithelium. *Front Pharmacol*, *12*, 727870. https://doi.org/10.3389/fphar.2021.727870

Yeo, S. Y., Kim, M., Kim, H. S., Huh, T. L., & Chitnis, A. B. (2007). Fluorescent protein expression driven by her4 regulatory elements reveals the spatiotemporal pattern of Notch signaling in the nervous system of zebrafish embryos. *Dev Biol*, *301*(2), 555-567. https://doi.org/10.1016/j.ydbio.2006.10.020

Yorston, D. (2014). Anti-VEGF drugs in the prevention of blindness. *Community Eye Health*, *27*(87), 44-46.

Yu, F., Guo, S., Li, T., Ran, J., Zhao, W., Li, D., . . . Zhou, J. (2019). Ciliary defects caused by dysregulation of O-GlcNAc modification are associated with diabetic complications. *Cell Res*, *29*(2), 171-173. https://doi.org/10.1038/s41422-018-0114-7

Yu, H. H., & Moens, C. B. (2005). Semaphorin signaling guides cranial neural crest cell migration in zebrafish. *Dev Biol*, *280*(2), 373-385. https://doi.org/10.1016/j.ydbio.2005.01.029

Zhang, S. S., Hu, J. Q., Liu, X. H., Chen, L. X., Chen, H., Guo, X. H., & Huang, Q. B. (2020). Role of Moesin Phosphorylation in Retinal Pericyte Migration and Detachment Induced by Advanced Glycation Endproducts. *Front Endocrinol (Lausanne)*, *11*, 603450. https://doi.org/10.3389/fendo.2020.603450

Zheng, L., Hill, J., Rumi, M. A. K., & Zheng, X. L. (2022). A Simple, Robust, and Cost-effective Method for Genotyping Small-scale Mutations. *J Clin Transl Pathol*, *2*(3), 108-115. https://doi.org/10.14218/JCTP.2022.00014

Zhou, M., Geathers, J. S., Grillo, S. L., Weber, S. R., Wang, W., Zhao, Y., & Sundstrom, J. M. (2020). Role of Epithelial-Mesenchymal Transition in Retinal Pigment Epithelium Dysfunction. *Front Cell Dev Biol*, *8*, 501. https://doi.org/10.3389/fcell.2020.00501

Zou, Z., Tao, T., Li, H., & Zhu, X. (2020). mTOR signaling pathway and mTOR inhibitors in cancer: progress and challenges. *Cell Biosci*, *10*, 31. https://doi.org/10.1186/s13578-020-00396-1

Zuppo, D. A., Missinato, M. A., Santana-Santos, L., Li, G., Benos, P. V., & Tsang, M. (2023). Foxm1 regulates cardiomyocyte proliferation in adult zebrafish after cardiac injury. *Development*, *150*(6). https://doi.org/10.1242/dev.201163

APPENDIX

Table 2 Raw data for percent GFP fluorescence

	0 dpr/6 dpf			1 dpr/7 dpf			3 dpr/9 dpf		
	mean	**SD**	**n**	**mean**	**SD**	**n**	**mean**	**SD**	**n**
Control WT	94.273	5.569	11	90.125	6.289	8	92.571	3.645	7
Control mutant	97.273	2.370	11	95.750	2.252	8	87.750	7.536	8
Injured WT	73.800	9.414	10	60.286	25.663	7	46.609	22.107	10
Injured mutant	70.626	12.746	11	56.125	12.194	8	65.571	17.624	7

Table 3 Raw data for aCsp3 counts

	0 dpr/6 dpf			1 dpr/7 dpf			3 dpr/9 dpf		
	mean	**SD**	**n**	**mean**	**SD**	**n**	**mean**	**SD**	**n**
Control WT	0.121	0.225	11	0.250	0.236	8	0.095	0.163	7
Control mutant	1.318	1.383	11	0.500	0.471	8	0.250	0.463	8
Injured WT	0.850	2.052	10	1.167	0.726	7	1.000	0.861	10
Injured mutant	2.242	4.681	11	0.926	1.152	9	4.944	4.494	7

Table 4 Raw data for RPE EdU counts

	0 dpr/6 dpf			2 dpr/8 dpf			4 dpr/10 dpf		
	mean	**SD**	**n**	**mean**	**SD**	**n**	**mean**	**SD**	**n**
Control WT	0.708	1.119	8	0.000	0.000	8	0.000	0.000	9
Control mutant	0.429	0.371	7	0.037	0.111	9	0.000	0.000	10
Injured WT	0.200	0.233	10	2.519	1.015	9	0.250	0.584	8
Injured mutant	0.970	0.690	11	2.848	0.874	11	0.111	0.236	9

Table 5 Raw data for ONL EdU counts

	0 dpr/6 dpf			2 dpr/8 dpf			4 dpr/10 dpf		
	mean	**SD**	**n**	**mean**	**SD**	**n**	**mean**	**SD**	**n**
Control WT	1.708	3.031	8	0.167	0.252	8	0.074	0.147	9
Control mutant	1.571	1.384	7	1.148	1.144	9	0.100	0.161	10
Injured WT	2.200	2.941	10	1.222	0.726	9	1.500	1.960	8
Injured mutant	2.606	2.820	11	3.576	1.694	11	0.926	0.795	9

Table 6 Raw data for INL EdU counts

	0 dpr/6 dpf			2 dpr/8 dpf			4 dpr/10 dpf		
	mean	**SD**	**n**	**mean**	**SD**	**n**	**mean**	**SD**	**n**
Control WT	0.500	0.471	8	0.083	0.154	8	0.037	0.111	9
Control mutant	0.810	0.539	7	0.185	0.242	9	0.133	0.233	10
Injured WT	0.700	0.793	10	0.889	0.782	9	0.500	0.891	8
Injured mutant	1.212	0.834	11	1.697	1.206	11	0.370	0.564	9